Gelatin nanoparticles & nanocrystals for dermal delivery

Inaugural-Dissertation

to obtain the academic degree

Doctor rerum naturalium (Dr. rer. nat.)

submitted to the Department of Biology, Chemistry and Pharmacy

of the Freie Universität Berlin

by

Xuezhen Zhai

from Henan, China

December 2013

The enclosed doctoral research work was performed at the Institute of Pharmacy, Department of Pharmaceutical Technology, Biopharmaceutics & NutriCosmetics, Freie Universität Berlin under the supervision of Prof. Dr. Rainer H. Müller from March 2011 until December 2013.

1st Reviewer: Prof. Dr. Rainer H. Müller

2nd Reviewer: Prof. Dr. Cornelia M. Keck

Date of defense: 10.February.2014

To my parents

With all love and gratitude

Table of contents

1 General introduction

1.1 Skin

1.1.1 Structure and functions of the skin

The skin acts as a remarkably efficient two-way barrier, controlling the unregulated loss of water, electrolytes and solutes, while preventing the invasion of pathogens and fending off physical and chemical assaults (Proksch et al., 2008). The skin has three layers: the epidermis, dermis, and subcutaneous layer, also called the fat layer. Hairs, sebaceous and sweat glands are regarded as derivatives of skin (Figure 1-1).

Being the outermost layer of the skin, epidermis is mainly responsible for the barrier function and mechanical resistance. In most parts of the human body the epidermis is approximately 0.1 mm thick, composed of proliferating basal and differentiated suprabasal keratinocytes. The epidermis consists from the inside to the outside of several layers, e.g. the basal layer, the spinous layer, the granular layer and the stratum corneum. The basal layer composes mainly of proliferating and non-proliferating keratinocytes and is mainly responsible for the constant renewing of the epidermis. The keratinocytes undergo a rapid differentiation in the spinosum and granulosum layers. The cells become flattened and lamellar granules are synthesized. These lamellar bodies migrate toward the cell periphery and are extruded to form the intercellular cement. Once at the base of the stratum corneum, keratinocytes lose their nucleus and organelles to form the so called cornecyte, which is also the final step of keratinocyte differentiation. Corneocytes are constantly replaced as they continuously slough off the surface of the skin in a process known as desquamation.

The dermis is composed of the upper papillary and lower reticular layers. The upper papillary layer is located directly under the epidermis and contains a thin arrangement of collagen fibers whereas the lower reticular layer consists of thick collagen fibers that are arranged parallel to the surface of the skin. The dermis is composed of three types of tissue like collagen, elastic tissue and reticular fibers. The highly organized network of them provides the mechanical properties of the skin. The dermis regulates temperature and supplies the epidermis with nutrient-saturated blood. It contains most of the skin's specialist cells and structures such as blood vessels, hair follicles, nerve endings, lymph vessels and sweat glands.

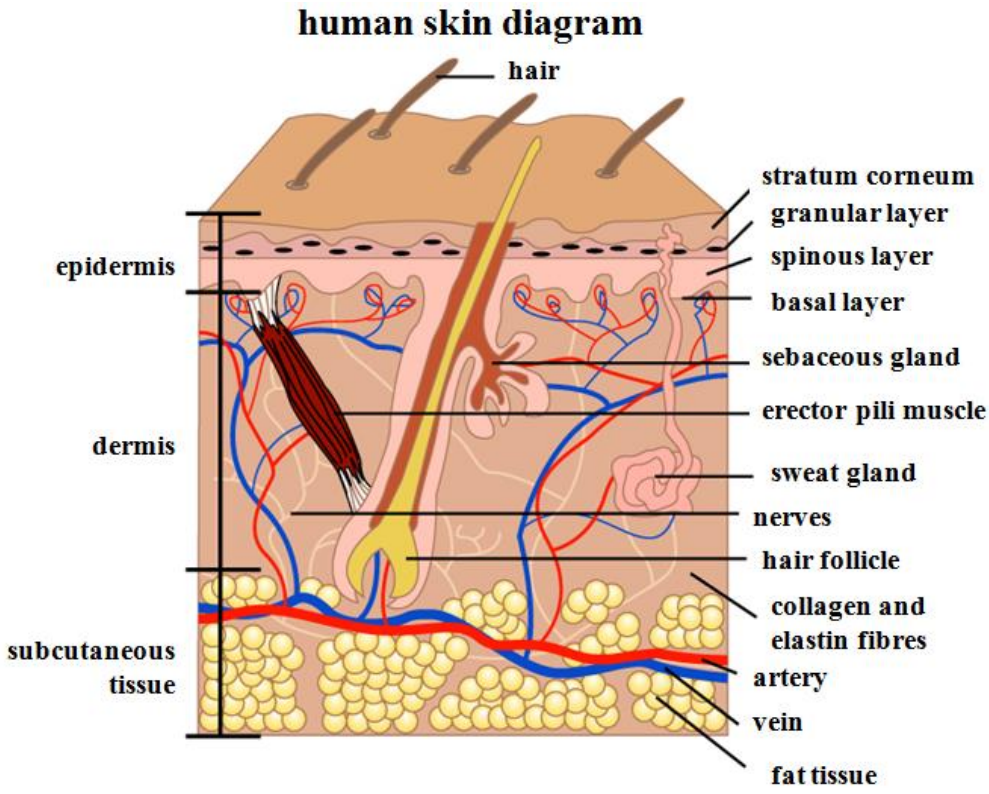

Figure 1-1: The human skin structure. Modified after (Seabuckthorn International Inc. (SII), UK).

The Subcutaneous layer is made up of adipose tissue. It is a layer of fat and also belongs to the deepest layer of the skin. Loss of subcutaneous layer causes facial sagging, leading to the formation of deep wrinkles associated with the process of aging. The fat cells work as shock absorbers protecting the body from mechanical trauma. They also act as heat insulators and help in stabilizing the body temperature.

1.1.2 Penetration pathways into the skin

Generally speaking, the penetration of topically applied substances through the skin includes three different pathways as illustrated in Figure 1-2. The first is the intercellular pathway, where the substances passively diffuse through the stratum corneum along the tortuous lipid matrix around the corneocytes. The second is the transcellular pathways which contemplates the direct transportation of substances through the lipid bilayers and the corneocytes. As the third option, the skin appendages like the hair follicles also represent an efficient penetration pathway. The

important role of hair follicles in skin penetration and the reservoir function have already been validated in many *in vitro* and *in vivo* investigations (Knorr et al., 2009). Nanoparticles have been demonstrated to be an efficient carrier for drug delivery into the hair follicles. The variations in penetration via follicular pathway were due to the difference in particle size and the density or length of the hair follicles (Otberg et al., 2004). The hair follicles also provide interesting immune targeting and gene targeting possibilities due to its distinctive structure and the presence of dendritic cells as well as stem cells.

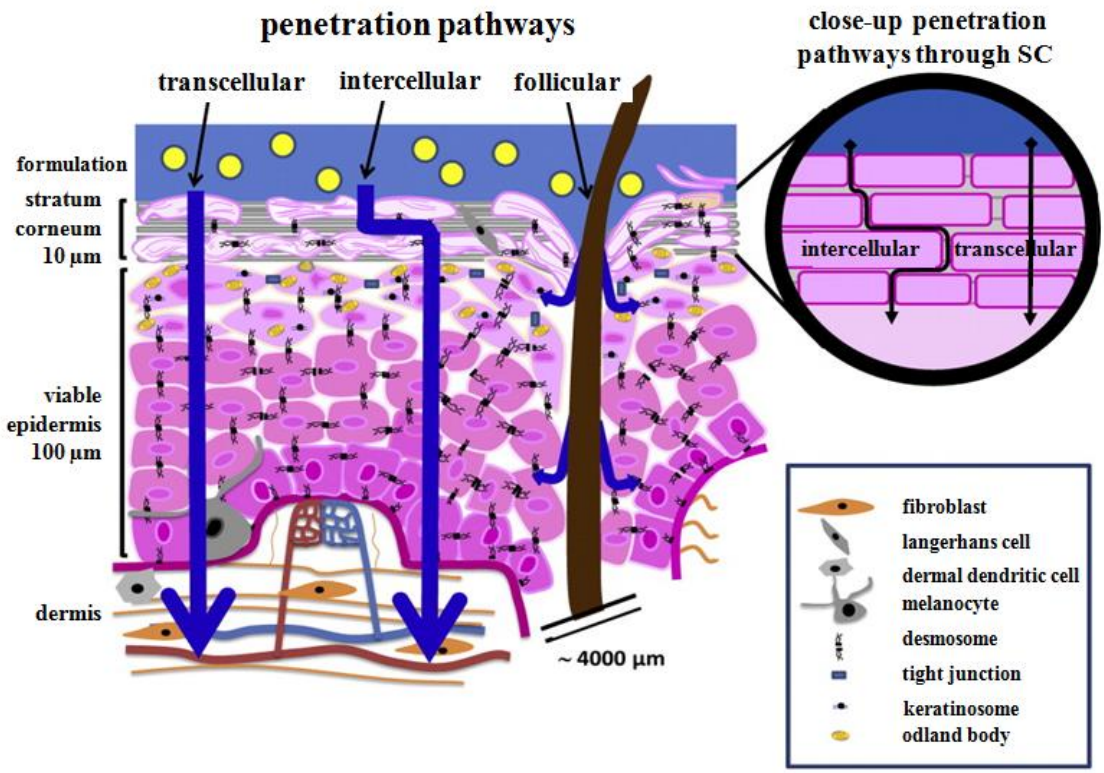

Figure 1-2: Sketch of the intracellular, intercellular and the hair follicular penetration pathways (modified with permission after (Bolzinger et al., 2012)).

1.1.3 Techniques for analyzing skin penetration

Several approaches have been developed to analyze the skin penetration of topically applied substances. The well-known tape stripping technique, firstly introduced in 1951 by Pinkus, is widely used as a minimally invasive technique to evaluate the localization and distribution of substances within the stratum corneum (Pinkus, 1951).

The development of the differential stripping technique enables the quantitatively evaluation of the hair follicular penetration process by combining the classical tape stripping process with the CSSB technique (cyanoacrylate skin surface biopsies technique) (Teichmann et al., 2005). Briefly, after application of a substance onto the skin, the tape stripping process is performed firstly to remove the partial substance within the stratum corneum. The rest which locates inside the hair follicle orifices can be removed by the CSSB technique. Thus the intercellular/transcellular transported and the hair follicle penetrated substance can be quantitatively evaluated separately. A further technique was developed in 2006, in which the hair follicle orifices are artificially blocked by nail varnish or wax within a predetermined skin region (Teichmann et al., 2006). This new approach allows the evaluation of the follicular rate of skin penetration *in vivo* by detecting and comparing the blood concentration of the substance in both hair follicle orifices blocked and unblocked groups.

1.2 Novel carrier systems for dermal delivery

1.2.1 Biodegradable gelatin nanoparticles

Gelatin is a denatured protein derived from animal collagen by partial acidic or alkaline hydrolysis. It is classified as GRAS (generally regarded as safe) material by the U.S. Food and Drug Administration (FDA) and has been safely used in foods, cosmetics and pharmaceutical products for a long time (Elzoghby et al., 2012; Rizzieri et al., 2006). Gelatin is also clinically used for intravenously administered applications like plasma expanders (e.g. Gelfoam®). It is a polyampholyte possesses cationic (lysine and arginine), anionic (aspartic and glutamic acid) along with hydrophobic groups (comprising valine, leucine, isoleucine and methionine) (Kommareddy et al., 2005). The amino acid composition of gelatin is dominated by approximately 33% glycine which orients into the core of the triple-helix, and a further 24% proline and 4-hydroxyproline. The rest are other residues. Gly-X-Y represents the continuously repeating amino acid sequence. A typical structure is "-Ala-Gly-Pro-Arg-Gly-Glu-4Hyp-Gly-Pro-" as shown in Figure 1-3 (Kommareddy et al., 2005). Commercially, two types of gelatin are available, gelatin type A, prepared by acidic hydrolysis of porcine skin type Ⅰ collagen, with an isoelectric point (IEP) of

6-9 and gelatin type B, prepared by alkaline hydrolysis of bovine collagen, with an IEP of 4.8-5.0.

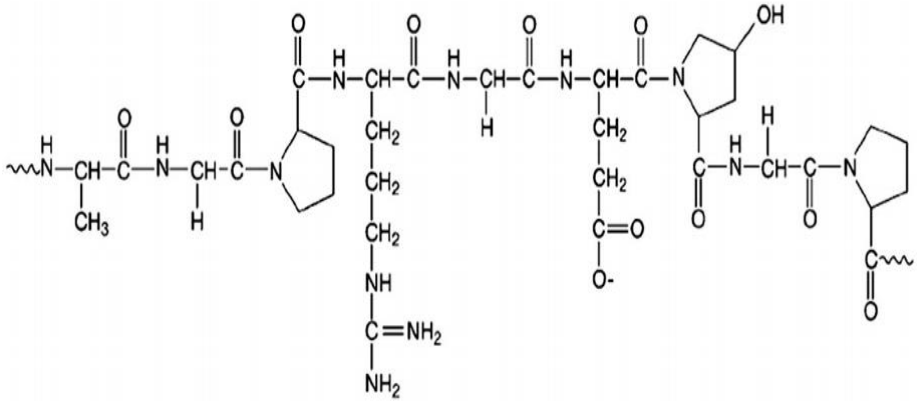

Figure 1-3: Basic chemical structure of gelatin (with permission from (Kommareddy et al., 2005)).

Over the past few decades, ongoing research interest has been conceded to gelatin based drug delivery systems (Young et al., 2005). The underlying rationale is due to their exceptional properties i.e. non-antigenicity, biodegradability, biocompatibility, chemical modification potential, extraordinary loading capacity, controllable drug release as well as good storage stability (Kawai et al., 2000; Yamamoto et al., 2001). Gelatin nanoparticles (GNPs) have been extensively investigated for the delivery of anti-cancer drugs, e.g. methotrexate (Cascone et al., 2002a), cytarabine (Bajpai and Choubey, 2006), resveratrol (Karthikeyana et al., 2013) and cisplatin (Jain et al., 2012). The preferable feature of GNPs for anti-cancer drug delivery concerns the passive targeting ability due to the enhanced permeability and retention effects (EPR effects), through which GNPs can remain at the tumor target for a long time to achieve the complete release of loaded drugs (Lu et al., 2004). GNPs also represent a promising vector for protein, vaccine and gene delivery. Insulin (Zhao et al., 2012), bovine serum albumin (BSA) (Li et al., 1998b), alkaline phosphatase (ALP) (Wang et al., 2012), and angiogenic basic fibroblast growth factor (bFGF) (Wang et al., 2013) have been successfully encapsulated into GNPs with retained *in vivo* bioactivity. After incorporating into the hydro-gel like matrix of GNPs, the plasmid DNA was found to be protected in the systemic circulation and upon cellular transport (Magadala and

Amiji, 2008). GNPs have been under investigation for various administration routes including peroral, ocular, pulmonary and parenteral (Elzoghby, 2013a). Limited report is available about the dermal delivery of GNPs. In the present study, the work focuses on the dermal application.

1.2.2 Nanocrystals

Drug nanocrystals, which are pure solid drug particles with nanodimension, were introduced in 1990s (Liversidge et al., 1992; Müller et al., 1999). The dispersion medium can be water, water-reduced mixtures or non-aqueous media. Typically a nanosuspension is stabilized by surfactants or polymers via electrical repulsion or steric effect (Keck and Müller, 2006). By reducing the size into the nano-range (below 1 µm), physicochemical properties of a substance might change. According to the Kelvin equation, the saturation solubility (C_s) of a substance increases with the decrease in particle size (Simonelli, 1970). Furthermore, dissolution velocity (dc/dt) increases as well, due to the specific surface area enlargement (Noyes and Whitney, 1897). Thus nanocrystal technology is widely used to solve the biopharmaceutical delivery problems of poorly soluble drugs. As displayed in Table 1-1, a variety of commercial products were developed exploiting different features of the nanocrystals.

Table 1-1: Marketed pharmaceutical products based on nanocrystal technology (modified after (Shegokar and Müller, 2010a)).

Trade name	Drug compound	Company	Applied technology
Rapamune®	sirolimus	Wyeth Pharmaceuticals	élan NanoCrystals®
Emend®	aprepitant	Merck & Co.	élan NanoCrystals®
Tricor®	fenofibrate	Abbott Laboratories	élan NanoCrystals®
Triglide®	fenofibrate	Sciele Pharma Inc.	IDD-P® technology
Megace ES®	megestrol acetate	Par Pharmaceutical Companies Inc.	élan NanoCrystals®
INVEGA® / XEPLION®	paliperidone palmitate	Janssen	élan NanoCrystals®

Besides the increased saturation solubility and dissolution velocity, nanocrystals also exhibit the property of increased adhesiveness to the skin which facilitated the dermal delivery. In 2007, nanocrystal technology was introduced to dermal application with the first rutin nanocrystals based cosmetic product emerging on the market. The commercial products are Juvedical Age-Decoder Face Fluid and Juvedical DNA skin optimizer cream (Juvena, Switzerland). It was followed by the Cellular Serum Platinum Rare from la prairie containing hesperidin nanocrystals (la prairie, Switzerland).

However, for a long time, totally neglected is the potential to apply this successful principle also to medium soluble actives such as caffeine. Caffeine is used in anti-cellulite products and specifically, the penetration of caffeine is concentration dependent. That is, increased caffeine concentration in the formulation results in higher skin penetration. Thus, transforming caffeine into nanocrystals and incorporating into dermal formulations (lotions, creams or gels) as dissolving depot might help to enhance its skin penetration by maintaining a constant dissolved caffeine concentration in the formulation as well as constant concentration gradient between the formulation and the skin. Preferably are nanocrystals compared to coarse powder or microcrystals due to the increased saturation solubility and dissolution velocity.

2 Aims of the thesis

Based on the introduction, the aim of the thesis includes:

1. Development of ultrafine GNPs with size below 100 nm or even 50 nm for dermal application using an adapted and modified two-step desolvation method.

The two-step desolvation method, developed by Coester in 2000, is widely used for the production of GNPs. However, the particle size of developed GNPs mostly exceeded 250 nm. Theoretically, smaller GNPs possess higher drug loading capacity via surface adsorption and faster drug release due to increased specific surface area. The aim was to evaluate the influence of different production parameters in the classical two-step desolvation method on particle size and stability of GNPs, and to produce ultrafine GNPs by optimization of the crucial parameters in the desolvation technique. The stability and compatibility of GNPs with a variety of preservatives were also investigated.

2. Characterization and comparison of ultrafine and traditional GNPs as dermal application carriers for proteins using lysozyme as a model drug.

Generally speaking, drug loading of GNPs can be performed in two different ways. The first way is to incorporate drug molecules into particle matrix during the production process of GNPs. And the other way is to allow surface adsorption of drug molecules onto GNPs by incubating the drug in the particle suspension. However, the fundamental relation between the drug loading behavior and the drug release pattern has not been thoroughly investigated. A deep understanding of the interactions between protein molecules and GNPs has not been obtained. The advantages of ultrafine GNPs for dermal application of proteins compared to traditional GNPs have not been demonstrated. Lysozyme was selected as model protein in the present study. The aim was to characterize and compare loaded ultrafine and traditional GNPs in terms of particle size, loading capacity, *in vitro* drug release, physical stability and biological activity, and to investigate the influence of different drug loading methods on particle size, drug loading and *in vitro* drug release.

3. Development of the novel concept and production technique of nanocrystals from medium soluble actives for improved dermal delivery.

The novel approach is to make nanocrystals also from medium soluble actives such as caffeine. By incorporating caffeine nanocrystals as dissolving depot, the concentration of caffeine in the applied dermal formulation remains stable, thus enhanced skin penetration can be obtained due to the constant penetration velocity. The aim is to produce caffeine nanocrystals via high pressure homogenization and pearl milling, in combination with the application of media with low dielectric constant (such as ethanol and propylene glycol) which helps to eliminate the crystal growth. As already has been documented, nanoparticles with appropriate size could be accumulated in the hair follicle orifices. Therefore, the present research mainly focuses on the production of caffeine nanocrystals with optimized particle size (600-700 nm) to enhance skin delivery by employing the reservoir functions of the hair follicles.

3 Theoretical background and technologies

3.1 Production techniques of GNPs

3.1.1 Coacervation

The coacervation and equally coined desolvation process are the most frequently applied methods to produce gelatin-based nanoparticles contributing to the relatively mild conditions. In brief, gelatin was initially dissolved and afterwards a colloidal system was created when the initial solvent was gradually extracted into an anti-solvent phase. Thereby, solid colloid dispersed in a second phase consisting of the initial solvent and the anti-solvent was obtained. The addition of alcohol or natural salt could promote the coacervation process and resulted in desired particle size. Consequently, solvent and anti-solvent must be miscible, e.g. water and acetone are often used to produce GNPs by a two-step desolvation technique (Langer et al., 2003; Weber et al., 2000). To stabilize freshly formed colloidal nanoparticles, chemical cross-linkers such as glyoxal and glutaraldehyde are widely used to establish covalent bonds between prime amino groups (Ofokansi et al., 2010).

3.1.2 Solvent extraction - emulsification

GNPs can be produced adopting a solvent evaporation technique based on a single water-in-oil (W/O) emulsion. In this technique, the aqueous phase containing gelatin and drug (in water or phosphate buffer) was mixed with the oil phase (i.e. organic solution of paraffin oil or polymethylmethacrylate) together with surfactants (e.g. Poloxamer-188) by vigorous shaking or high speed homogenization followed by cross-linking of glutaraldehyde (Cascone et al., 2002b; Zhao et al., 2012). GNPs were obtained after the evaporation of organic solvent either by increasing the temperature or continuous stirring. In general, a high encapsulation rates can be observed by this technique. The effect of process variables on the properties of resulted GNPs was investigated. The water-in-oil-in-water (W/O/W) double emulsion technique has also been used to allow the encapsulation of hydrophilic drugs and proteins (Sussman et al., 2007).

3.1.3 Nanoprecipitation

In a precipitation process, water phase containing both gelatin and drug (solvent phase) was added slowly to the non-solvent phase such as ethanol or acetone and afterwards glutaraldehyde was added to stabilize GNPs by cross-linking. The GNPs turned out to be mono-dispersed with a mean particle size of 251 nm and a polydispersity index of 0.096 after freeze-drying (Lee et al., 2012). Possible mechanism for the formation of GNPs could be attributed to the interfacial turbulence generated during solvent replacement followed by a violent spreading due to the mutual miscibility between the solvents. Probably nano-sized droplets are torn from the interface. These ultra-small droplets are immediately stabilized by the stabilizer (e.g. poloxamer), until diffusion of the solvent is complete and polymer solidification is finished (Quintanar-Guerrero et al., 1998). Nanoprecipitation technique possesses many advantages, in that it is a straightforward method, rapid to perform. The formation of particles is instantaneous and the entire procedure is easy to carry out. All these points make this method widely used for the production of various polymeric nanoparticles. It enables the production of nanoparticles with smaller particle size as well as narrower size distribution. Moreover, no sonication, extended stirring rate, or high temperature is needed.

3.1.4 Self-assembly

GNPs can also be performed by self-assembly of gelatin molecules through chemical modification. The distinctive structure of hydrophilic gelatin provides varied possibilities to chemically conjugate with hydrophobic molecules and form an amphiphilic polymer. When dissolving in an aqueous phase, modified gelatin molecules are capable of self-assembling to form micelle-like nanospheres through conformational rearrangement. The self-assembled GNPs possess a hydrophilic outer shell and a hydrophobic core formed by inward aggregation of hydrophobic segments. Hydrophobic drugs with solubility problems could be entrapped into the core of the GNPs. An example is the camptothecin loaded self-assembled GNPs in which hexanoyl anhydride was utilized for the hydrophobic modification of gelatin (Figure 3-1). In addition, a controllable sustained release could be obtained by adjusting the substitution degree of gelatin (Li et al., 2011).

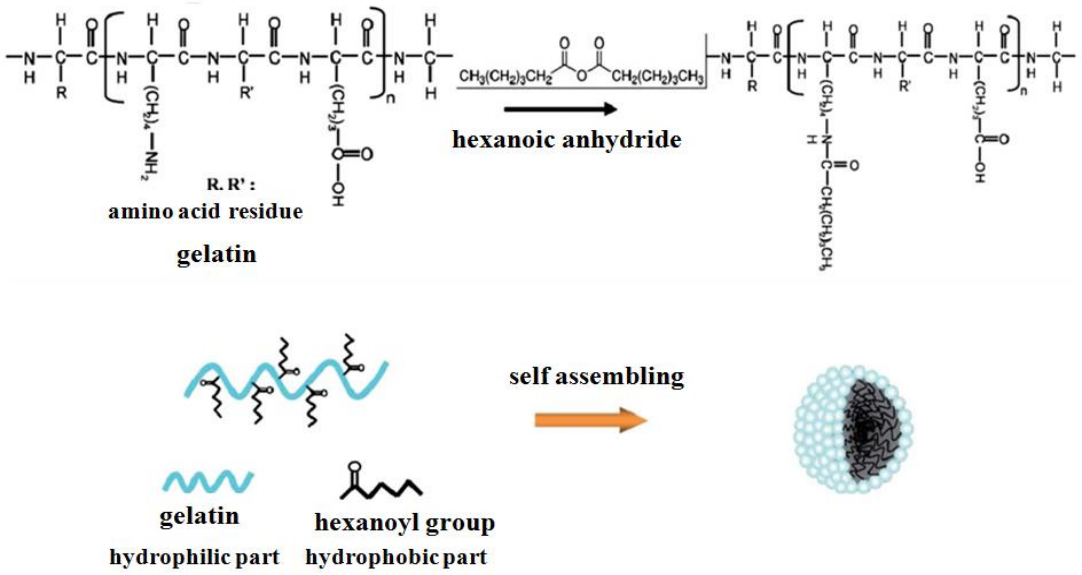

Figure 3-1: The reaction scheme for the synthesis of self-assembled hexanoyl-modified GNPs (modified with permission after (Li et al., 2011)).

3.2 In vitro characterization of GNPs

3.2.1 Drug loading

Drug loading into GNPs can be performed by either entrapped into the matrix during the production or adsorption onto the surface of the performed nanoparticles. Possible mechanisms could be electrostatic attraction, covalent conjugation, hydrogen bonding as well as physical entrapment (Kommareddy et al., 2005). For matrix incorporation of hydrophilic drugs, drug loading was performed by dissolving the drug in aqueous gelatin solution prior to the desolvation and formation of GNPs. As with hydrophobic drugs, a concentrated drug solution in water-miscible organic solvent was mixed with gelatin solution under sonication or gentle stirring (Nahar et al., 2008; Zhao et al., 2004). Thus drug loading was performed before formation and cross-linking of GNPs. Entrapment of hydrophobic drugs into GNPs is based on the preferential localization as the nanoparticulate core is less hydrophilic than the outer aqueous environment (Nahar et al., 2008). For surface drug loading of GNPs, drugs were incubated together with freshly produced nanoparticles suspension to allow the surface adsorption through electrostatic attraction or entrapment in between the extended segments on the surface of nanoparticles due to steric effects. The extent of drug loading efficiency

is dominated by the nature of the substance incorporated and also the molecular weight of gelatin. Saxena *et al.* reported that 300 bloom gelatin possessed higher drug loading efficiency than that of 75 and 175 bloom gelatins (Saxena et al., 2005).

3.2.2 Drug release

Three possible mechanisms including desorption, hydration and matrix erosion are related to the drug release from GNPs (Kaul and Amiji, 2002; Kommareddy et al., 2005). Varied factors have been demonstrated to influence the drug release rate from GNPs, e.g. the degree of cross-linking, the particle size and the presence of proteolytic enzymes. Since glutaraldehyde is a hydrophilic cross-linker, linkages in the GNPs matrix serve as hydrophilic channels which allow the water molecules to penetrate into the core of the particles. Thus, obviously increased cross-linking density facilitates the drug release (Bajpai and Choubey, 2006). Another factor is the particle size. Smaller particles possess larger specific surface area and therefore, most of the incorporated drug molecules will be near or just beneath the particle surface leading to a faster drug release. Furthermore, the presence of a proteolytic enzyme also accelerates the biodegradation of GNPs and correspondingly the drug release. The release of doxorubicin from GNPs was reported to increase from 9% to 30% by addition of protease (Leo et al., 1999).

3.2.3 Particle size and surface charge

Utilizing the above mentioned production methods GNPs with particle sizes ranging from 220 to 500 nm could be obtained. The particle size is a pivotal property of GNPs which influences the drug loading efficiency, drug release, storage stability and cell internalization kinetics *etc*. The effect of various parameters like gelatin concentration, temperature, pH, type of desolvation agent and degree of cross-linking has been intensively investigated by several groups (Ethirajan et al., 2008; Qazvini and Zinatloo, 2011). Zhai *et al* reported that increasing the gelatin concentration caused a significant increase in particle size of GNPs produced by a modified two-step desolvation technique, while an obvious reduction in particle size was observed by increasing the amount of cross-linking agent (Zhai et al., 2011). This could be

attributed to the cross-linking of free amino groups on the surface of particles and consequently hardening of GNPs. A temperature of 50°C was recognized as the optimum temperature for the production of GNPs with desired particle size and low polydispersity index because of the high viscosity of gelatin at room temperature. Furthermore, formulation pH at the second desolvation step was of critical importance as it dominates the cross-linking reaction. The optimum pH for type A gelatin was found to be 3, and 11 for type B gelatin (Zhai et al., 2011). Zeta potential is an efficient tool to forecast the stability of nanoparticles. A high absolute value of zeta potential indicates high electric charge on the surface and strong electrostatic repulsion, which can efficiently prevent the agglomerations of particles (Wissing and Müller, 2002b).

3.3 Production technologies of nanocrystals

3.3.1 Bottom up technologies

The existing nanocrystal production strategies can be classified into “bottom up” and “top down” technologies. In term of bottom up process drug nanocrystals are fabricated from molecule state via classical precipitation techniques. In brief, the drug is dissolved in a solvent and the obtained solution is then added to an anti-solvent, thus nanocrystals are generated by precipitation. Examples for precipitation techniques are Nanomorph™ from Soliqs/Abbott (previously Knoll, belonged to BASF) and hydrosols developed by Sucker (Sandoz, nowadays Novartis). Various parameters are critical for the production of predefined nanocrystals via precipitation techniques, i.e. solvent and anti-solvent properties, mixing efficiency, degree of supersaturation and the nucleation process (Sinha et al., 2013).

There are various other bottom up technologies, e.g. sonocrystallization, supercritical fluids, spray-drying based droplet evaporation and multi-inlet vortex mixing (Müller et al., 2011). The basic advantages of precipitation techniques are low cost, scale-up potential and reduced denaturation of APIs (active pharmaceutical ingredients) due to high energy input (Sinha et al., 2013; Zhong et al., 2005). However, the precipitation techniques are not really widely used for the production of commercial used drug nanocrystals. There are several challenges stunting the widespread application of

precipitation techniques, i.e. drug solubility in at least one solvent, crystal growth due to Ostwald ripening, formation of amorphous drugs, poor re-dispersity and the organic solvent residue (Sinha et al., 2013). Therefore, typically the top down technologies are commonly applied in pharmaceutical industries.

3.3.2 Top down technologies

In the top down technologies, nanocrystals are produced from large sized drug powders and go down to the nano-dimension by disintegration processes. There are basically two disintegration technologies: pearl milling/ball milling and high pressure homogenization (microfluidization and piston-gap homogenization)

3.3.2.1 Pearl milling

Pearl milling is a low energy milling technology developed by G. Liversidge and co-workers (Liversidge and Cundy, 1995). Nowadays this technology is used by the company élan (previously Nanosystems, now belonging to Alkermes), being the NanoCrystal® technology. In a pearl milling process, the coarse drug powder is firstly dispersed in a surfactant solution, and the obtained presuspension is poured into the milling chamber containing milling beads. Size diminution is obtained by the shear forces generated by the movement of milling beads, driven by either a stirrer or by moving the chamber itself. The critical process parameters dominating nanocrystal formulation and stabilization have been identified, i.e. size of milling beads, milling time, temperature and the concentration of drug (Ofokansi et al., 2010). The general problem with pearl milling is the potential product contamination caused by erosion of milling beads. The erosion mainly depends on the hardness of the drug and the milling beads as well as the milling time. Most nanocrystal based pharmaceutical products on the market are produced by this technology, e.g. RAPAMUNE® from Wyeth and EMEND® from Merck.

3.3.2.2 High pressure homogenization

Another frequently used disintegration process is the high pressure homogenization. Microfluidizer, developed by the company RTP, is a jet stream homogenizer. The suspension is accelerated and passes a “Z” type or “Y” type chamber at very high velocity and crystals are generated via particle collision and shear forces (Khan and Pace, 2002). Problems associated with microfluidization are the high numbers of passes through the chamber and the high potential presence of a large fraction of microcrystals in the final production.

Alternatively, nanocrystals can be produced by using a piston-gap homogenizer developed by Müller and co-workers (Müller et al., 2000). The first trademarked technology based on piston-gap homogenization is DissoCubes®, of which the dispersion media is pure water. Take the APV LAB 40 as an example, coarse suspension is forced from the wide cylinder (3 cm) into the very narrow gap (5 µm to 25 µm) at high pressure and velocity (Figure 3-2, left). When arriving at the gap, the dynamic pressure increases and the static pressure decreases according to the law of Bernoulli that the flow volume of a liquid remains constant per cross section in a closed system. The liquid starts boiling when the static pressure drops to or even below the vapor pressure of the liquid at room temperature. After leaving the gap, the bubbles formed by liquid boiling implode under normal air pressure conditions. Nanocrystals are fabricated via this so called cavitation process. The follow-up technology is Nanopure® developed by PharmaSol. In a typical Nanopure® homogenization process, water-reduce media (e.g. water/glycerol mixtures) or water-free media (oils or liquid polyethylene glycols, i.e. PEG 400 and PEG 600) are used as dispersion media. This kind of media possesses lower vapor pressure than water, and the drop in the static pressure is not sufficient to initiate cavitation or only limited cavitation is obtained (Figure 3-2, right). Thus nanocrystals are generated mainly via particle collision and shear disintegration.

The particle size of nanocrystals produced by high pressure homogenization mainly depends on the hardness of the drug, the power density of the homogenizer, the number of homogenization cycles and the production temperature (Keck and Müller, 2006).

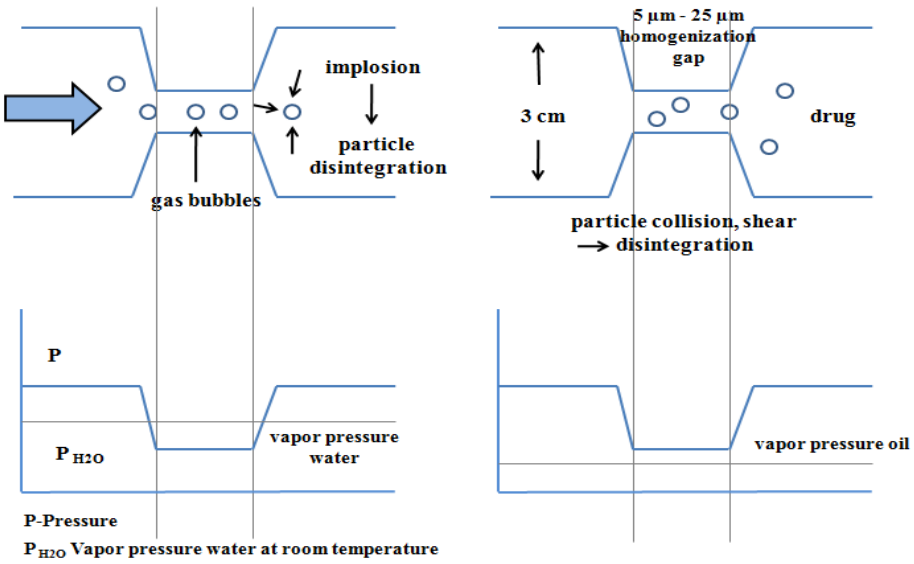

Figure 3-2: Illustration of the nanocrystal fabrication in a piston-gap homogenizer, from the large diameter cylinder to the narrow homogenization gap. The diagrams below present the actual ranges of the static pressure (left: homogenization in pure water, right: homogenization in water-reduce media or water-free media) (with permission from (Keck and Müller, 2006)).

3.3.3 Combinative technology

The combination of a pre-treatment step and subsequent high pressure homogenization are introduced to compensate the limitations of the single "bottom up" and "top down" technologies. The NANOEDGE™ technology developed by Baxter is performed by precipitation at the first step, and the obtained suspension is further subjected to high pressure homogenization. The smartCrystal® technology developed by PharmaSol (owned by Abbott Lab since 2007) in composed of a variety of combinative techniques (Table 3-1). Spray-drying, precipitation, lyophilization and pearl milling are applied as pretreatment followed by high pressure homogenization as the main treatment (Shegokar and Müller, 2010a). By applying this technology, ultra small nanocrystals with particle size below 100 nm can be produced (Müller et al., 2011).

Table 3-1: The second generation of drug nanocrystals, the members of the smartCrystal® technology (modified with permission after (Shegokar and Müller, 2010a)).

Process	Pre-treatment	Main treatment	Patent No. and date of filling
H42	spray-drying	high pressure homogenization	DE/102005 011 786.4, 2005
H69	precipitation	high pressure homogenization	PCT/EP 2006/009930, 2007
H96	lyophilization	high pressure homogenization	PCT/EP 2006/003377, 2007
CT	Pearl milling	high pressure homogenization	PCT/EP 2007/009943, 2006

3.4 In vitro characterization of nanocrystals

3.4.1 Particle size analysis

3.4.1.1 Photon correlation spectroscopy

Photon correlation spectroscopy (PCS), also called dynamic light scattering or quasi-elastic light scattering, is a widely used technique to determine the particle size and size distribution of particles in the submicron range. PCS analysis is based on the random movements of particles diffusion. The particle suspension is illuminated with a laser light and the fluctuations of the scattered light caused by the particles are measured. Small particles possess higher diffusion velocity and the fluctuations of the scattered light are rapid. In contrast, for large particles the fluctuations of the scattered light are slow due to the lower diffusion velocity. An autocorrelation function g(τ) is calculated from the time dependent intensity fluctuation of the scattered light. The diffusion coefficient D of particles is obtained from the decay of the correlation function. Hence the particle diameter can be calculated using the well known Stokes-Einstein equation:

$$d\,(\mathrm{H}) = \frac{kT}{3\pi\eta D}$$

d(H) is the hydrodynamic diameter

D is the diffusion coefficient

k is the Boltzmann's constant

T is the absolute temperature

η is the dynamic viscosity

Besides the particle diameter, the polydispersity index (PI), which is a measure of the width of the size distribution, is also obtained by the PCS measurement. If all the particles in a suspension possess the same size, g(τ) is a single exponential. Whereas if more than one size of particles present, g(τ) is poly-exponential. The PI describes mathematically the deviation between the calculated and the fitted correlation function g(τ). Generally speaking, PI values of less than 0.2 indicate a relatively narrow size distribution (Malvern Instruments, UK).

3.4.1.2 Laser diffractometry

Laser diffractometry (LD), also known as static light scattering, is another preferable technique for particle sizing of materials ranging from tens of nanometers up to about two millimeters. LD analysis is based on the fact that the pattern of diffracted light by particles is size dependent. The surface of a large particle is less curved and the diffraction angle is small, whereas for a small particle, the diffraction angle is large (Figure 3-3). The particle size is calculated using the Mie theory of light scattering based on the collected scattering intensity data, assuming the particles possess spherical shapes. Thus the particle size obtained by LD is a volume equivalent sphere diameter. The advantages related to LD include the wide dynamic range, the rapid measurement and the instant feedback.

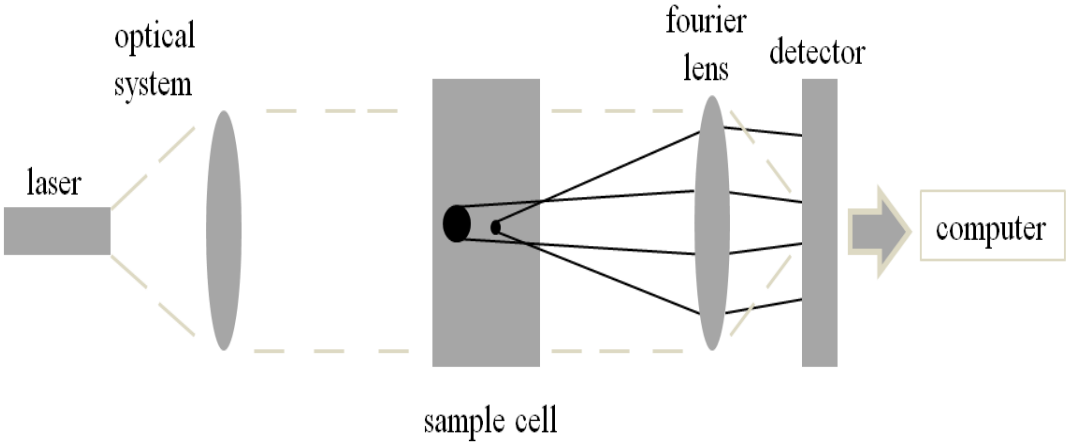

Figure 3-3: Schematic assemble of the laser diffractometry (modified with permission after (Keck, 2006)).

3.4.2 Zeta potential analysis

Zeta potential is well known to predict the long term stability of colloidal systems. Most particles in a suspension possess a surface charge due to ionization of surface groups or adsorption of ions. According to the DLVO theory (Derjaguin and Landau, Verwey and Overbeek theory), the liquid layer surrounding the particle is divided into two layers: the Stern layer containing strongly bounded ions which move together with the particle and the diffuse layer where the ions diffuse more freely (Malvern Instruments, UK). There exists a theoretical boundary in the diffuse layer, i.e. the hydrodynamic plane of shear which is also called the slipping plane. The ions within the slipping plane move together with the particle. The zeta potential refers to the electrical potential at this slipping plane.

The zeta potential can be measured using a technique of Laser Doppler Anemometry. When applying an electrical field across the suspension, particles will migrate toward the oppositely charged electrode with a constant velocity (electrophoretic mobility). The zeta potential can be calculated from the detected electrophoretic mobility by the Henry equation. Several factors are crucial for the detection of zeta potential, i.e. the pH of the medium, the conductivity of the medium and the concentration of a particular additive in the suspension (ionic surfactants) (Müller, 1996). The relationship between the zeta potential values and the stability of colloidal systems

has been evaluated by Müller. Generally speaking, a suspension system possesses an absolute zeta potential value higher than 30 mV is expected to show a good physical stability (Müller, 1996).

4 Preparation, characterization and stability of ultrafine gelatin nanoparticles for dermal application

4.1 Introduction

The lipid nanoparticles, submicron emulsions, liposomes, nanocrystals etc. are the most active research areas in nanotechnology concerned with pharmaceuticals and cosmetics during the past decade. These delivery systems exhibit attractive advantages regarding good physical stability, controllable release and modifiable organ distribution (Barratt, 2003). They are of particular interest to provide new delivery methods for traditional drugs and also genes, peptides, proteins and oligonucleotides (Liang et al., 2006a).

In the development process of particulate drug carriers, both synthetic and natural polymers have been extensively investigated due to their known biodegradability and biocompatibility (Soppimath et al., 2001). With regards to nanoparticles based on natural polymers, gelatin and gelatin based derivatives represent a focal point of interest. As a kind of proteinaceous origin carrier with unique amino acid structure, gelatin bears numerous accessible functional groups which can provide various modification opportunities for particular drug delivery applications (Kuo et al., 2011b). In 1969, Schwick and Heide reported the advantages of gelatin over other homologues, i.e. lower immunogenicity and higher physiological tolerance (Schwick and Heide, 1969). Due to its outstanding beneficial properties, gelatin is generally accepted as safe by the U.S. Food and Drug Administration (FDA). Gelatin has been employed in cosmetic industries for decades as “hydrolyzed animal protein” in conditioners, lipsticks and shampoos. It has been demonstrated to be able to boost skin hydration, improve skin feeling, decrease the depth and extent of wrinkles (Rizzieri et al., 2006). On the other hand, gelatin nanoparticles (GNPs) have been applied in the delivery of various drugs, i.e. doxorubicin, paclitaxel, cycloheximide and chloroquine phosphate (Bourquin et al., 2010; Hoffmann et al., 2009; Nezhadi et al., 2009a).

In general, two types of gelatin are available for the preparation of GNPs: gelatin type A (acidic) extracted from porcine skin and gelatin type B (basic) obtained mostly from bovine bones. Several methods like coacervation (Mohanty et al., 2005), emulsification (Cascone et al., 2002a), nanoencapsulation (Li et al., 1998a), and desolvation have been developed for the preparation of GNPs (Coester et al., 2000a).

The two-step desolvation method developed by Coester *et al.* enabled the preparation of homogeneous and high concentrated nanoparticles by separating the higher molecular weight fractions from the lower molecular weight fractions (Coester et al., 2000a). In the following years, the influence of several preparation parameters such as concentration of cross-linking reagent, cross-linking degree and type of desolvation reagent on properties of GNPs have been intensively investigated by several research groups (Azarmi et al., 2006; Jahanshahi et al., 2008; Saxena et al., 2005). However, the size of the GNPs reported so far mostly exceeded 250 nm. In general, particulate carriers have different mechanisms of penetrating or crossing the human skin barrier like the intercellular pathway, the transcellular pathway and via hair follicles (Prow et al., 2011). The stratum corneum also represents the first main physical barrier against the percutaneous penetration of pathogens and chemicals. Therefore only small molecules are able to move freely across the stratum corneum. However, it has been reported that free movement of small particles and macromolecules might be physically restricted within the inter-corneocyte-cluster spaces with dimensions varied from 0.4 nm to 100 nm (Cevc, 2004b; Charalambopoulou et al., 2000; Vogt et al., 2006a). In addition, very small particles are highly adhesive to surface, i.e. they stick strongly to the skin, and remain there being beneficial for drug delivery.

Based on the facts and assumptions mentioned above, ultra small nanoparticles possess extremely high potential for dermal application. Therefore, the main goal of this study was to develop GNPs with size below 100 nm or even 50 nm for dermal application using an adapted and modified two-step desolvation method.

4.2 Materials and methods

4.2.1 Materials

Gelatin type A, Bloom 175, derived from porcine skin was obtained from Naumann Gelatine and Leim GmbH (Memmingen, Germany). Glutaraldehyde aqueous solution (25% w/w, grade I) and acetone (HPLC grade) were purchased from VWR International GmbH (Darmstadt, Germany), Euxyl® PE 9010 (EUX9010) from Schülke & Mayr GmbH (Norderstedt, Germany), and Hydrolite®-5 (Pentylene glycol) from Dragoco Gerberding & Co AG (Holzminden, Germany). Thiomersal was

purchased from Sigma-Aldrich GmbH (Taufkirchen, Germany). Freshly prepared double distilled and ultra purified water (Milli-Q, Millipore GmbH, Germany) were used as dispersion medium. All the other reagents and chemicals used in this study were of analytical grade and were used as received.

4.2.2 Methods

4.1.1.1 Preparation of GNPs

GNPs were prepared by a new modified two-step desolvation method. Gelatin type A was dissolved in 25 ml Milli-Q water under constant magnetic stirring (300 rpm) and heating at various temperatures, till a clear gelatin solution was obtained. First addition of 25 ml desolvating agent (ethanol, acetone or isopropanol) was done for rapid desolvation and sedimentation of high molecular weight gelatin fractions. Turbid supernatant containing lower molecular weight gelatin fractions was discarded after various times. Additional 3 ml of water were added to remove the traces of lower molecular fractions on the surface of hydrogel-like sediment after slightly shaking. Finally, the hydrogel-like sediment was redissolved in 25 ml water and the pH of the solution was adjusted. Then gelatin aqueous solution was again desolvated by adding desolvating agent. The solution was observed for the endpoint like turbidity or formation of blue ring (approximately 50 ml desolvating agent). After stirring for 10 minutes at 200 rpm, desolvating agent was added again dropwise. Afterwards, 0.8 ml of glutaraldehyde (8% w/w) was added for the cross-linking of GNPs. The freshly prepared nanoparticle suspension was stirred for 12 hours at 200 rpm. The cross-linked particles were then purified by centrifugation and redispersion in 50 ml of Milli-Q water. Possible remaining desolvating agent was evaporated by using a Buchi RE-121 Rotavapor (Buchi Laboratoriums-Technik AG, CH-9230 Flawyl/Schweiz, Switzerland).

Effect of various preparation parameters like the starting gelatin concentration (2.5, 5, 10 and 20% w/v), the precipitation time (2, 5, 10, 20 and 30 min), the temperature at the first desolvation step (35, 40, 45, 50, 55, 60 and 65°C), the pH at the second desolvation step (2, 2.5, 3, 3.5 and 4), the type of desolvating agent (ethanol, acetone

and isopropanol) and the amount of dropwise added desolvating agent (20, 25, 30 and 35 ml) on particle size were studied.

4.1.1.2 Characterization of GNPs

Photon correlation spectroscopy (PCS)

GNPs were characterized for mean particle size (mean intensity weighted diameter, z-average) and polydispersity index (width of the size distribution, PI) by photon correlation spectroscopy (PCS), using a Zetasizer Nano ZS (Malvern Instruments, UK). For size determination, all samples were diluted fivefold with Milli-Q water and measured 10 subruns in triplicate at 25°C.

Yield of GNPs

About one milliliter of the freshly prepared GNPs aqueous suspension was dropped in an aluminum sample pan and was dried in the oven at 60°C for 3 hours until a constant weight was obtained. The particle yield was calculated using equation (4-1).

$$\text{GNPs yield (\%, w/w)} = \frac{\text{amount of recovered GNPs}}{\text{total amount of suspension}} \times 100\% \qquad (4\text{-}1)$$

Light microscopy

Light microscopy was also performed for the detection of possible larger particles or aggregates at different magnifications. An Orthoplan microscope (Leitz, Germany) connected to a CMEX-1 digital camera (Euromex microscopes, Netherlands) was employed.

Transmission electron microscopy

Morphology of GNPs was analyzed by a transmission electron microscope (Tecnai F20 TEM, FEI Company, USA). Droplets of the nanoparticle suspension (approximately 5 µl) were applied to the hydrophilized carbon film covered microscopical copper grid (400 mesh) and stained after 30 seconds by 1% (w/v),

uranyl acetate. Subsequently, the supernatant fluid was removed with filter paper and the grid was allowed to air dry. TEM analysis was performed at an acceleration voltage of 160 kV.

Zeta potential determination

The zeta potential (charge on the particles) of GNPs was analyzed by using a Zetasizer Nano ZS (Malvern Instruments, UK). The electrophoretic mobility of GNPs in an electric field was measured directly by the Zetasizer and then converted to the zeta potential by Helmholtz-Smoluchowski equation. All samples were diluted tenfold and measured in triplicate. The zeta potential of GNPs and gelatin solution (1% w/w) was also analyzed at different pH values (2-10) and varying conductivities (2-60 μS/cm). The pH of the media was adjusted by hydrochloric acid (37% w/w) or sodium hydroxide. The conductivity of the media was adjusted by sodium chloride solution (0.9% w/w).

Physical compatibility of GNPs with different gelling agents

For the preparation of GNP-loaded gels, different gelling agents were selected to screen the suitability without affecting the physical stability of GNPs. As a first step, an adequate production procedure has to be verified. Gelatin type A was firstly dissolved in water under heating at 45°C and cooled to room temperature. Sodium Carboxymethyl Cellulose (CMC-Na) was dispersed in water and allowed to swell overnight. As for Carbopol® 940, it was firstly dispersed in water and then the pH was adjusted to 6.0 by adding sodium hydroxide solution (1% w/v) under stirring. Three concentrations (1%, 2% and 5%) of each gelling agents were applied for the preparation of gels. The GNPs aqueous suspensions were mixed with the various gels (50:50) and left overnight. The physical compatibility of the GNPs with the added gelling agents was investigated over three months at 4°C by particle size analysis. For the preparation of the samples for PCS measurements, various GNP-loaded gels were diluted tenfold by Milli-Q water under constant stirring at 300 rpm over night.

4.1.1.3 Long term stability

To examine the physical stability of GNPs, a long term stability test was carried out. On the day of preparation, GNPs were divided into three vials and stored at three different temperatures (4°C, room temperature and 40°C) for two years. Samples were analyzed for particle size on the days 0, 30, 90, 180, 360 and 720. The influence of three preservatives (1% Euxyl® PE 9010, 5% Hydrolite®-5 and 0.002% Thiomersal, w/w) on physical stability of GNPs was also investigated.

4.3 Results and discussion

4.3.1 Preparation of GNPs

For the preparation of ultrafine GNPs for dermal application (50-100 nm), the modification of the existing preparation method became the most crucial challenge of this study. Therefore, several parameters of the two-step desolvation method were modified and optimized. In the following, each parameter separately is presented and the effect on particle size was discussed.

4.3.1.1 Effect of starting gelatin concentration on particle size of GNPs

The starting concentration of gelatin solution is a main factor in order to achieve predefined parameters for the reproducibility of specifically sized particles using a desolvation method. Although the preparation of GNPs was already described in 1978 by Marty *et al.*, the low starting gelatin concentration (0.1-1%) needed for the preparation of stable particles did not lead to much further use of GNPs due to very low concentrated nanoparticle suspensions after preparation and purification (Marty et al., 1978). Therefore the first parameter investigated was the starting concentration of gelatin which has direct effect on the amount of sediment after the first desolvation step and the corresponding yield of nanoparticles in the final product. Gelatin concentrations in a range of 2.5 to 20% (w/v) were chosen and GNPs were prepared according to the standard production protocol as described in methods (section 4.2.2.1). Gelatin was dissolved in 25 ml Milli-Q water at 50°C. 25 ml of acetone was added to the gelatin solution and the turbid supernatant was discarded after 5 minutes.

The traces of low molecular weight fractions on the surface of the sediment were also removed. After redissolution of the sediment, the pH of the solution was adjusted to 3.0. Then the gelatin solution was desolvated again by direct addition of 50 ml acetone followed by dropwise addition of another 25 ml acetone. Glutaraldehyde solution was added as a cross-linking agent. After stirring for 12 hours, the particles were purified and possible remained acetone was evaporated.

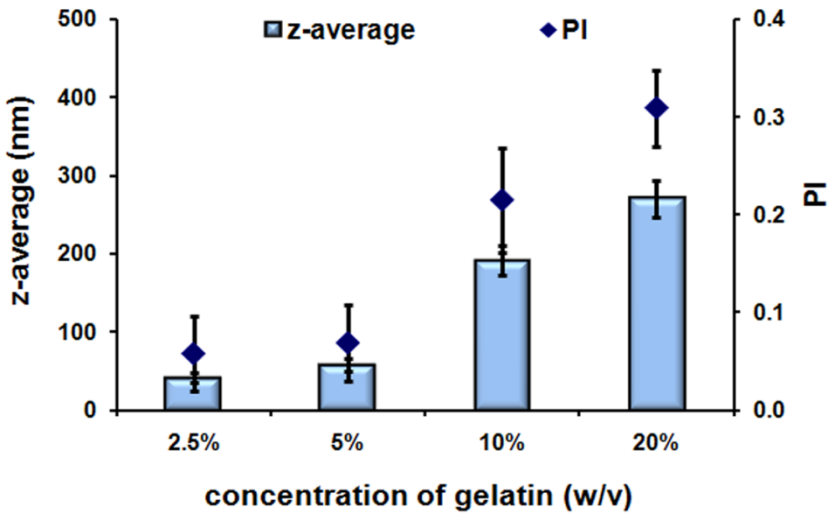

Figure 4-1: Effect of starting gelatin concentration on z-average and PI of GNPs. The evaluated gelatin concentrations were 2.5%, 5%, 10% and 20% (w/v), respectively.

A noticeable increase in the mean particle size was observed as the concentration of gelatin increased from 2.5 to 5% (w/v) (Figure 4-1). The results show that the particle size of GNPs increased from 56 nm (5% w/v) to 270 nm when the starting gelatin concentration increased to 20% (w/v). The increase in gelatin concentration affected not only the mean particle size but also resulted in flocculation. Already after the doubling of the starting concentration from 5% to 10%, the PI value already increased from 0.069 to 0.215. All these changes might be associated with the insufficient segregation of the low molecular weight gelatin fractions which hinders the formation of GNPs itself as well as results in interaction between particles during or after cross-linking by forming unstable agglomerate. This means that the starting concentration of gelatin for the preparation of uniform and stable ultrafine GNPs using the modified two-step desolvation technique was a maximum of 5% (w/v). Based on these results

no higher starting concentrations than 5% (w/v) were applied in the following experiments.

4.3.1.2 Effect of precipitation time on particle size of GNPs

Gelatin type A is prepared by acidic hydrolysis of porcine skin type I collagen. During the extraction process, covalent inter- and intramolecular bonds which have direct influence on the basic characters of collagen like solubility and stability undergo cleavage. Afterwards the obtained tropocollagen is further subjected to denaturation by the breakage of hydrophobic interactions and hydrogen bonds which are responsible for the stabilization of the triple-helix structure (Flory and Weaver, 1960). Therefore, a heterogeneous proteinaceous product with a broad range of molecules with various molecular weights is generated instead of a homogeneous decomposition material. The molecular heterogeneous property of gelatin represents a particular challenge for the production of homogeneous GNPs. The most creative step is the development of the two-step desolvation technique which separates the higher molecular weight fractions from the lower molecular weight fractions before the preparation of GNPs.

In the two-step desolvation method, the first desolvation step is performed by addition of anti-solvent to gelatin aqueous solution. When molecules of a solvent with different polarity and hydrogen-bond-forming capacity such as acetone replace some or all of the water molecules, the solute-solvent interactions which determine the solubility of the protein will be strongly affected (Lee, 2011). The higher molecular weight fractions (microgel, δ and ζ fractions, > 700 kDa) which need more water molecules to form an aqueous solution precipitate first, followed by the intermediate molecular weight fractions (ε, γ and β fractions, 125-700 kDa) and last the lower molecular weight fractions (α, sub-α fractions and hydrolysis fragments, < 125 kDa) (Farrugia and Groves, 1999). The separation efficiency of various gelatin molecules, which is the key point to produce homogeneous and ultrafine gelatin particles, depends mainly on the precipitation time. Thus the precipitation time has definitive impact on the particle size, extent of tendency to aggregate as well as the nanoparticles concentration in the final product.

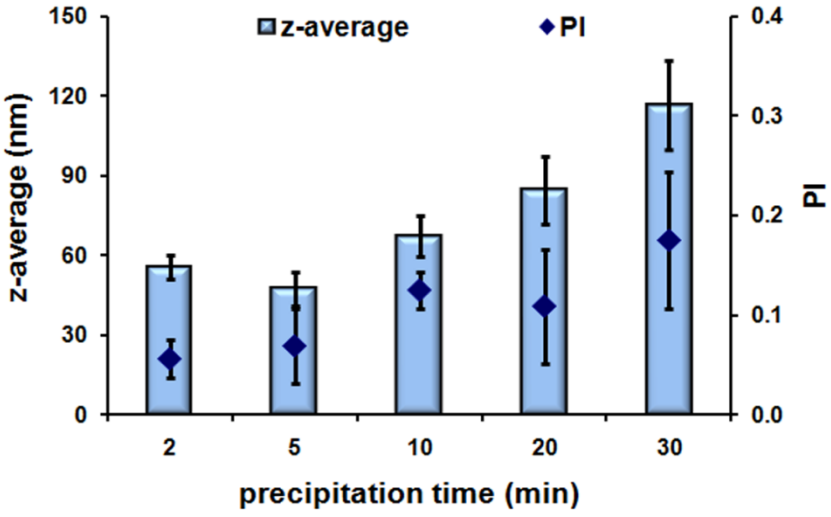

Figure 4-2: Effect of precipitation time on z-average and PI of GNPs. Precipitation times in a range of 2 to 30 minutes were applied at the first desolvation step. Acetone was used as desolvating agent. The gelatin starting concentration was 5% (w/v).

In the experiments, a defined precipitation time from 2 to 30 minutes was used. As shown in Figure 4-2, by increasing precipitation time from 2 to 30 minutes, the mean particle size of GNPs ascended from around 55 nm to about 120 nm and the PI increased from 0.05 to approximately 0.2. When the precipitation time exceeded 10 minutes, flocculation was induced after 12 hours cross-linking. The influence of precipitation time below two minutes has already been explored by Zwiorek (Zwiorek, 2006). Contrary to our experience, the particle size of GNPs produced by the traditional two-step desolvation method was 250 nm utilizing a precipitation time of 20 seconds. This could be attributed to the assumption that the sediment contains both high molecular weight gelatin fractions and parts of low molecular weight fractions in very short time after the addition of acetone. In the following time up to 5 minutes, a redistribution of low molecular weight gelatin fractions could occur from the sediment to the supernatant (mixture of acetone and water). Summarizing the above results, five minutes seems to be the maximum precipitation time to achieve nanoparticles below 100 nm without agglomeration. Only a proper adjusted precipitation time during the first desolvation step can segregate high molecular weight gelatin fractions efficiently for the subsequent preparation of ultrafine GNPs.

4.3.1.3 Effect of temperature on particle size of GNPs

As the third parameter, the temperature at the first desolvation step was investigated. It has been demonstrated that factors like temperature and pH have considerable effect on the molecular-weight profile of gelatin and its precipitation property (Farrugia and Groves, 1999). The helical tropocollagen structure characteristic of higher molecular weight gelatin fractions (microgel and δ fractions) could be denatured due to the disruption of hydrogen bonds under heating. As documented, the percentage content of the microgel gelatin fraction decreased from 30% at 20°C to 0.6% at 80°C (Farrugia and Groves, 1999). Decreased content of higher molecular weight fractions could result in heterogeneous GNPs. Azarmi *et al.* reported that high desolvation temperature may enlarge the GNPs due to the gelling properties of gelatin (Azarmi et al., 2006). To clarify the optimum parameter, the influence of temperature at the first desolvation step on the physical properties of GNPs was studied.

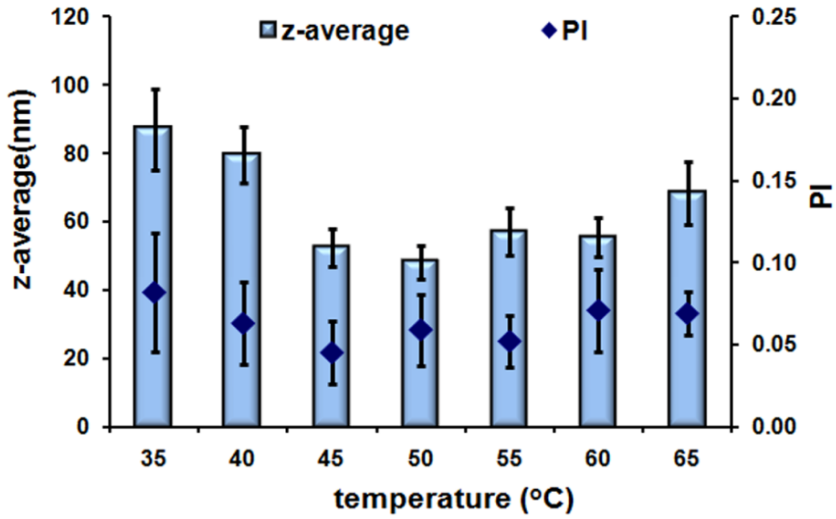

Figure 4-3: Effect of temperature at the first desolvation step on z-average and PI of GNPs. Temperatures in a range of 35 to 65°C were applied at the first desolvation step. The other parameters were kept as optimized (desolvating agent: acetone, gelatin starting concentration: 5% (w/v), precipitation time: 5 minutes).

Figure 4-3 shows the influence of temperature at the first desolvation step on the resulting mean particle size and PI. The smallest and homogeneous particles were achieved at 50°C with a particle size of 55 nm and a PI of 0.062. Increasing the

temperature from 45 to 65°C did not considerably change the particle size. GNPs with particle size of approximately 80 nm could be produced at lower temperatures (35 and 40°C). In terms of dispersivity, all PI values were below 0.1 and no agglomeration or flocculation was observed.

Drug loading of GNPs can be performed during the production process of GNPs via incorporation into the matrix of the particles. As demonstrated by the present results, ultrafine GNPs could be prepared at relatively low temperatures. This feature will contribute to the application of GNPs as carriers for enzymes and peptides, as most proteins from mammals possess an optimum temperature of around 37°C to achieve a maximum biological activity. High temperatures above 55°C will denature most mammalian proteins within one or two hours.

4.3.1.4 Effect of pH on particle size of GNPs

The pH value of the redissolved gelatin solution at the second desolvation step is the fourth important investigated parameter. Gelatin is an amphoteric biopolymer and possesses both positive and negative charges. The pH condition of the media determines the net charge and charge density of gelatin molecules in solution and therefore influences the final properties of GNPs. To investigate the effect of pH on the particle size of GNPs, only the pH was changed while the other parameters were kept constant. In Figure 4-4, the influence of pH at the second desolvation step on the average size and PI of GNPs is shown. The average sizes of nanoparticles at pH 2.0, 2.5 and 3.0 were 53, 56 and 88 nm, respectively. At pH values above 3.5, the average size was strongly increased up to 315 nm. Within the pH range of 2.0-4.0 the PI increased from 0.022 to 0.360 which may indicate persistent widening of the particle size distribution. Since the isoelectric point (IEP) of gelatin type A is between 6 and 9, within the pH region investigated gelatin molecules should possess a positive net charge. These observations could be explained as the consequence of a decrease in net charge on the gelatin molecule in acidic condition, thereby facilitating the intermolecular reactions and co-aggregation. Larger particle size and widened size distribution are in correlation with the decrease of intermolecular electrostatic repulsion forces which could have stabilized *in situ* pre-formed nanoparticles.

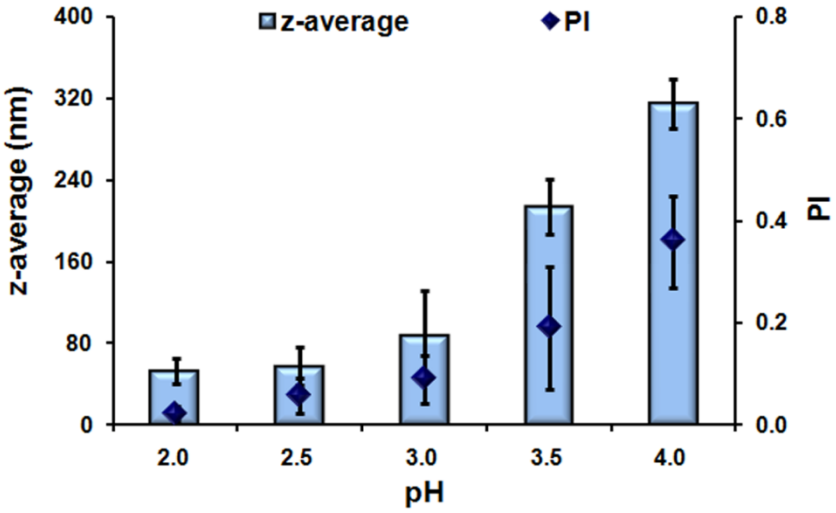

Figure 4-4: Effect of pH of the gelatin solution at the second desolvation step on z-average and PI of GNPs. pH values in a range of 2.0 to 4.0 were investigated. The other parameters were kept as optimized (desolvating agent: acetone, gelatin starting concentration: 5% (w/v), precipitation time in first desolvation step: 5 minutes, temperature at the first desolvation step: 50°C).

Moreover, the pH value of the gelatin solution is also a pivotal factor which dominates the cross-linking reaction between gelatin and glutaraldehyde and consequently influences the final particle size. It is commonly accepted that the cross-linking mechanism of glutaraldehyde is related to the formation of Schiff's bases between ε-amino groups of lysine and the aldehyde groups (Schreiber and Gareis, 2007). However, the reactions may also involve the hydroxyl groups of hydroxylysine and hydroxyproline, leading to the formation of hemiacetals, especially at low pH (Farris et al., 2010). Thus when the second desolvation was performed at lower pH, ultrafine GNPs were obtained due to the enhanced cross-linking reactions which hardened the freshly formed particles.

Furthermore, cross-linking reactions might occur both inside and on the surface of the nanoparticles. Internal cross-linking helps to harden the performed particles whereas covalent interparticle cross-linking may introduce particle agglomeration (Farris et al., 2010). The diversification of cross-linking reactions may assist in the explanation why gelatin based particles prepared at different pH conditions exhibited distinctive particle size.

4.3.1.5 Effect of desolvating agent on particle size and yield of GNPs

Gelatin possesses various hydrophobic and hydrophilic amino acids and the solubility of gelatin in water is due to the formation of hydrogen bonds between hydrophilic amino acids and water molecules. Addition of desolvating agent into the gelatin solution decreases the water molecules surrounding the gelatin chains and consequently reduces the intermolecular hydrogen bonds (Azarmi et al., 2006). All these lead to the shrinkage and rolled-up conformation of gelatin chains. At a certain point the hydration is too low and the loosely packed gelatin chains precipitate as nanoparticles. The following cross-linking step by glutaraldehyde helps to tighten and maintain the performed particle structure.

Different desolvating agents such as alcohols, ketones and inorganic salts in high concentrations have been applied in the production of collagen based nanoparticles. In the present study, the influence of three different desolvating agents (ethanol, acetone and isopropanol), their amounts used in dropwise addition on particle size and yield of GNPs was evaluated. The results are displayed in Table 4-1. The results show that all desolvating agents under evaluation were able to achieve nanoparticulate gelatin desolvation. With acetone, it was possible to produce highly monodispersed GNPs in a sub-100 nm size range between 45 and 58 nm by slight variation of the volume of the desolvating agent. Ethanol and isopropanol could be used for the production of GNPs with particle sizes range from approximately 70-90 nm and 70-140 nm, respectively (Table 4-1). All the PI values obtained by PCS in this study were below 0.15 which stands for a good size uniformity of produced GNPs.

In fact, the influence of acetone and ethanol on particle size has been studied previously in the case of bovine α-lactalbumin (α-LA) and human serum albumin (HSA) nanoparticles (Arroyo-Maya et al., 2012; Storp et al., 2012). In both cases acetone was demonstrated to be more efficient than ethanol in the production of smaller particles. As documented, two possible properties may dominate the performance of a desolvating agent: the polarity and the ability to form hydrogen bonds. Higher polarity of the desolvating agent reduces the hydrophobic interactions and favors the formation of smaller particles (Arroyo-Maya et al., 2012; Storp et al., 2012). The presence of hydrogen bonds facilitates the formation of larger lattices and

consequently larger particle size (Arroyo-Maya et al., 2012; Storp et al., 2012). The results from the present study agree well with the hypothesis, as smaller particle size was obtained by ethanol which possesses higher polarity index than isopropanol. Acetone is a polar aprotic solvent and can only act as a hydrogen bond acceptor, while ethanol and isopropanol are polar protic solvents which can act as both donors and acceptors of hydrogen bonds. Less formation of hydrogen bonds by acetone enables the production of the smallest particles.

Table 4-1. The effects of the type of desolvating agent and the amount used in dropwise addition on particle size and yield of GNPs. The other parameters were kept as optimized (desolvating agent: acetone, gelatin starting concentration: 5% (w/v), precipitation time in first desolvation step: 5 minutes, temperature at the first desolvation step: 50°C, pH at the second desolvation step: 3.0).

Formulation code	Desolvating agent		Z-average (nm)*	PI*	Yield of GNPs*
E-20	ethanol	20 ml	69 ± 7	0.032 ± 0.038	3.3 ± 0.2%
E-25		25 ml	88 ± 5	0.025 ± 0.039	3.8 ± 0.2%
E-30		30 ml	96 ± 4	0.068 ± 0.054	4.6 ± 0.4%
E-35		35 ml	93 ± 7	0.089 ± 0.039	4.7 ± 0.1%
A-20	acetone	20 ml	45 ± 4	0.023 ± 0.012	3.9 ± 0.4%
A-25		25 ml	58 ± 6	0.039 ± 0.005	5.2 ± 0.3%
A-30		30 ml	56 ± 4	0.038 ± 0.019	5.2 ± 0.1%
A-35		35 ml	55 ± 3	0.033 ± 0.011	5.1 ± 0.2%
I-20	isopropanol	20 ml	75 ± 5	0.065 ± 0.054	2.9 ± 0.4%
I-25		25 ml	107 ± 5	0.078 ± 0.052	3.7 ± 0.3%
I-30		30 ml	139 ± 9	0.098 ± 0.076	4.3 ± 0.2%
I-35		35 ml	142 ± 12	0.103 ± 0.035	4.5 ± 0.2%

* Values are expressed as mean ± S.D. (n = 3).

As already described in section 4.2.2.1, desolvating agent was added dropwise after the observation of turbidity or formation of blue ring. And the amount of desolvating agent was controlled between 20 and 35 ml in the present experiments. The particle size of obtained GNPs was found to be amount-dependent on the dropwise added desolvating agent. Increased amount of desolvating agent led to larger particle diameter until a plateau was achieved. Taking ethanol for example, an increase in particle size from 69 to 96 nm was obtained by increasing the amount of ethanol from 20 to 30 ml. However no obvious fluctuation in particle size was noticed when the amount of ethanol was further increased to 35 ml (Table 4-1). Similar behavior was observed in the change of the particle yield. The plateau was achieved by addition of 25 ml acetone, 30 ml of ethanol or isopropanol, respectively. The final yields of the three batches GNPs desolvated by ethanol, acetone and isopropanol were 4.7%, 5.2% and 4.4%, respectively (Figure 4-1). The increase in particle size and yield of GNPs with increased desolvating agent could be attributed to the increase of particle concentration (Gaihre et al., 2008). Along with the gradual addition of a desolvating agent, the number of precipitated particles increases and consequently the interparticle distance decreases. The increasingly crowded condition facilitates the interparticle interactions and/or cross-linking, which results in the formation of larger particles.

4.3.2 Characterization of GNPs

4.3.2.1 GNPs prepared under optimized parameters

After thorough investigation of the effect of different parameters on the characteristics of resulting GNPs, the optimized production parameters are as follows:

1. starting gelatin concentration: 5% (w/v)
2. precipitation time at the first desolvation step: 5 minutes
3. temperature at the first desolvation step: 50°C
4. pH at the second desolvation step: 3.0
5. desolvating agent: acetone 25 ml
6. amount of dropwise added desolvating agent at the second desolvating step: 25 ml

Optimized GNPs showed good reproducibility in production. They possessed a mean particle size of 56 ± 4 nm, a polydispersity index of 0.039 ± 0.018 when analyzed by PCS. GNPs produced under optimized conditions were characterized in detail (formulation A-25 from Table 1).

4.3.2.2 Light microscopy

Light microscopy technique was used for measurement of potential aggregates or large particles in aqueous dispersion. In optimal preparation, the particle size is too small (56 nm) to be observed using this method (Figure 4-5, A). Agglomerations and tremelloid structures can be potentially introduced because of increased pH value or precipitation time which can be clearly detected by light microscopy (Figure 4-5, B and C). As already discussed in section 4.3.1.4, the pH of the gelatin solution at the second desolvation step dominates the cross-linking reaction between gelatin and glutaraldehyde. Increased pH facilitated the intermolecular interaction and resulted in the formation of larger particles or even agglomerations (Figure 4-5, B).

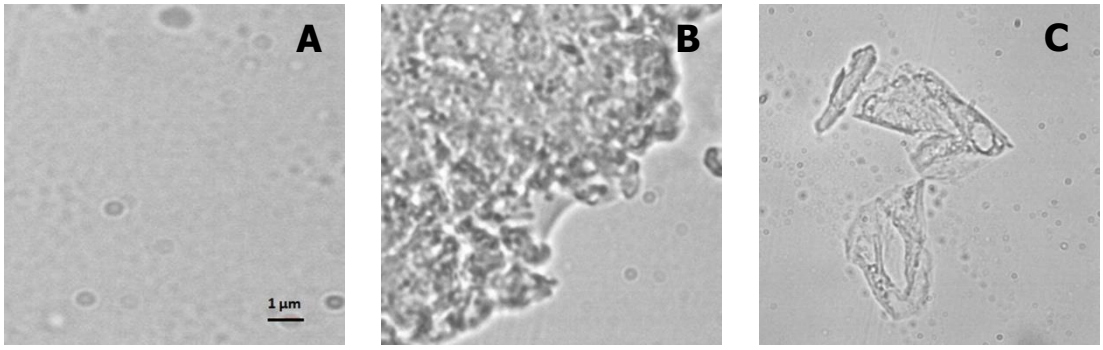

Figure 4-5: Micrographs (magnification 1000×) of GNPs (formulation A-25): A. GNPs prepared under condition of pH value 2.5 (particles were too small to be observed clearly); B. GNPs prepared under condition of pH value 3.5 (visible agglomeration); C. GNPs prepared under condition of precipitation time 10 minutes and after 12 hours cross-linking (tremelloid structures).

Increased precipitation time induced lower molecular weight gelatin fractions (α, sub-α fractions and hydrolysis fragments) in the formulation. After addition of the desolvating agent, these fractions were not able to precipitate as homogeneous

particles due to their weak folding or bending ability, and hence led to insufficient cross-linking by glutaraldehyde. Thus the tremelloid structures were obtained by the sedimentation of lower molecular weight gelatin fractions (Figure 4-5, C).

4.3.2.3 Transmission electron microscopy

Due to the different measuring conditions, PCS and TEM are reported to give different results about particle size and size distribution of polymer based nanoparticles (Ethirajan et al., 2008). PCS measures the hydrodynamic diameter based on the analysis of intensity fluctuations of the light randomly diffused by particles diffusing due to the Brownian motion of the dispersion medium. It shows particle size slightly larger than their real size. TEM generally measures non-dispersed dry nanoparticles and yields smaller diameters than PCS as during the preparation of samples for TEM, air drying and vacuum drying conditions might induce shrinking or collapsing of the particles structure to a different extent. Literature reports have demonstrated the ability of trehalose to maintain morphology and diameter of GNPs during freeze drying and rehydration procedure (Zillies et al., 2008). Hence in the current study trehalose (5% w/w) was applied to stabilize GNPs during TEM measurements.

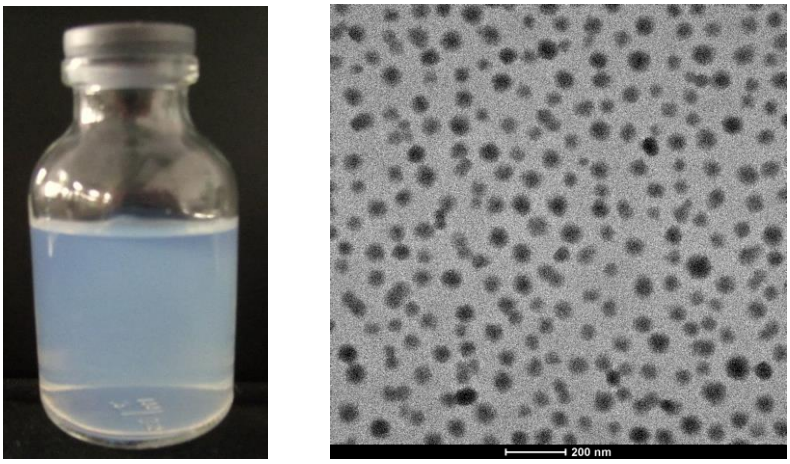

Figure 4-6: Photograph of the GNPs aqueous suspension (formulation A-25, z-average: 58 ± 6, PI: 0.039 ± 0.005): GNPs aqueous suspension had slightly bluish appearance due to Tyndall effect (left). Transmission electron microscopy micrograph of GNPs with trehalose (5% w/w): GNPs were found to be monodispersed (right).

As shown in Figure 4-6, GNPs aqueous suspension had slightly bluish appearance (left) and particles possessed a spherical shape and homogeneous size distribution (right). The average size observed by TEM relatively agreed with the one obtained by PCS, i.e. about 58 nm.

4.3.2.4 Zeta potential analysis

Gelatin type A possesses an IEP between 6 and 9, thus optimized GNPs prepared under acidic condition should possess positive charge. The zeta potential of optimized GNPs was found in rage of approximately +25 to +28 mV in Milli-Q water. This indicates good physical stability of GNPs prepared by the modified two-step desolvation method. As zeta potential values around +30 mV are normally considered sufficient for a good physical stability of nanoparticles due to high electrostatic repulsion between particles (Wissing and Müller, 2002a).

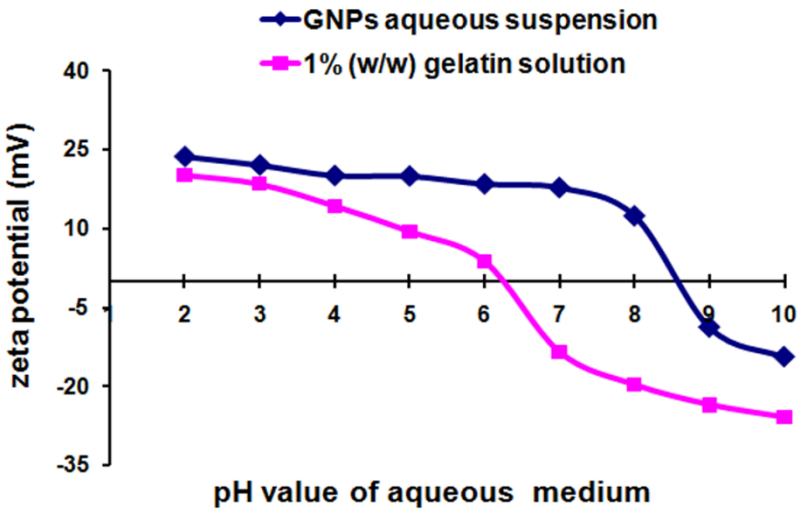

Figure 4-7: Zeta potential of GNPs aqueous suspension (formulation A-25, z-average: 58 ± 6, PI: 0.039 ± 0.005) and gelatin solution (1% w/w) in dependence on the pH value.

Additionally, the effect of the pH value on the zeta potential of GNP suspensions in comparison with the gelatin solution was further explored in a pH range of 2 to 10. The results revealed that the increase in the pH value led to a decrease in the zeta potential of both nanoparticles and gelatin solution and they showed different break-

over points of net charge from positive to negative (Figure 4-7). Produced GNPs contained mainly higher molecular weight gelatin fractions as the lower molecular weight fractions were separated and discarded at the first desolvation step. Thus the proportions of various amino acids with different IEP values were redistributed. Moreover, the cross-linking between aldehyde groups of glutaraldehyde, amino groups of lysine as well as hydroxyl groups of hydroxylysine and hydroxyproline could also influence the final IEP of resulted GNPs (Farris et al., 2010).

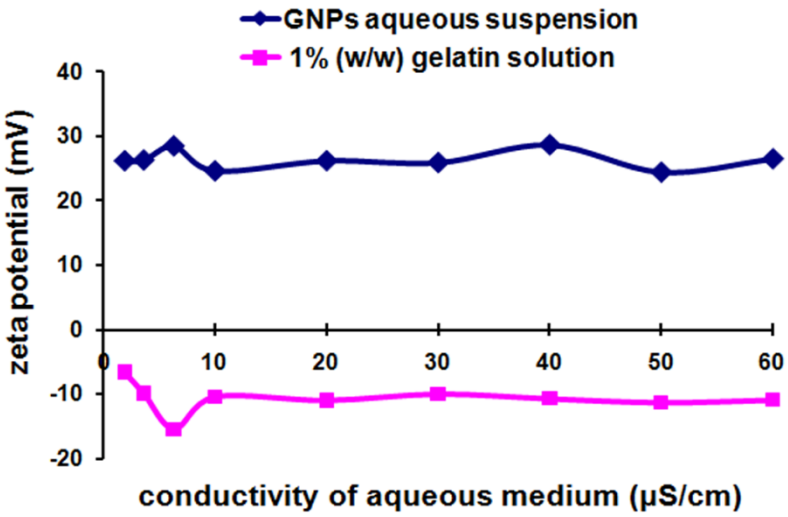

Figure 4-8: Zeta potential of GNPs aqueous suspension (formulation A-25, z-average: 58 ± 6, PI: 0.039 ± 0.005) and gelatin solution (1% w/w) in correspondence to the medium conductivity.

Zeta potential refers to the electric potential at the interface between slipping plane of the dispersed particle and the dispersion medium. The zeta potential can be influenced by several factors, i.e. pH, conductivity (type and/or concentration of salt) and the concentration of an additive (ionic surfactant or polymer). The thickness of the double layer depends upon the concentration of ions in solution and can be calculated from the ionic strength of the medium. The higher the ionic strength, the more compressed the double layer becomes.

In the present experiment, when conductivity adjusted water (1.9-60 µS/cm) was used as dispersion medium for the determination of zeta potential of GNPs, only slight fluctuations in zeta potential were observed (Figure 4-8). As for 1% gelatin solution,

the value of the zeta potential reached a platform when the conductivity of the medium increased to 10 µS/cm. The zeta potential of GNPs was about +25 mV, while 1% gelatin solution showed a zeta potential of approximately -10 mV, which was consistent with the former results (Figure 4-8). In low conductivity media, there is no influence of the electrolyte concentration on the physical stability.

4.3.2.5 Physical compatibility of GNPs with different gelling agents

As a next step for transferring the GNPs in applicable dermal dosage forms, the GNPs were incorporated in various gels for the aim of dermal application. After incorporation into different gels the particle size and polydispersity index of GNPs remained stable over three months as shown in Figure 4-9. This might be attributed to the firmly package of GNPs through cross-linking and the high viscosity in gels which hinders diffusion and subsequent agglomeration.

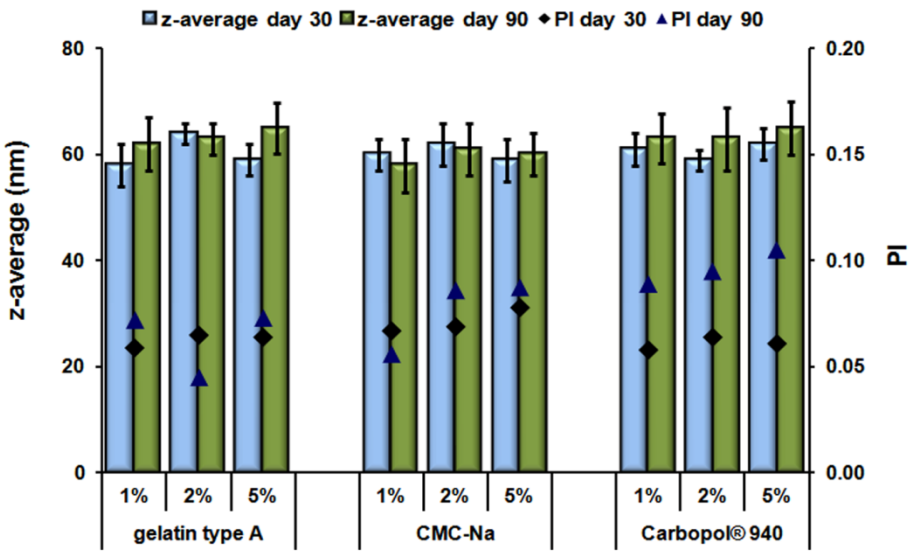

Figure 4-9: Effect of different viscosity enhancers on z-average and PI of GNPs (formulation A-25, z-average: 58 ± 6, PI: 0.039 ± 0.005). Three different gelling agents (gelatin type A, CMC-Na and Carbopol® 940) were applied in concentrations of 1%, 2% and 5%.

4.3.3 Long term stability study

Long term stability test was carried out for optimized GNPs at three different temperatures (4°C, room temperature (RT) and 40°C) for two years. As gelatin is susceptible to microbial attack, addition of preservatives during production or in the final dermal formulations like gels or creams is essential. The compatibility of different preservatives like Euxyl® PE 9010, Hydrolite®-5 and Thiomersal with GNPs was investigated in this study. Each preservative was used in a concentration specified in the literature.

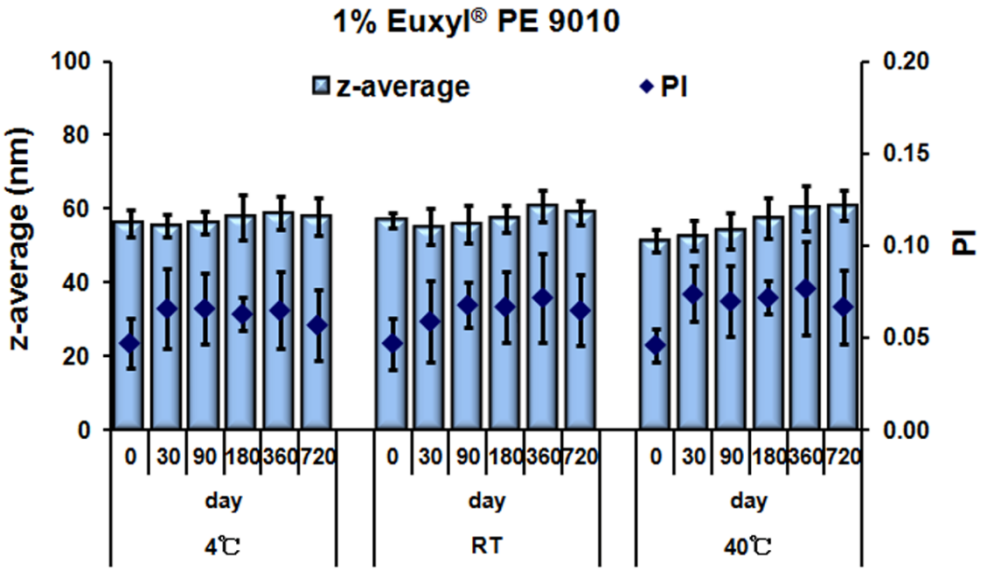

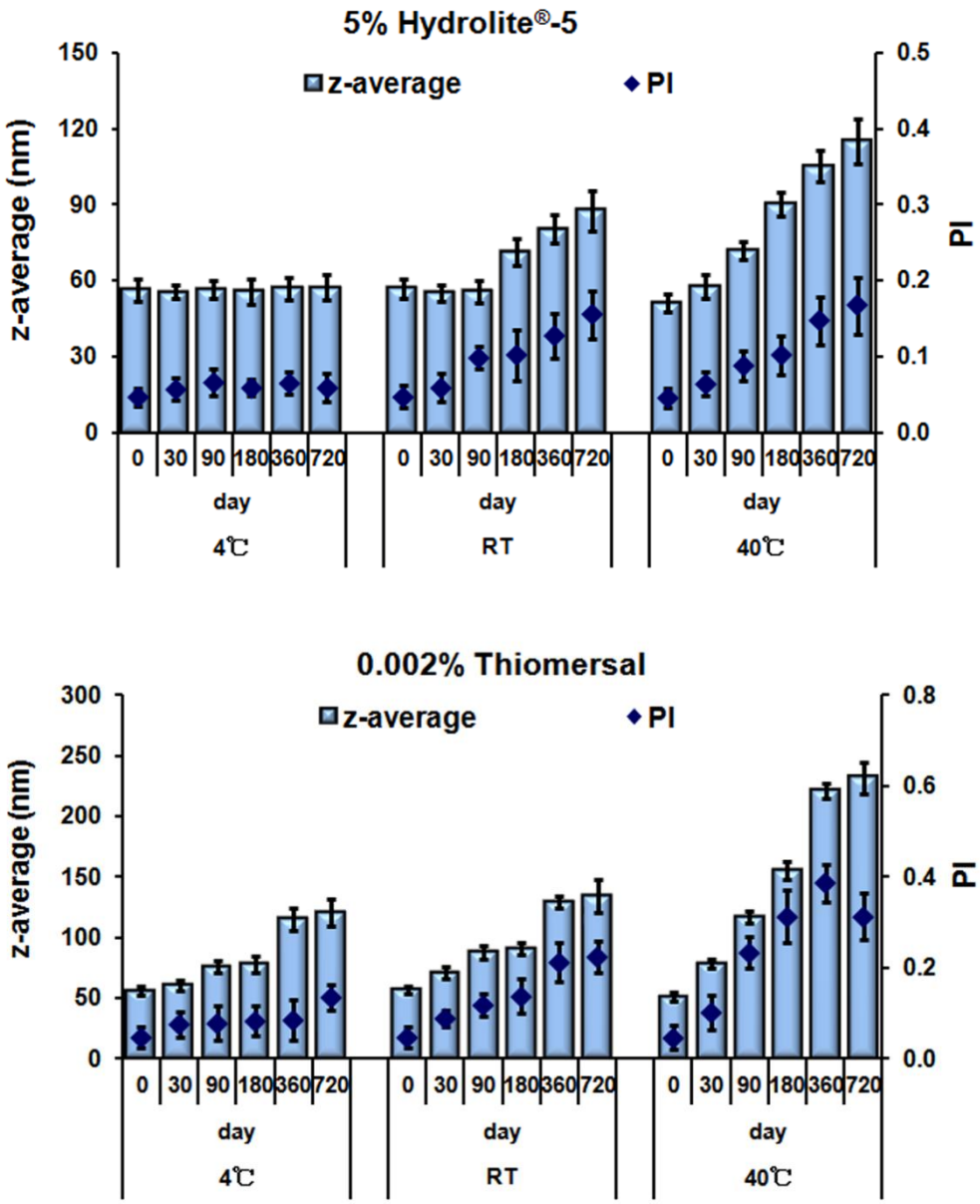

Figure 4-10: Particle size analysis of preserved GNPs (formulation A-25, z-average: 58 ± 6, PI: 0.039 ± 0.005) at different temperatures: 4°C, room temperature (RT) and 40°C over a period of two years. GNPs were preserved with 1% (w/w) Euxyl® PE 9010 (previous page), 5% (w/w) Hydrolite®-5 (middle) and 0.002% (w/w) Thiomersal (above).

Figure 4-10 shows the results of z-average and PI analysis at three different temperatures in the presence of three preservatives during two years storage. Nanoparticles preserved with 1% (w/w) Euxyl® PE 9010 showed the best stability with stable particle size and negligible increase of PI at all temperatures. In the

presence of Hydrolite®-5, mean particles size and PI of GNPs were stable during storage at 4°C. However, at room temperature and 40°C, 5% (w/w) Hydrolite®-5 preserved GNPs showed increases in particle size to varying degrees. Strong increase in z-average and PI was noticed for 0.002% (w/w) Thiomersal preserved GNPs at all three temperatures. At 40°C, particle size was significantly increased from around 60 nm to approximately 250 nm and PI was increased from 0.07 to approximately 0.4.

The activity of a preservative depends on the concentration, the adsorption affinity onto particle surfaces and the hydrophilic/lipophilic properties. An optimum preservative should possess certain hydrophilicity to remain in the water phase where the bacteria are present as well as certain lipophilicity to interact with the lipophilic membranes of bacteria (Shaal, 2011). Thiomersal is ethylmercurithiosalicylic acid sodium salt, and the salicylic acid residues are able to attach onto the positive charged GNPs surfaces when dissolved in water. Thus the surface charge of GNPs decreases to +14 mV (Table 4-2) which leads to weakened electronic repulsion and impaired physical stability. Hydrolite®-5 is pentylene glycol, relatively hydrophilic and therefore having some affinity to the GNPs surface. Thus the stability of GNPs could be decreased due to the interactions with preservative molecules especially when undergoes stress condition (40°C). Euxyl® PE 9010 contains 90% of phenoxyethanol and 10% of ethylhexylglycerin. Due to the lipophilic benzene ring in phenoxyethanol the interaction with the hydrophilic GNPs surface is supposed to be limited, making this preservative the best one for GNPs.

Table 4-2. Zeta potential values of preserved GNPs suspensions (formulation A-25, z-average: 58 ±6, PI: 0.039 ±0.005) in conductivity adjusted water (50 µS/cm).

GNPs formulations	Zeta potential (average ±S.D.) in mV
unpreserved GNPs suspension	+25 ±4
GNPs preserved with 1% Euxyl® PE 9010	+27 ±5
GNPs preserved with 5% Hydrolite®-5	+19 ±3
GNPs preserved with 0.002% Thiomersal	+14 ±3

The deduction mentioned above can be well supported by the results of zeta potential analysis (Table 4-2). Unpreserved and Euxyl® PE 9010 preserved GNPs possessed zeta potentials of +25 mV and +27 mV. Addition of Hydrolite®-5 and Thiomersal decreased the zeta potential values to +19 mV and +14 mV due to the adsorption of preservative molecules onto the particle surface.

4.4 Conclusion

GNPs with mean diameter in the range of 50 to 100 nm were successfully prepared using modified two-step desolvation method. Compared with traditional desolvation technique, the modified two-step desolvation method enabled the production of GNPs below 100 nm with narrow size distribution and excellent stability. After intensive study of six crucial parameters of the modified two-step desolvation method, it could be concluded that, gelatin starting concentration, precipitation time and pH value were the most crucial parameters in determining the synthesis of ultra small GNPs. GNPs produced by modified two-step desolvation technique might provide a promising carrier system for both pharmaceutical and cosmetic applications. The preparation temperature can also be lowered to 40°C for temperature sensitive actives. The ultra small size of particles, the collagen derived structure and high physiological tolerance of gelatin can further contribute to the effective dermal delivery of actives.

5 Characterization and loading with lysozyme as model enzyme

5.1 Introduction

During the past few decades nanoparticulate colloidal systems based on gelatin have been extensively investigated as carriers for various hydrophilic molecules like genes, peptides, proteins and nucleic acids (Elzoghby, 2013b; Liang et al., 2006b; Zwiorek et al., 2005). Numerous investigations have confirmed the attractive advantages of gelatin nanoparticles (GNPs) regarding controllable drug release, modifiable biodistribution and sub-cellular particle size (Kuo et al., 2011a; Nezhadi et al., 2009b; Rajan and Raj, 2013). Moreover, the application of proteins and peptides in medicine is partly limited due to their rapid degradation by proteolytic enzymes in the gastrointestinal tract, thus they need to be administered through parenteral routes. However, limited report is available till now for dermal application of such actives by ways of GNPs. For dermal delivery systems, the stratum corneum represents the first main physical barrier against the percutaneous penetration of pathogens, chemicals as well as nanoparticulate carriers. It has been reported that macromolecules, nanomaterials and small particles might be able to permeate into epidermal layers of skin through aqua pores or intercellular space with dimensions varied from 0.4 to 100 nm (Cevc, 2004a; Charalambopoulou GC, 2000; Vogt et al., 2006b). Therefore, small particles possess extremely high potential for increasing skin penetration of particulate carrier systems. However, the particle size of GNPs produced by the classical two-step desolvation method reported so far mostly exceeded 250 nm (Coester et al., 2000b; Narayanan et al., 2013).

To load proteins into GNPs, two general methods can be performed: one is by incorporating the drug at the time of particle preparation (in step of particle formation) or secondly by incubating the drug in the freshly prepared particle suspension to allow surface adsorption (Nahar et al., 2008; Vandervoort and Ludwig, 2004). It is thus evident that a large amount of drug can be incorporated into the core of particles by the first method while limited drug is adsorbed onto the surface of particles by the second method. Moreover, the quantitative differentiation between the amounts of surface adsorbed and matrix incorporated drug is of immense benefit to achieve a deeper understanding of loading behaviors and release mechanisms of proteins from various polymer based nanoparticles. As to the adsorption process, both electrostatic and van der Waals interactions could be governing factors for the adsorption of proteins (Gady et al., 1996; Roth and Lenhoff, 1995). However, the fundamental interactions between protein molecules and GNPs have not been thoroughly

evaluated yet. The factors that are crucial to protein adsorption efficiency and the protection of biological activity have not been distinguished.

Lysozyme (N-acetylmuramide glycanhydrolase), also known as muramidase, is one of the commonly used model proteins to investigate the effects of protein formulation, preparation and storage on activity and function (Cal et al., 2008; Peng et al., 2004). It is a basic protein with a weight of 14.4 kDa and a high isoelectric point between 10.5 and 11.0. In this study, lysozyme was used as the model drug because of its easy characterization and straightforward evaluation of the biological activity.

In the previous studies, ultrafine GNPs with particle size approximately 50 nm had been successfully and reproducibly prepared by a modified two-step desolvation technique. The influence of various preparation parameters like pH, precipitation time, volume of acetone and temperature had been intensively investigated and optimized (Zhai et al., 2011). The aim of the present study was to develop and compare ultrafine with traditional GNPs as dermal application carriers for proteins using lysozyme as a model drug. Ultrafine GNPs were prepared by a modified two-step desolvation method, while traditional GNPs were produced by the classical two-step desolvation method. Drug loading was performed at different preparation steps of particles and achieved via surface adsorption or matrix incorporation. Loaded ultrafine and traditional GNPs were characterized and compared in terms of particle size, zeta potential, loading behavior, *in vitro* drug release, stability and biological activity.

5.2 Materials

Gelatin type A, Bloom 175, derived from porcine skin was obtained from Naumann Gelatin and Leim GmbH (Memmingen, Germany). Hen egg lysozyme was a gift from Handary (Brussels, Belgium). Acetone (HPLC grade) and glutaraldehyde aqueous solution (25% w/w, grade I) were purchased from VWR International GmbH (Darmstadt, Germany), hydrochloric acid (37% w/w) from Merck (Darmstadt, Germany). Sodium chloride solution (NaCl, 0.9% w/w) was obtained from B. Braun Melsungen AG (Melsungen, Germany). Freshly obtained double distilled ultra pure water (Milli-Q, Millipore GmbH, Germany) was used as dispersion medium. All the other reagents and chemicals used in this study were of analytical grade and were used as received.

5.3 Methods

5.3.1 Preparation of ultrafine GNPs

Ultrafine GNPs with particle size approximately 50 nm were produced by a modified two-step desolvation technique as reported previously (Zhai et al., 2011). In brief, 1.25 g of gelatin was dissolved in 25 ml Milli-Q water at 50°C under magnetic stirring (300 rpm). 25 ml of acetone was added to the gelatin solution at 50°C for rapid desolvation and sedimentation of high molecular weight gelatin. The obtained turbid supernatant was discarded after 5 minutes and another 3 ml of water was applied to remove traces of low molecular weight fractions on the surface of the sediment by slightly shaking (the first desolvation step). The sediment was redissolved in 25 ml Milli-Q water and the pH of the gelatin solution was adjusted to 3.0 using hydrochloric acid (37% w/w). Then the gelatin solution was desolvated again by direct addition of 50 ml acetone followed by dropwise addition of another 25 ml acetone (the second desolvation step). Glutaraldehyde solution (800 µl, 8% w/w) was added as a cross-linking agent. After stirring for 12 hours, the particles were purified by centrifugation and redispersed in 50 ml of Milli-Q water. Possible remained acetone was evaporated by using a Büchi RE-121 Rotavapor (Büchi Laboratoriums-Technik AG, CH-9230 Flawyl/Schweiz, Switzerland).

5.3.2 Preparation of traditional GNPs

Traditional GNPs with particle sizes between 250 and 300 nm were produced by the classical two-step desolvation method (Coester et al., 2000b). Briefly, Gelatin type A (1.25 g) from porcine skin was dissolved in 25 ml Milli-Q water under heating. To achieve the rapid desolvation of gelatin, 25 ml of acetone was added to this solution (the first desolvation step). The supernatant was discarded when hydrogel-like sediment was observed by eyes (approx. 20 minutes) and the remaining sediment was redissolved in 25 ml of water. The pH of the redissolved gelatin solution was adjusted to 2.5 using hydrochloric acid (37% w/w) and was then desolvated again by addition of 40 ml acetone (the second desolvation step, in contrast to addition of 50 ml + 25 ml acetone for ultrafine GNPs). At the end, 0.5 ml glutaraldehyde (8% w/w) was added to crosslink the particles. The purification and evaporation steps were followed as described in section 5.3.1.

5.3.3 Drug loading experiments

Figure 5-1 illustrates detailed the two-step desolvation process. To achieve drug loading by matrix incorporation or surface adsorption, lysozyme loading was performed in three different ways, i.e. after the first step desolvation, during the second step desolvation and after the purification of GNPs (Figure 5-1, D, F and H).

Method 1: Lysozyme was added to the formulation after the first desolvation step (Figure 5-1, D). The sediment was redissolved in 25 ml water together with 100 mg of lysozyme.

Method 2: Lysozyme was added to the formulation during the second desolvation step (Figure 5-1, F). 100 mg of lysozyme was dissolved in the pH adjusted gelatin solution.

Method 3: Lysozyme was loaded after the purification of performed GNPs (Figure 5-1, H). Lysozyme solution (2 mg/ml, 50 ml) was incubated with the purified GNPs aqueous suspension (50 ml) for 45 min at 40°C under magnetic stirring (500 rpm) to allow surface adsorption.

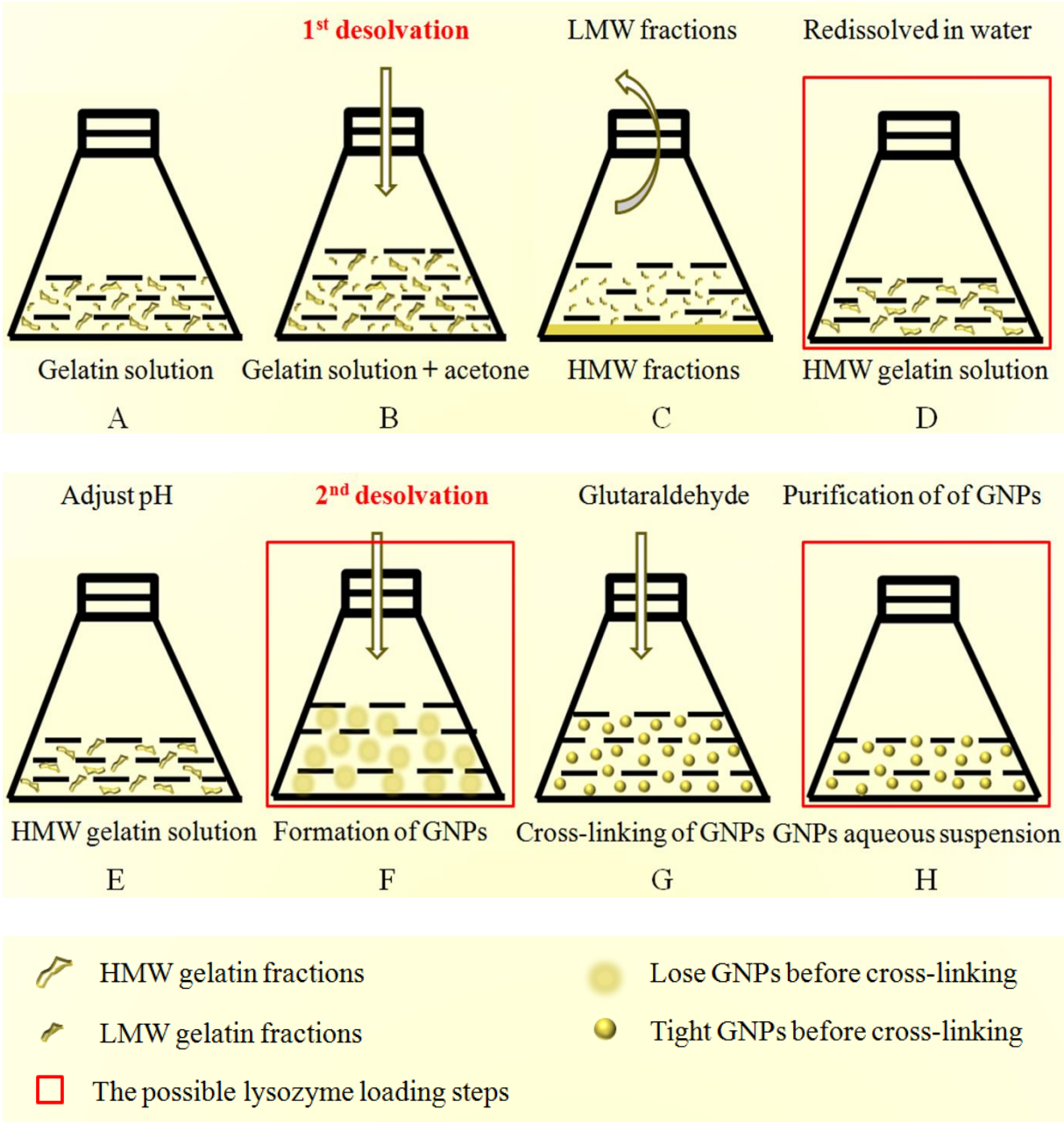

Figure 5-1: Illustration of the two-step desolvation technique applied for the production of GNPs and the possible drug loading steps. The first desolvation was performed for the separation of HMW gelatin fractions (B). The second desolvation was performed for the formation of GNPs (F). Lysozyme loading was performed in three different ways: after the first step desolvation (D), during the second step desolvation (F) and after the purification of GNPs (H). (HMW: high molecular weight; LMW: low molecular weight).

5.3.4 Characterization of GNPs

5.3.4.1 Yield of GNPs

About one milliliter of the freshly prepared GNPs aqueous suspension was dropped in an aluminum sample pan and was dried in the oven at 60°C for 3 hours until a constant weight was obtained. The particle yield was calculated using equation (1).

$$\text{GNPs yield (\%, w/w)} = \frac{\text{amount of recovered GNPs}}{\text{total amount of formulation}} \times 100\% \qquad (1)$$

5.3.4.2 Size analysis

The mean particle size (z-average) and polydispersity index (PI) of various developed GNPs were determined by photon correlation spectroscopy (PCS) using a Zetasizer Nano ZS (Malvern Instruments, UK). For size determination, samples were diluted fivefold with Milli-Q water and measured in triplicate. All measurements were carried out at 25°C.

Laser diffraction (LD, static light scattering) was performed by using a Mastersizer 2000 (Malvern Instruments, UK). The volume weighted diameters *d(v)*50%, *d(v)*90%, *d(v)*95% and *d(v)*99% were used as characterization parameters. All parameters were analyzed by using the Mie theory with 1.59 as the real refractive index and 0.01 for the imaginary refractive index. The real refractive index was determined by using an Abbe Refractometer (Carl Zeiss Microscopy GmbH, Germany).

5.3.4.3 Zeta potential

The zeta potential reflects the net electrical charge on the particle surface and indicates the physical stability of colloidal systems. The zeta potential was analyzed by using a Zetasizer Nano ZS (Malvern Instruments, UK) in conductivity adjusted Milli-Q water (50 µS/cm) using sodium chloride solution (0.9%, w/v) as described by Müller (Müller, 1996). All samples were diluted tenfold and measured in triplicate.

5.3.4.4 Determination of lysozyme loading

The drug loading efficiency (DLE) was calculated by the difference between the total amount used in the formulation and the amount of free drug (equation 2). The amount of free lysozyme in the formulation was determined spectrophotometrically (UV-1700, Pharma Spec, Shimadzu Deutschland GmbH, Germany) at 280 nm in the clear supernatant obtained by separation of GNPs using ultracentrifuge at 50,000 g for 3 hours (25°C, Optima™ MAX-XP Ultracentrifuge, Beckman Coulter, USA). The loading capacity of GNPs was calculated using equation (3).

$$\text{DLE (\%, w/w)} = \frac{\text{Amount of drug used in formulation - Amount of free drug}}{\text{Amount of drug used in formulation}} \times 100\% \qquad (2)$$

$$\text{Loading capacity of GNPs (w/w, mg/g)} = \frac{\text{Amount of lysozyme loaded in GNPs}}{\text{Amount of recovered GNPs}} \qquad (3)$$

5.3.4.5 Recovery rate of lysozyme from GNPs

In order to verify the influence of particle preparation process on the stability and activity of lysozyme, the recovery rate of lysozyme extracted from GNPs was also detected. In brief, 10 ml of lysozyme loaded nanoparticle suspension was concentrated by removing water using a rotary evaporator until 2 ml of the dispersion was left. The concentrated suspension of GNPs was subjected to ultracentrifugation as described in section 5.3.4.4. The recovered sediment was redispersed in pH adjusted Milli-Q water (pH 5.5) and shaken for 2 hours to dissolve any lysozyme associated to the surface of the particles and further subjected to ultracentrifugation. The resulted final supernatant was then analyzed to determine the amount of lysozyme adsorbed onto the surface of the GNPs. The final sediment was dispersed in 2 ml of trypsin solution (0.5 mg/ml) under stirring at 500 rpm until a complete digestion of the GNPs and release of the matrix incorporated lysozyme was achieved.

Concentration of extracted lysozyme was determined by using a validated high performance liquid chromatography (HPLC). The chromatographic system was equipped with KromaSystem 2000 (Kontron Instrument) and a UV detector operated at 250 nm. A Eurospher, 100-5 C18 (5 μm, 250×4.6 mm) column was used. Acetonitrile, water and

trifluoroacetic acid in a ratio of 48:48:2 was used as a mobile phase. The HPLC measurement was performed at a flow rate of 1 ml/min at 25°C.

The recovery rate of lysozyme of GNPs was calculated according to the following equations (equations 4, 5 and 6). The possible degradation of lysozyme during the production process could be estimated by the recovery rate as well as the chromatogram obtained by HPLC.

$$\text{Amount}_{\text{theoretical lysozyme}} = \text{Amount}_{\text{total applied lysozyme}} - \text{Amount}_{\text{free lysozyme}} \quad (4)$$

$$\text{Amount}_{\text{recovered lysozyme}} = \text{Amount}_{\text{surface adsorbed lysozyme}} + \text{Amount}_{\text{incorporated lysozyme}} \quad (5)$$

$$\text{Recovery rate (\%, w/w)} = \frac{\text{Theoretical amount of loaded lysozyme}}{\text{Recovered amount of loaded lysozyme}} \times 100\% \quad (6)$$

5.3.4.6 In vitro release study

In vitro lysozyme release study was performed by using static Franz diffusion cells. Cellulose acetate membrane filters (0.01 µm) were used as barrier membranes and were mounted on the Franz diffusion cells with a surface area of 0.64 cm^2. A total amount of 300 µl of lysozyme loaded GNPs aqueous suspension was placed in the donor compartment and the receptor compartment was filled with 6 ml pH adjusted Milli-Q water (pH 5.5). The medium was stirred by magnetic stirrer at 800 rpm to minimize the differentiation of concentration in the acceptor medium. During the experiments, the temperature of the medium was controlled at 32 ± 1°C by a water jacket to mimic the human skin temperature. Samples of 500 µl were withdrawn at fixed time intervals over 48 hours, being replaced with the same volume of freshly prepared acceptor medium. The *in vitro* release study was performed in triplicate for each formulation under the same conditions. The collected samples were then spectrophotometrically analyzed at 280 nm.

5.3.4.7 Physical and chemical stability test

To evaluate the physical stability of unloaded and lysozyme loaded GNPs, a short term stability test was carried out. On the day of production (day 0), GNPs aqueous suspension was divided into three vials and stored at three different temperatures (4°C, room temperature (RT) and 40°C). Stored samples were analyzed for particle size and zeta potential on days 0, 30 and 90. The amounts of lysozyme recovered from GNPs were also determined at settled time intervals. A control study by lysozyme solution was simultaneously performed.

5.4 Results and discussion

5.4.1 Preparation of ultrafine and traditional GNPs

The optimized production conditions of classical two-step desolvation technique and modified two-step desolvation technique resulted in the formulation of unloaded traditional GNPs (UTG) of 250 nm and unloaded ultrafine GNPs (UUG) of 50 nm, respectively. The controllable parameters included optimized gelatin concentration, segregation of extremely high molecular weight gelatin fraction, precipitation time and pH value.

The lysozyme loading to GNPs at the first or second desolvation step, which means prior to the formation of particles, drug loading were mainly achieved by matrix incorporation. When drug loading was done after the formation and cross-linking of particles, lysozyme was expected to be loaded by surface adsorption. These deductions are made since lysozyme, being an amphoteric enzyme, is reported to contain various ionizable groups by virtue of the presence of amino acid residues which are capable of attaching to a positively charged polyelectrolyte and acidic functionalities which are capable of attaching to a negatively charged polyelectrolyte via electrostatic interactions (Menendez-Arias et al., 1985). Three types of lysozyme loaded ultrafine GNPs (LUG) were produced and labeled according to the step of drug addition: LUG 1 (addition of drug was performed after the first desolvation step), LUG 2 (addition of drug was performed at the second desolvation step) and LUG 3 (addition of drug was performed after the preparation of GNPs). Similarly, we got another three types of lysozyme loaded traditional GNPs: LTG 1, LTG 2 and LTG 3. The preparative variables and batch codes are shown in Table 5-1. In the following sections the effect of different loading methods on the characteristics of GNPs are discussed in detail.

Table 5-1: List of the type of drug loading methods and the steps at which drug loading was performed for ultrafine and traditional GNPs prepared by two step desolvation methods. Lysozyme was loaded by two methods like matrix incorporation or surface adsorption.

GNPs	Drug loading step	Type of drug loading	Batch No.
unloaded ultrafine GNPs	---	---	UUG
lysozyme loaded ultrafine GNPs	first desolvation step	matrix incorporation	LUG 1
	second desolvation step	matrix incorporation	LUG 2
	after GNPs preparation	surface adsorption	LUG 3
unloaded traditional GNPs	---	---	UTG
lysozyme loaded traditional GNPs	first desolvation step	matrix incorporation	LTG 1
	second desolvation step	matrix incorporation	LTG 2
	after GNPs preparation	surface adsorption	LTG 3

5.4.2 Characterization of ultrafine and traditional GNPs

5.4.2.1 Size analysis

Particle size measurement results are presented in Figure 5-2. PCS diameters of ultrafine GNPs were in most cases remarkably lower than that of traditional GNP. All batches of lysozyme loaded GNPs showed increase of z-average and PI to different extends compared with unloaded ones. The loading method of lysozyme affected the PCS diameters of varied GNPs as well. The average particle size of LUG 1 was found to be 209 nm which was almost four times higher than that of UUG (56 nm). This might be attributed to the formation of some small clumps between lysozyme molecules and high molecular weight gelatin fractions. On the other hand, the addition of lysozyme at the first desolvation step decreased the pH value of redissolved gelatin solution which in turn reduced the necessary amount of hydrochloric acid in the pH adjustment at the second desolvation step. During the formation of particles, part of lysozyme was incorporated into GNPs, resulted in higher pH value of the medium. This speculation can be verified by the fact that freshly prepared LUG 1 aqueous

suspension possessed a pH of 3.5 while UUG possessed a pH of 2.7. Since the IEP of gelatin type A is between 6 and 9, decreased net charge in acidic condition leads to a weaker positive net charge of gelatin molecule, thereby facilitates the intermolecular reactions or co-aggregation.

Addition of lysozyme at the second desolvation step resulted in increased particle size of LUG 2 to 74 nm. This could be due to the matrix incorporation of lysozyme molecules. The slight increase in particle size of LUG 3 could be attributed to the anchoring of the lysozyme molecules at the surface of the nanoparticles through electrostatic interaction and Schiff's base formation. A very low PI of less than 0.1 was obtained for all ultrafine formulations, indicating a narrow size distribution of the nanoparticles and consequently homogeneous suspension. Traditional GNPs possessed mean particle sizes range from 245 to 292 nm. Different from the formulation LUG 1, comparatively lower drug loading of LTG 1 ensured the regular sedimentation, particle formation and consequently slight increase of particle size compared to UTG.

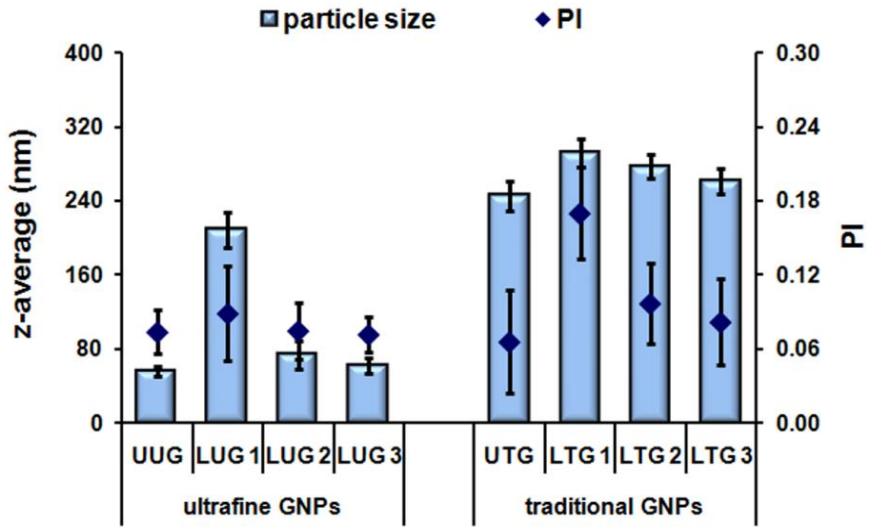

Figure 5-2: Comparative mean particle sizes (z-average) and polydispersity indices (PI) of prepared unloaded ultrafine and traditional GNPs (UUG and UTG) and lysozyme loaded GNPs (LUG 1, 2, 3 and LTG 1, 2, 3) on the day of production based on different drug loading methods 1 to 3.

The LD data of developed gelatin formulations were evaluated using the diameter *d(v)*50%, *d(v)*90%, *d(v)*95% and *d(v)*99% which means that either 50%, 90%, 95% or 99% (volume

distribution) of the measured particles are below the given size (Figure 5-3). A slight increase in mean particle size of LUG 2 and LUG 3 after drug loading was revealed by PCS measurement while the *d(v)*50% and *d(v)*90% of UUG, LUG 2 and LUG 3 obtained by LD showed no notable difference. Obviously, drug incorporation affected mainly the size of the bulk population (detected by PCS measurements being highly sensitive in the nano range). A few large particles might have also been found, but were not detected by LD due to its lower sensitivity.

Less sensitivity of LD in detecting slight changes in the particle size of ultrafine nanoparticles can be explained by the different measuring ranges, being approximately 20 nm to 2,000 µm for LD (very broad range, less sensitive) but 0.6 nm to 6 µm for PCS (small range, higher sensitivity in range of nanometer and lower micrometer range). The LD results of traditional formulations were in agreement with the previous PCS data. The diameter *d(v)*99% is a parameter very sensitive towards large particles. The *d(v)*99% of GNPs when lysozyme loading was performed at the first desolvation step (LUG 1 and LTG 1) was approximately 600 nm. As aforementioned, the possible explanation for the presence of large particles can be attributed to the increased pH value during the formation and cross-linking of particles as pH dominates the cross-linking reaction between gelatin chains and glutaraldehyde and consequently the final particle size. Internal spheres cross-linking reaction leads to hardening of particles and reduction of particle size, while when it occurs on the surface of the nanoparticles covalent intermolecular reaction may induce particle aggregation.

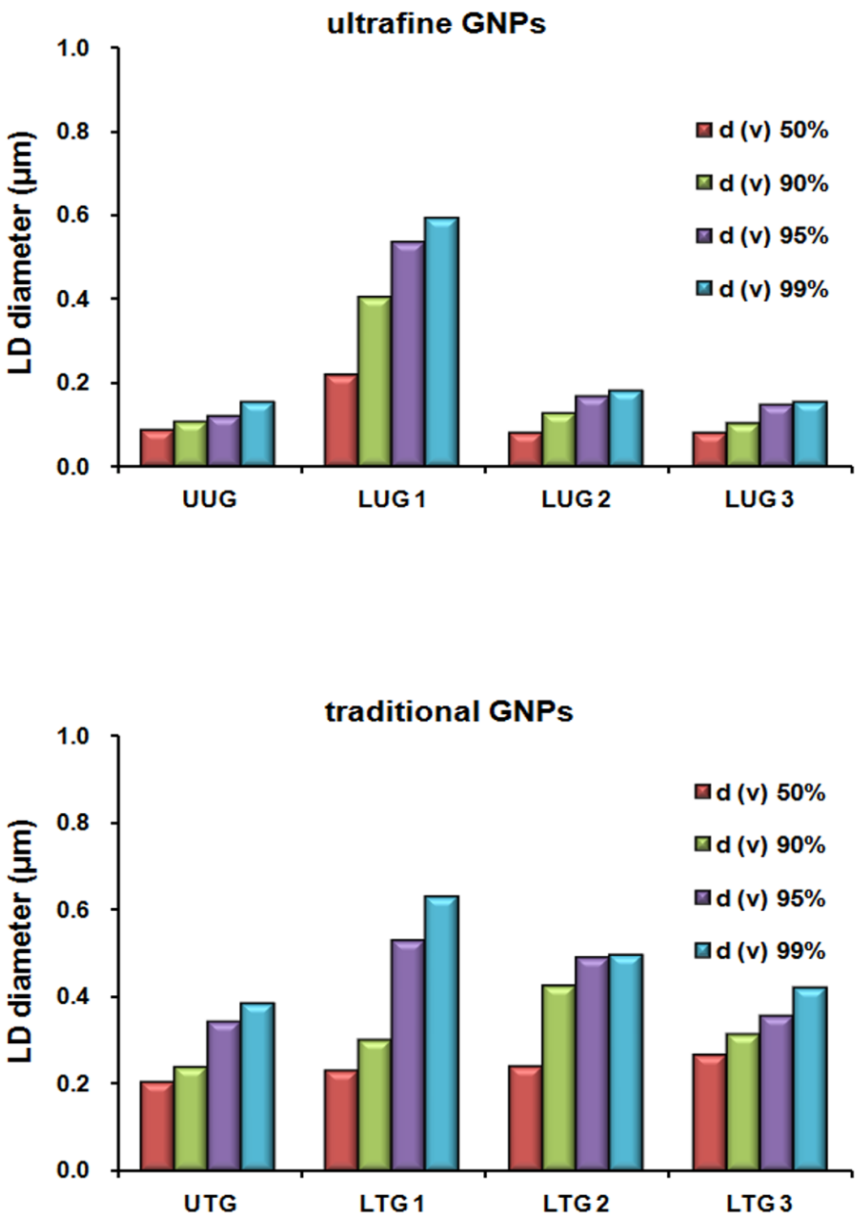

Figure 5-3: LD diameters *d(v)*50%, *d(v)*90%, *d(v)*95% and *d(v)*99% of prepared unloaded ultrafine and traditional GNPs (UUG and UTG) and lysozyme loaded GNPs (LUG 1, 2, 3 and LTG 1, 2, 3) on the day of production based on the type of drug loading.

5.4.2.2 Zeta potential

To investigate the surface charge of GNPs, the zeta potential was measured in Milli-Q water adjusted to a conductivity of 50 µS/cm. According to the DLVO theory (Derjaguin and Landau, Verwey and Overbeek theory) the physical stability of a dispersed system depends on the electrostatic repulsion energy of particles which increases with increased surface charge

and the thickness of the diffusion layer (Kobierski et al., 2011). The zeta potential values of all types of GNPs were found to be above 25 mV as shown in Figure 5-4.

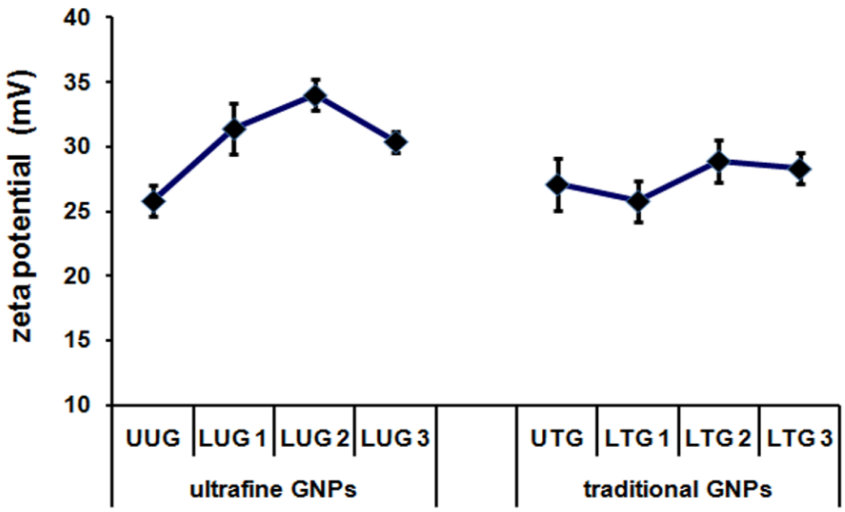

Figure 5-4: Zeta potential of unloaded GNPs (UUG and UTG) and lysozyme loaded GNPs (LUG 1, 2, 3 and LTG 1, 2, 3) in conductivity adjusted water (50 µS/cm) on the day of production. Ultrafine GNPs after drug loading showed slightly higher zeta potential values compared with traditional GNPs.

The positive charge could be explained by the predominance of NH_3^+ groups on the surface of type A GNPs acquired during the formation of particles in acidic pH. The loading of lysozyme led to an increase in net positive charge from 25 mV to approximately 35 mV for the ultrafine GNPs. In contrast only slight fluctuations of zeta potential were observed for the traditional GNPs which may be due to the comparatively lower drug loading. This observation was expected since the amphoteric peptide lysozyme, after anchoring at the surface of GNPs, introduced higher density of NH_3^+ groups on the surface of particles in acidic conditions. Furthermore, the increase in positive zeta potential as lysozyme was loaded into the GNPs is a definite indication that a considerable fraction of lysozyme was attached onto the surface of the particles which will be further confirmed later in the depiction of lysozyme loading behavior (section 5.4.2.5).

5.4.2.3 Lysozyme loading into GNPs

Particle yields, drug loading efficiencies and loading capacities of gelatin particles are summarized in Table 5-2. Traditional formulations possessed a mean particle yield of approximately 7.5%, which was relatively higher than that of ultrafine ones (around 5%). The highest loading of lysozyme among all the formulations was presented by LUG 2 with a drug loading efficiency of 90.2% and a loading capacity of 121 mg (lysozyme per gram GNPs). However, all traditional formulations possessed drug loading efficiencies less than 60% and loading capacities not more than 35 mg (lysozyme per gram GNPs). When drug loading was performed after the formation of the particles surface adsorption dominated the loading of lysozyme. As ultrafine particles possesses high specific surface area for drug anchoring, the drug loading efficiency of LUG 3 was calculated to be 62.0%, while the one of LTG 3 was found to be only 39.5%.

Table 5-2: Mean particle size (PCS), percentage particle yields, percentage drug loading efficiencies (DLE %) and loading capacities of ultrafine and traditional gelatin based formulations.

Formulation	Particle size* (nm)	GNPs yield (%)*	DLE (%)*	Loading capacity of GNPs (mg/g, lysozyme/GNPs)*
UUG	56 ± 5	5.1 ± 0.1	---	---
LUG 1	209 ± 17	4.8 ± 0.2	60.5 ± 2.5	87 ± 5
LUG 2	74 ± 8	5.0 ± 0.1	90.2 ± 2.8	121 ± 4
LUG 3	62 ± 9	5.0 ± 0.1	62.0 ± 1.9	82 ± 7
UTG	245 ± 16	7.2 ± 0.2	---	---
LTG 1	292 ± 13	8.0 ± 0.1	49.2 ± 3.3	24 ± 4
LTG 2	277 ± 13	6.9 ± 0.2	59.5 ± 2.6	35 ± 6
LTG 3	261 ± 8	7.5 ± 0.3	39.5 ± 2.1	20 ± 6

* Values are expressed as mean ± S.D. (n = 3).

5.4.2.4 Recovery rate of lysozyme from GNPs

The preparation, processing and storage of enzyme loaded particulate carriers may induce changes in the native structure of the protein, which could in turn result in a reduction in the therapeutic activity. The turbidimetric method relying upon spectrophotometrical measurement of the clearance rate of lysozyme lysed turbid suspension of Micrococcus lysodeikticus is commonly used as standard for the detection of lysozyme activity (Morsky, 1983). Since already documented, lysozyme concentrations obtained from HPLC can be well correlated with the result of the turbidimetric method (Liao et al., 2001). The concentrations of extracted lysozyme from GNPs were detected by using HPLC method and the recovery rates are presented in Figure 5-5.

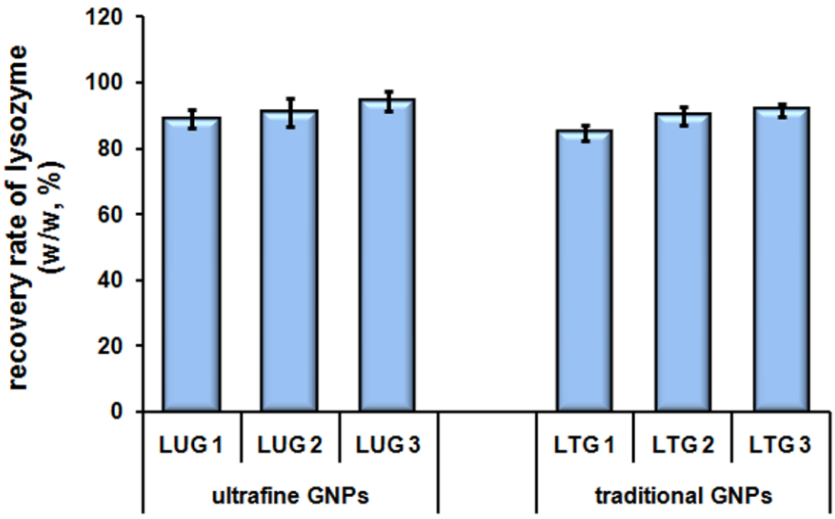

Figure 5-5: Recovery rates of lysozyme from varied loaded GNPs. The relatively high recovery rates indicated that the gentle production and drug loading process of both ultrafine and traditional GNPs maintained the structure and activity of lysozyme.

Slight differences between the recovered lysozyme concentrations and the theoretical ones were observed for all formulations and recovery rates ranging from 85% to 93% were obtained. As displayed in Figure 5-5, LUG 1 and LTG 1 possessed relatively slightly lower recovery rates than the other formulations. They showed recovered concentrations around 85% of the theoretical ones. The observed loss of activity can be deduced to the bridging of amino groups in free lysozyme molecules and aldehyde groups in glutaraldehyde. During the

ultracentrifugation free lysozyme molecules could be trapped in between nanoparticles which can also contribute to the relatively lower determined concentration. Activity of an enzyme depends on its stability when exposed to various experimental conditions like temperature, pH, buffers etc., of all these, thermal inactivation was demonstrated to be the primary cause for enzyme inactivation. A recent study aimed at understanding the relationship between thermal stability, pH and activity of lysozyme showing that no noticeable change in the secondary structure of lysozyme was observed until the temperature was increased to 65°C (Venkataramani et al., 2013). Also, the lysozyme was demonstrated to be stable at relatively lower pH (2.0-5.0) and its activity would be significantly affected at higher pH (> 7.0). In the production and lysozyme loading process of both ultrafine and traditional GNPs, the temperature was controlled at 50°C and the pH ranged from 2.5 to 3.0, which is beneficial to maintain the protein structure and activity of lysozyme.

5.4.2.5 Depicts of lysozyme loading behavior

Lysozyme loading behavior concerning surface adsorbed, matrix incorporated and free lysozyme of various developed GNPs is depicted in detail in Figure 5-6. When drug loading was performed prior to the formation of particles, most lysozyme molecules were expected to be incorporated into the core of GNPs. However, in this study, remarkable amount of lysozyme molecules was anchored at the surface of particles for the ultrafine formulations. For LUG 2, up to 44% of the lysozyme applied in the formulation was surface associated whereas 46% was incorporated into the core of GNPs and the rest was unloaded free lysozyme. As with LUG 1, the surface adsorbed and matrix incorporated lysozyme accounted for 27% and 33% of the applied lysozyme. These are attributable to strong electrostatic interactions between the positively charged type A GNPs (IEP of 6 to 9) and the numerous basic functionalities of lysozyme which are capable of attaching to a positively charged polyelectrolyte such as gelatin (type A) in an acidic pH medium. There are further aspects that have to be taken in consideration. Glutaraldehyde, a well-known non-zero length cross-linking agent, is commonly accepted to induce poly- or bi-functional cross-links into the network structure of polymers by the formation of Schiff's bases between free amino groups of lysine and aldehyde groups (Migneault et al., 2004). It is reasonable to infer that similar bridging may also occurs between lysozyme-lysine, gelatin-lysine and two aldehyde groups of glutaraldehyde on the surface of GNPs, which in turn leads to a higher surface adsorbing of lysozyme molecules. Matrix incorporation played a key role in the loading of lysozyme prior

to particle formation for the traditional formulations. The surface adsorbed percentages of lysozyme in LTG 1 and LTG 2 were found to be only 14% and 21%, respectively. Larger particle size of the traditional GNPs leads to smaller specific surface area and consequently lower surface adsorption of lysozyme.

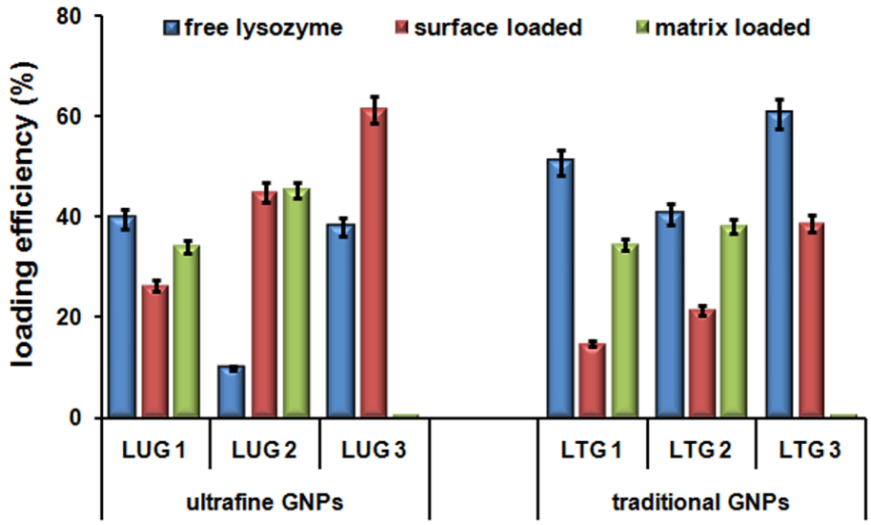

Figure 5-6: Depiction of the loading efficiency of ultrafine and traditional GNPs with respect to free lysozyme, surface adsorbed and matrix incorporated lysozyme.

By adding lysozyme to the formulation after formation of the particles, drug should theoretically be preferably loaded by surface adsorption. Approximately 60% of the lysozyme applied in the formulation was adsorbed onto the particle surface for LUG 3. This could be due to the smaller particle size and consequently high specific surface area. A surface associated lysozyme loading of only 40% was obtained by LTG 3 due to relatively smaller surface area for drug anchoring. For both particle types only very little was found in the particle matrix (< 5%).

5.4.2.6 In vitro release study

The *in vitro* drug release profiles of lysozyme loaded ultrafine and traditional GNPs were studied using Franz diffusion cells and are presented in Figure 5-7. A fast drug release was obtained when lysozyme was adsorbed onto the surface for both ultrafine and traditional GNPs. The release of lysozyme from LUG 1, 2 and LTG 1, 2 showed a biphasic pattern which is characterized by an initial burst in the first 4 hours followed by a prolonged release.

Taking LUG 2 as an example, a burst release of 38% was observed for LUG 2 within the first 4 hours. The cumulative release percentage was obtained by comparing the amount of released lysozyme to the total amount of loaded lysozyme. As estimated in the loading behavior experiments, surface adsorbed lysozyme accounted for 27% of the lysozyme applied in the formulation. This corresponded to 43% of the total amount of loaded lysozyme both by surface adsorption and matrix incorporation. It is not difficult to decipher a correlation between the burst release data (38%) and the surface loading data (43%) to get a conclusion that the initial bust drug release is mainly due to desorption of the surface adsorbed lysozyme or release of incorporated lysozyme just beneath the surface of the nanoparticles. Similar phenomenon was observed with LUG 2, for which surface adsorbed lysozyme accounted for 49% of the total loaded lysozyme and a burst release of approximately 46% were obtained. After four hours, 90% of lysozyme was released from LUG 3, while 80% of lysozyme was released from LTG 3 over a period of 6 hours.

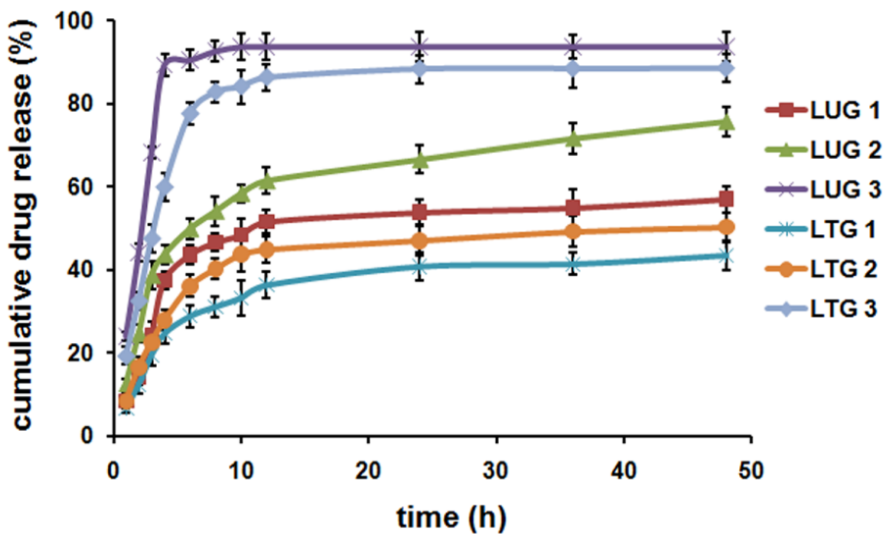

Figure 5-7: Percent cumulative release in Milli-Q water (pH 5.5) of lysozyme from ultrafine and traditional GNPs at 32 $\pm 1^{\circ}$C. The fastest drug release was observed for surface loaded ultrafine GNPs LUG 3 (60 nm) and approximately 90% of lysozyme was released after 4 hours which was nearly 3 times higher than that of traditional GNPs batch LTG 1 (290 nm).

Additional factors such as hydration, swelling and matrix erosion of nanoparticles could have caused the prolonged release of matrix incorporated drug. Gelatin type A, also known as acidic gelatin, is obtained from acid treated precursors and would be expected to undergo

marked swelling in a acidic environment (pH 5.5) (Goswami et al., 2010). The release rate of matrix incorporated drug depends strongly on the size of the particles. Smaller spheres have larger specific surface area and, therefore, most of the incorporated lysozyme molecules will be near or just beneath the particle surface leading to a faster drug release whereas larger spheres have larger cores which allowing slow diffusion of lysozyme. This theory could be an ideal explanation for the result that the formulations LUG 1, LTG 1 and LTG 2 which possess larger particle size showed much slower drug release (less than 60%) than LUG 2 (75%) over a period of 48 hours. Strictly speaking, the release could even be considered as biphasic. After an initial burst release in about 5-7 hours (depending on the formulation), a slow release period follows. This period can be subdivided in medium slow release from 5 or 7 to 12 hours, followed by a very slow release period up to 60 hours. The medium slow period is due to release of some remaining surface adsorbed lysozyme and lysozyme beneath the surface. After its desorption lysozyme is released mainly from particle core leading to very slow release.

5.4.2.7 Physical stability test

In the development of a new drug carrier system physical stability plays a decisive role. Figure 5-8 depicts the physical stability of all formulations stored at refrigeration (4°C), room temperature (RT) and at 40°C conditions over a time period of three months. At all three storage temperatures, the ultrafine formulations UUG, LUG 2 and LUG 3 possessed practically unchanged mean particle size (z-average) and all PI values obtained were below 0.1 as shown in Figure 5-8 (upper). Similar behaviors were observed for the traditional formulations UTG, LTG 2 and LTG 3 (Figure 5-8, lower). Continuous increase in mean particle size along with the PI was noticed for LUG 1 and LTG 1 at both room temperature and 40°C. The z-average of LTG 1 increased up to approximately 500 nm at the end of three months when stored at 40°C, which indicated possible particle aggregation. This could be correlated with the drug loading step as for both LUG 1 and LTG 1 lysozyme loading was performed after the first desolvation step. As already discussed in particle size analysis (section 5.4.2.1), addition of lysozyme to the formulation after the first desolvation step led to a higher pH of the particle suspension obtained by the followed second desolvation. The pH is a pivotal factor dominating the cross-linking reaction of glutaraldehyde. Increased pH could decrease the cross-linking density and induce covalent intermolecular cross-linking which

would facilitate the particle aggregation during both production and storage (Farris et al., 2010; Zhai et al., 2011).

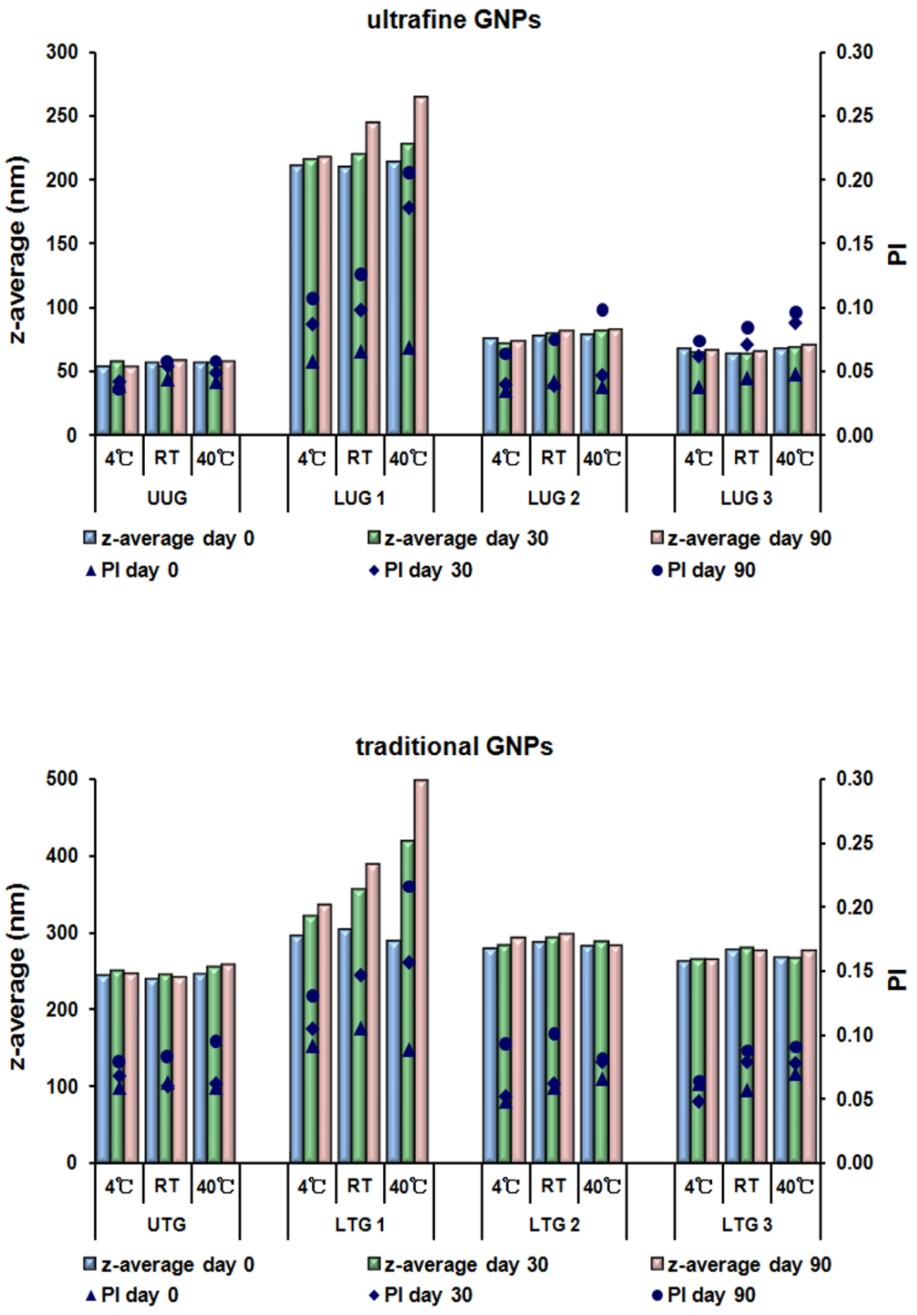

Figure 5-8: Mean PCS particle size and PI of unloaded and lysozyme loaded ultrafine and traditional GNPs stored at 4°C, room temperature (RT) and 40°C over a time period of three months.

The zeta potential of each formulation was also analyzed. The results displayed in Figure 5-9 are well in agreement with the observed excellent stabilities and minor instabilities in particle size (LUG 1, LTG 1).

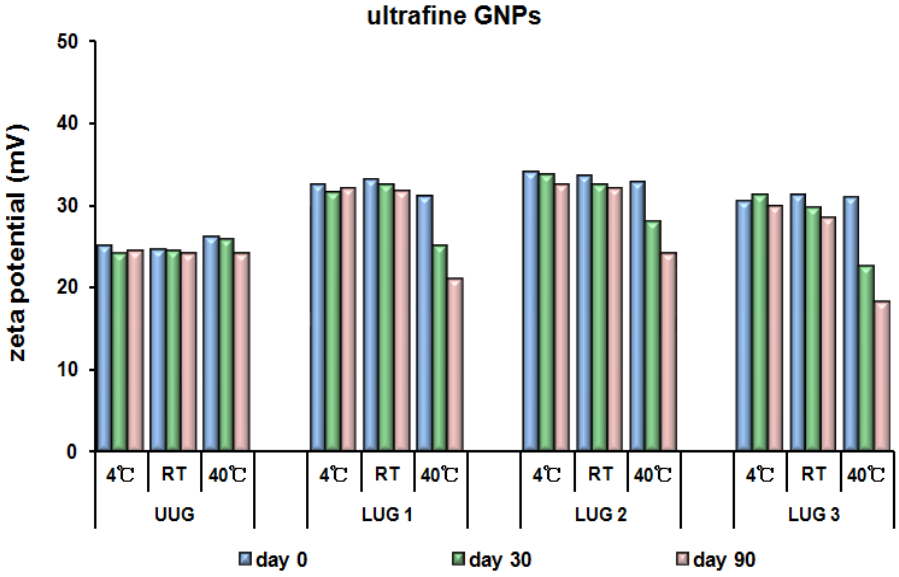

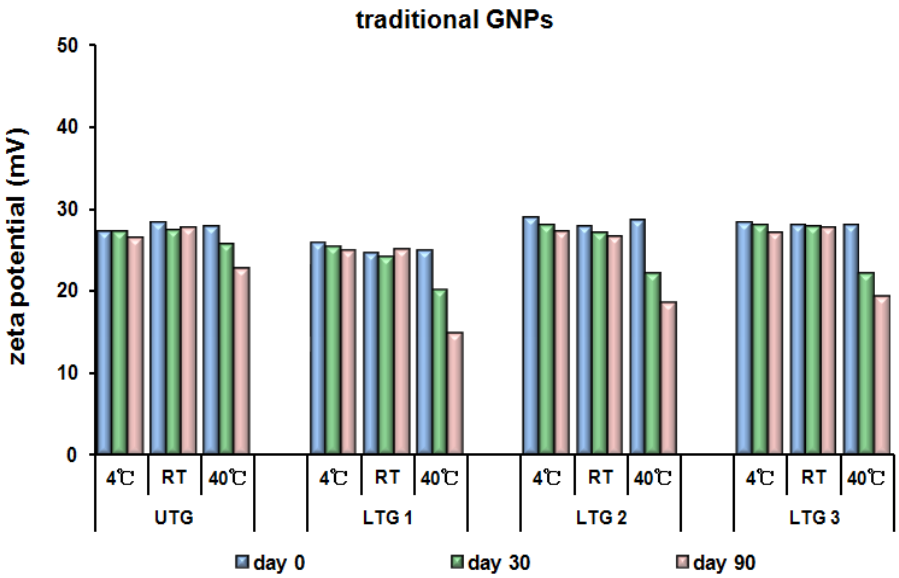

Figure 5-9: Zeta potential of unloaded and lysozyme loaded ultrafine and traditional GNPs stored at 4°C, room temperature (RT) and 40°C over a period of three months. A continuous decrease in zeta potential was observed for both ultrafine and traditional GNPs when stored at 40°C.

Unloaded ultrafine and traditional GNPs possessed stable zeta potential values throughout the whole observation time at all temperatures. Continuous pronounced decrease in zeta potential was observed for both LUG 1 and LTG 1 when stored at 40°C. The zeta potential of LTG 1 even decreased to approximately 15 mV at 40°C over a period of three months, which was well in agreement with the particle size data as decreased electrostatic repulsion facilitated the aggregation of GNPs. Slight decrease in zeta potential was noticed at 40°C for formulations of which drug loading was performed at the second desolvation step (LUG 2 and LTG 2) or after formation of GNPs (LUG 3 and LTG 3). This could potentially be attributed to desorption of the surface associated lysozyme. Surface loading of lysozyme in GNPs is correlated with two possible mechanisms: electrostatic attraction and surface mount due to steric effects. Anchoring of lysozyme molecules on the surface of GNPs introduces higher density of NH_3^+ groups and thus a higher net positive charge. But there exists an adsorption and desorption balance of surface associated lysozyme molecules. Higher temperature increases the kinetic energy of a system which results in the diffusion of lysozyme molecules from the surface of GNPs to the less concentrated dispersion medium and therefore a lower zeta potential.

5.4.2.8 Chemical stability test

The chemical stability of loaded lysozyme was also investigated over three months. At settled time intervals the suspension of lysozyme loaded GNPs was subjected to ultracentrifugation and then lysozyme was extracted following the procedure described in section 5.3.4.4. The concentration of lysozyme extracted from each GNPs formulation was detected by using the HPLC method and is displayed in Figure 5-10. When stored at lower temperatures (4°C or room temperature) lysozyme concentration remained stable over three months for all batches of GNPs. Whereas slight decrease in lysozyme concentration was observed when stored at 40°C for ultrafine GNPs (LUG 1 and LUG 2) and traditional GNPs (LTG 1 and LTG 2) of which drug loading was performed prior to the formation of particles. Continuous decrease in lysozyme concentration was noticed at 40°C for formulations LUG 3 and LTG 3 of which drug loading was performed after the formation of particles. For these two batches GNPs, lysozyme loading was achieved by surface adsorption. When stored at a higher temperature the increased kinetic energy disrupts the

established balance between adsorption and desorption thus some of the surface associated lysozyme molecules diffuse to the less concentrated dispersion medium. For both ultrafine batch and traditional batch, two vials of lysozyme solution with equivalent concentration to each formulation composition were also tested in parallel. The concentration of lysozyme in the solutions remained stable at all tested temperatures over three months due to its good thermal stability. This phenomenon supported the assumption that the decreased lysozyme concentration in GNPs was due to desorption of the surface associated lysozyme molecules.

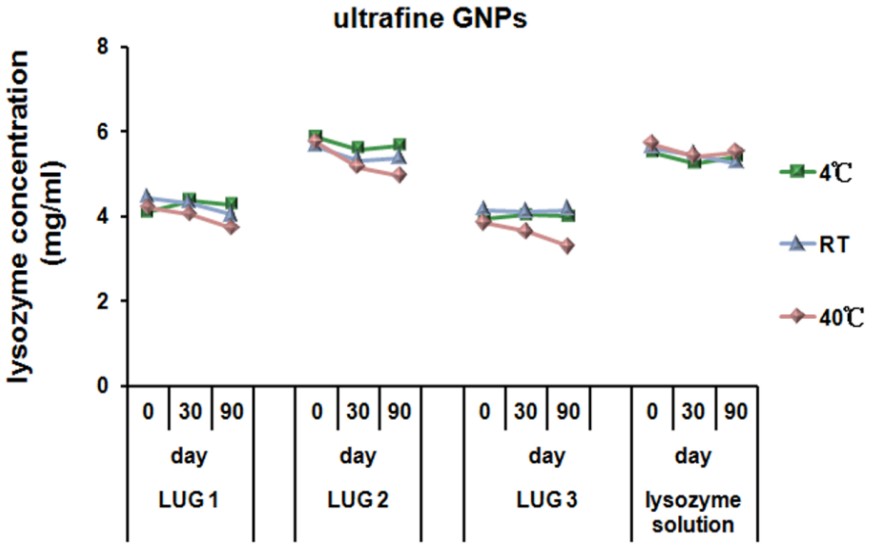

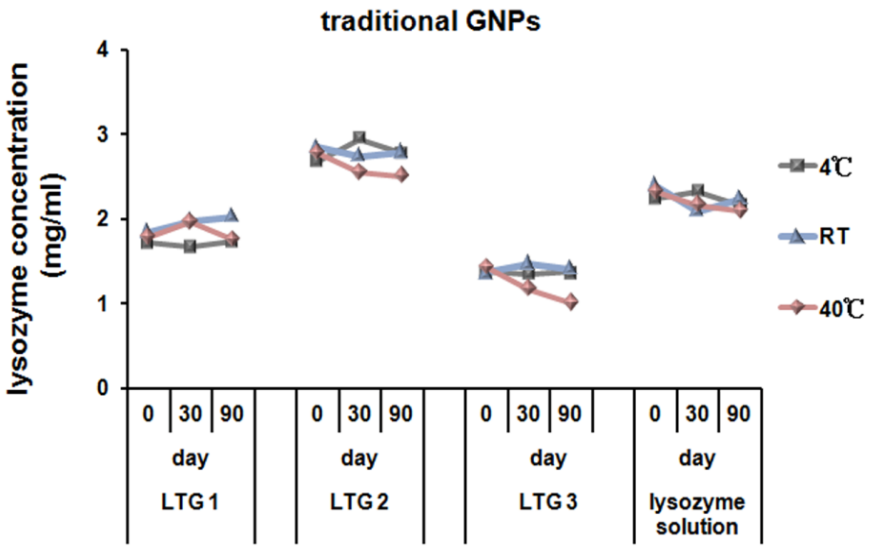

Figure 5-10: Recovered concentration of lysozyme from ultrafine and traditional GNPs when stored at 4°C, room temperature (RT) and 40°C over a time period of three months. Stability of lysozyme solutions with equivalent concentration were also investigated in parallel.

5.5 Conclusion

Lysozyme loaded ultrafine GNPs were developed and compared with traditional GNPs. The ultrafine GNPs possess promising characteristics for dermal delivery of lysozyme compared with traditional GNPs regarding ultra small particle size, high loading efficiency, fast drug release and preserved biological activity. When drug loading was performed prior to the formation of particles, remarkable amount of lysozyme molecules were adsorbed onto the surface of ultrafine GNPs, while matrix incorporation played a key role in the loading of lysozyme into the traditional ones. Loaded GNPs showed a biphasic pattern of drug release, which was characterized by an initial burst release of surface adsorbed drug within 5-7 hours (= relevant for dermal application) followed by a prolonged release of drug from the particle matrix. High loading capacity and fast drug release were observed for ultrafine GNPs due to increased specific surface area. Further studies involving the surface modification of GNPs to further increase loading capacity are planned. The developed ultrafine GNPs possess great potential for dermal delivery of enzymes.

6 Caffeine nanocrystals – developed production method & novel concept for improved skin delivery

6.1 Introduction

Nanocrystals represent a focal point of interest to overcome the limited application of new chemical entities which have dissolution problems such as the BCS class II drugs (Junghanns and Müller, 2008; Rachmawati et al., 2013; Shegokar and Müller, 2010b). Nanonization of coarse drug powders increases the saturation solubility (C_s) and related dissolution velocity (dc/dt) according to the Kelvin and Noyes-Whitney equations, which in turn lead to increased membrane penetration and consequently bioavailability (BA) (Müller et al., 2011). Nanocrystals can be applied by various routes of administration but by now product developments focused mainly on the oral route. One of the most successful examples is the block buster Tricor®, with an annual sale of more than 1 billion dollars in US.

For a long time no attention was given to the exploitation of nanocrystals for dermal application. Things changed when this successful principle was employed to improve the dermal BA of cosmetic ingredients rutin and hesperidin. Since 2007, the anti-aging and skin-protective cosmetic products based on nanosuspensions of poorly soluble antioxidants rutin (Juvena) and hesperidin (la prairie) have been introduced to the market. Compared with water soluble rutin derivative, rutin nanocrystals showed a 500-fold higher antioxidant activity *in vivo* (Petersen, 2006). Similarly, when it comes to pharmaceutical dermal formulations, the drug permeability of diclofenac sodium across the skin was increased up to approximately 4 fold by transferring into nanocrystals tested using Yucatan micropig (YMP) skin model (Piao et al., 2008).

The novel approach is to formulate nanocrystals also from medium soluble actives, and specifically for dermal application. At first glance, it does not make any sense at all to transfer medium soluble actives into nanocrystals, as they are soluble anyway! However, it will benefit compounds like caffeine (used in anti-cellulite products), of which the skin penetration is mainly a function of the active concentration in the applied dermal formation. Due to the penetration into the skin, the concentration of caffeine in the applied formulation decreases, thus the penetration decreases as well. Therefore, it makes sense to incorporate additional caffeine nanocrystals as dissolving depot to maintain a constant concentration gradient and consequently a steady skin

penetration. Favorably are nanocrystals with higher C_s and faster dissolution compared to macro-crystals.

The hair follicles are currently esteemed to be an important shunt route in the percutaneous penetration of topically applied substances (Lademann et al., 2001; Patzelt and Lademann, 2013). Nanoparticles have been identified as an efficient carrier for various drugs and chemicals into the skin, specifically via the hair follicular pathway. The influence of particle size on follicular penetration regarding to the penetration depth has been evaluated utilizing a multitude of models (Lademann et al., 2012; Ossadnik et al., 2007). It was found that nanoparticles with sizes range from 650 to 750 nm penetrated deeper than smaller or larger ones (Alexa Patzelt et al., 2011; Toll et al., 2004). Developing caffeine nanocrystals with optimized size could increase skin absorption via hair follicle accumulation.

Basically, for the production of nanocrystals from poorly soluble actives, two principle methods, i.e. “top-down” and “bottom-up” techniques, are being extensively used (Müller et al., 2011). However, the production of nanocrystals from medium soluble actives is challenging. In the production process, the saturation solubility increases with the reduction of size. Supersaturation effect can cause pronounced re-crystallization and crystal growth, e.g. formation of fibre-like microcrystals. The aim of the present investigation was to develop a specific production technique which allows the production of nanocrystals from actives with medium solubility.

6.2 Materials and methods

6.2.1 Materials

Caffeine was purchased from BASF SE (Ludwigshafen, Germany). Polyvinylpyrrolidone (PVP 40) was purchased from Sigma Aldrich (Deisenhofen, Germany). Carbopol® 981 was a kind gift from Lubrizol Advanced Materials Europe BVBA (Brussels, Belgium). Tween® 80 was purchased from Uniqema GmbH & Co. KG (Emmerich, Germany), propylene from VWR International GmbH (Darmstadt, Germany). Freshly produced double distilled ultrapurified water (Milli-Q, Millipore

GmbH, Germany) was used as dispersion medium. Ethanol 96% and acetonitrile were of analytical grade and used as received.

6.2.2 Methods

6.2.2.1 Production of caffeine nanocrystals

Firstly, caffeine pre-suspensions were processed by using an Ultra-Turrax T25 (Janke & Kunkel GmbH, Germany) at 8,000 rpm for 20 seconds. Afterwards, both high pressure homogenization (HPH) and low energy milling (pearl milling, PM) were applied for the production of caffeine nanocrystals.

High pressure homogenization (HPH)

Caffeine pre-suspension formulated with 15% (w/w) caffeine, 1% (w/w) stabilizer (PVP 40, Carbopol® 981 and Tween® 80) and 84% (w/w) water-ethanol mixture (1:9) was subjected to pre-milling at low homogenization pressure (250 bar, 2 cycles) to diminute very large crystals. Followed by 20 cycles of homogenization at higher pressures of 500, 800 and 1,200 bar, respectively, using a Micron LAB 40 high pressure homogenizer (APV Deutschland GmbH, Germany), cooled to 5°C (three formulations were produced at different conditions). The samples were withdrawn after 5, 10, 15 and 20 cycles of homogenization.

Pearl milling (PM)

The prepared pre-suspensions of caffeine (10% and 20% w/w) in water-ethanol mixtures (1:9, 3:7 and 5:5) with varied stabilizers (PVP 40, Carbopol® 981 and Tween® 80; 1% and 2% w/w) were milled by using a pearl mill PML 2 (Bühler AG, Switzerland) at 2,000 rpm. Power beads type yttria-stabilized zirconia (YSZ) with a size of 0.4-0.6 mm were used as milling material. The solubility of caffeine is substantially temperature dependent, thus the cooling system is obviously necessary. To reduce the recrystallization phenomena, the whole system was cooled to 5°C during production. The samples were withdrawn at time of 5, 30, 60, 120 and 180

minutes. The influence of varied dispersion mediums and stabilizers on particle size and stability of caffeine nanocrystals was investigated.

6.2.2.2 Particle size and shape analysis of caffeine nanocrystals

Photon correlation spectroscopy (PCS, Zetasizer Nano ZS, Malvern Instruments, UK) was employed to determine the particle size of developed caffeine nanocrystals. PCS calculates the mean particle size (mean diameter of the bulk population, z-average) and polydispersity index (width of the size distribution, PI). For size determination, samples were diluted with water-ethanol mixture (1:9) saturated with caffeine and measured in triplicate. All measurements were carried out at 20°C.

An Orthoplan microscope (Leitz, Germany) connected to a CMEX-1 digital camera (Euromex microscopes, Netherlands) was used to detect the presence of potential large particles, agglomerations or even fibre-like structures during production and over storage. Samples were analyzed at magnifications of 630 and 1,000 folds.

6.2.2.3 High performance liquid chromatography (HPLC) analysis of caffeine

Caffeine concentrations were determined by high performance liquid chromatography (HPLC). The HPLC system consisted of a KromaSystem 2000 version 1.7 (Kontron Instruments GmbH, Germany), an auto sampler model 560, a solvent delivery pump and an UV detector model 430 (Kontron Instruments SpA, Italy), measuring at 272 nm. The analytical column was an Eurospher-100 C18 5 µm (4.6 × 250 mm) with a flow rate of 1 ml/min at 25°C with 175 bar. The mobile phase consisted of acetonitrile and water in a ratio of 15:85 (v/v).

6.2.2.4 Saturation solubility

To determine the saturation solubility of caffeine, the coarse powder was suspended in water-ethanol mixture (1:9) to a final active concentration of 5% (w/w). For preparation of the nanosuspension samples, 2.5 ml of each nanosuspension with an active content of 20% (w/w) was added to 10 ml of water-ethanol mixture (1:9). The samples were stored at 32°C shaking at 100 rpm in an Innova 4230 refrigerated incubator shaker (New Brunswick Scientific, USA). The same procedure was

performed when applying ethanol-propylene glycol mixture (3:7) as dispersion medium. Samples were withdrawn at settled time intervals over a period of one week. Batches were centrifuged for 1 hour at 10,000 g (32°C, Optima™ MAX-XP Ultracentrifuge, Beckman Coulter, USA). Caffeine concentration in the supernatant was analyzed using the developed HPLC.

6.2.2.5 Short term stability

For stability investigations, caffeine nanosuspensions stabilized with PVP 40, Carbopol® 981 and Tween® 80, respectively, were stored at three different temperatures (4, 25 and 40°C) for two months. The particle size was analyzed on the day of production and after 7, 14, 30 and 60 days of storage. Light microscopy was also performed to determine the presence of possible agglomerations.

6.3 Results and discussions

6.3.1 The novel concept

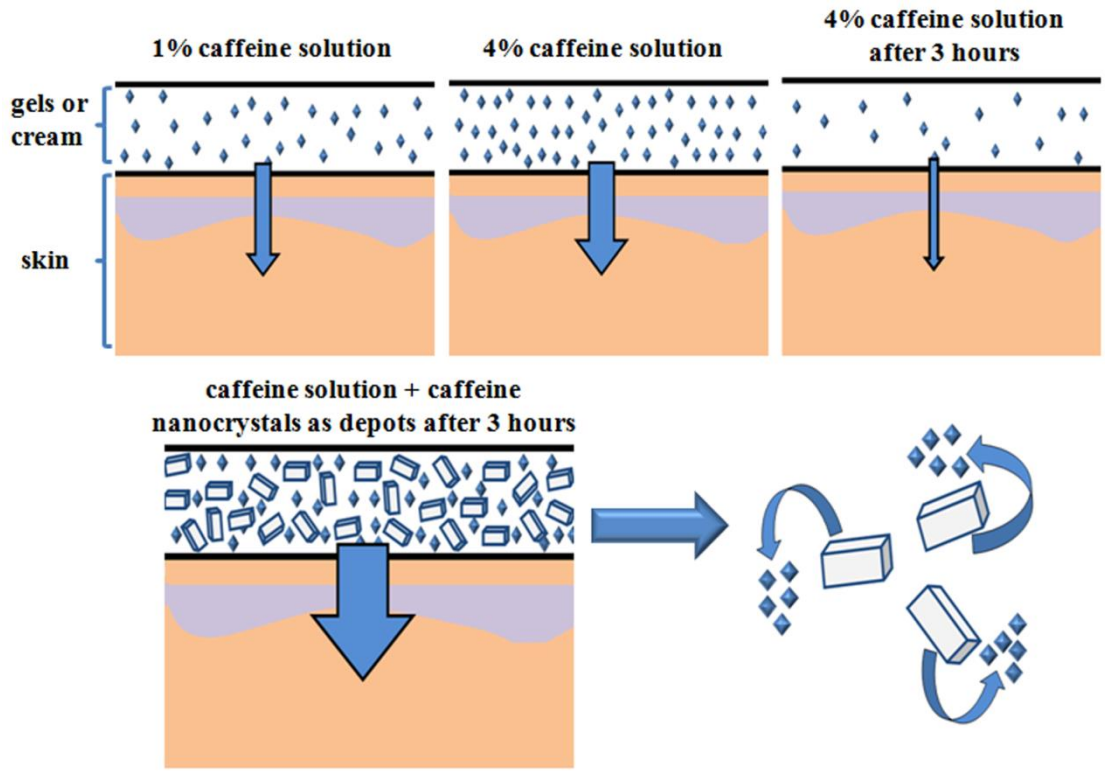

Figure 6-1: Novel nanocrystal concept to increase skin delivery of medium soluble actives: the skin penetration increases with the concentration of caffeine in the formulation (upper left and middle). Incorporating caffeine nanocrystals as depot could avoid reduction of the caffeine concentration in the formulation due to skin penetration (lower), thus maintaining a constant concentration gradient and constant skin penetration.

The novel idea is to transfer medium soluble actives into nanocrystals to increase the skin penetration. As illustrated in Figure 6-1, the penetration into the skin increases with the concentration of caffeine in the dermal applied formulation, i.e. increase from 1% to 4% (upper left and middle, blue arrows, stripping test data - unpublished). After certain application time, i.e. after three hours, the caffeine concentration in the formulation (4%) decreases due to its penetration into the skin. Thus, penetration slows down owing to the reduced concentration gradient (Figure 6-1, upper right). By

applying additional nanocrystals in the formulation, caffeine penetrated into the skin is supplemented by the dissolved caffeine from the nanocrystals, which act as depot (Figure 6-1, lower left). Advantage of nanocrystals is that they show a higher kinetic saturation solubility compared with micronized crystals and dissolve faster (Figure 6-1, lower right).

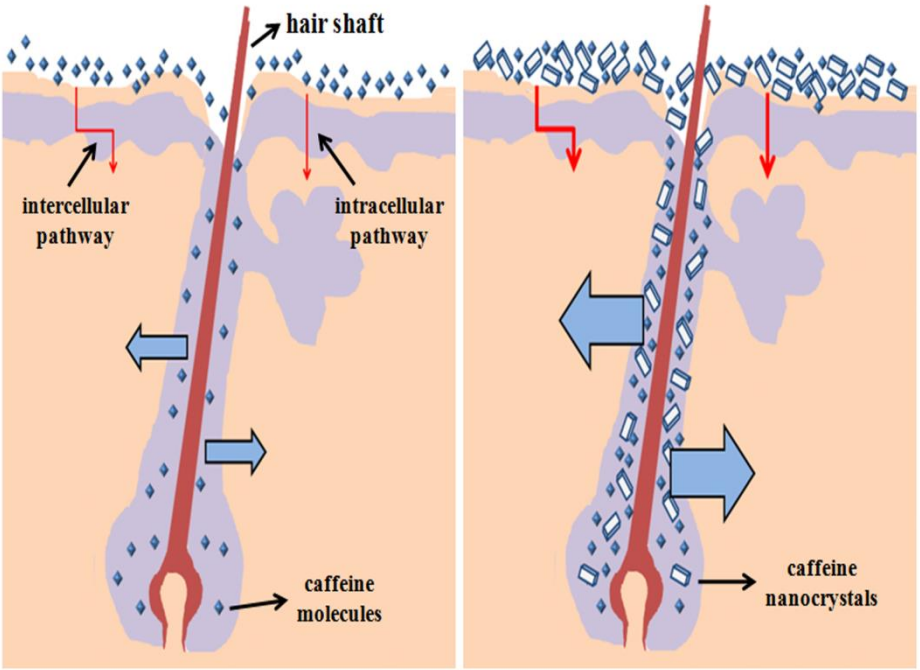

Figure 6-2: Combination of novel nanocrystal concept and hair follicle accumulation: Caffeine nanocrystals on skin surface possess higher saturation solubility increasing intercellular and transcellular penetration pathways (left). Besides, nanocrystals can preferentially accumulate in hair follicles, increasing the penetration into surrounding cells (right).

At present, three penetration pathways have been theoretically proposed: the intercellular, transcellular and follicular pathways (Figure 6-2, left). It used to be assumed that the intercellular route was the only relevant penetration pathway (Bouwstra et al., 2001; Hadgraft, 2001). Therefore, attempts were made to develop ultra small particles to facilitate the particle diffusion inside the lipid layers surrounding the corneocytes. However, recent investigations have revealed that hair follicles play a significant role in skin penetration (Knorr et al., 2009; Otberg et al., 2008). Nanocrystals with appropriate particle size (approximately 700 nm) could

penetrate into or be entrapped within the hair follicles to specific depths (Figure 6-2, right), which could be even enhanced by mechanical massage (Alexa Patzelt et al., 2011). Nanonization of caffeine powder increases its saturation solubility and concentration gradient, thus the skin penetration via intercellular and transcellular pathways is increased. Furthermore, accumulation of caffeine nanocrystals in hair follicles increases the penetration into surrounding cells.

6.3.2 Production and characterization of caffeine nanocrystals

Caffeine nanocrystals were produced by HPH or PM according to the listed formulation compositions in Table 6-1. Water-ethanol mixtures (1:9, 3:7 and 5:5) and ethanol-propylene glycol mixture (3:7) were used as dispersion medium. Various stabilizers like PVP 40, Carbopol® 981 and Tween® 80 were applied.

Table 6-1: Production techniques and composition of caffeine formulations applied in this study.

Formulation	Production method	Active (w/w)	Stabilizer (w/w)	Dispersion medium quantum satis 100% (w/w)
A			0.5% PVP 40	
B	HPH	10% Caffeine	0.5% Carbopol® 981	water-ethanol 1:9
C			0.5% Tween® 80	
D				water-ethanol 1:9
E	PM	20% Caffeine	1% Tween® 80	water-ethanol 3:7
F				water-ethanol 5:5
G			2% PVP 40	
H	PM	20% Caffeine	2% Carbopol® 981	water-ethanol 1:9
I			2% Tween® 80	
J	PM	20% Caffeine	2% Carbopol® 981	ethanol-propylene glycol 3:7

6.3.2.1 HPH

HPH is a typical disintegration process for nanocrystal production. A pre-suspension is forced by a piston-gap homogenizer at high pressure and speed to pass through a tiny gap, and the nanocrystals are generated via cavitation and crystal collision (Keck and Müller, 2006). Theoretically, enhanced power density of the homogenizer leads to smaller crystal size. In this experiment, premilling at 250 bar was performed for two times, followed by 20 cycles homogenization at 500, 800 and 1,200 bar, respectively. The performance of three different stabilizers was investigated. Figure 6-3 describes the fluctuation of particle size (*d(v)* 50%, obtained by LD) during homogenization.

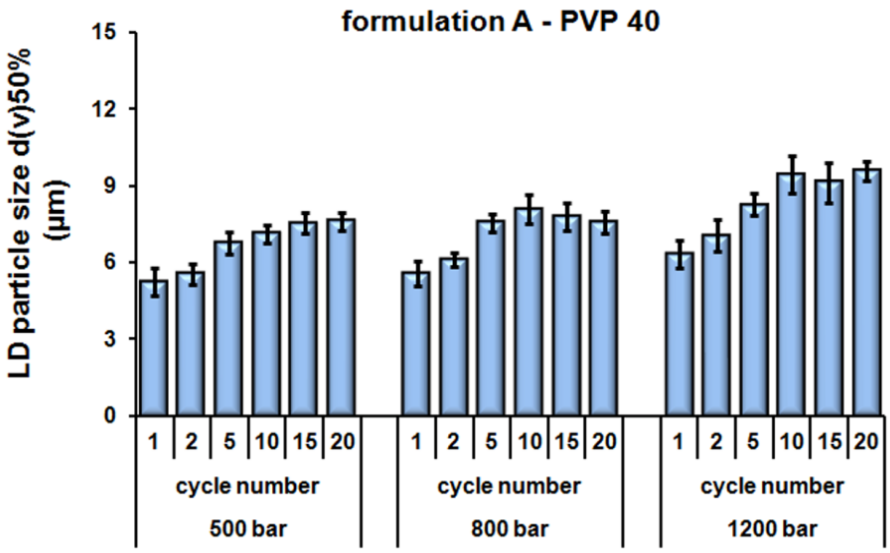

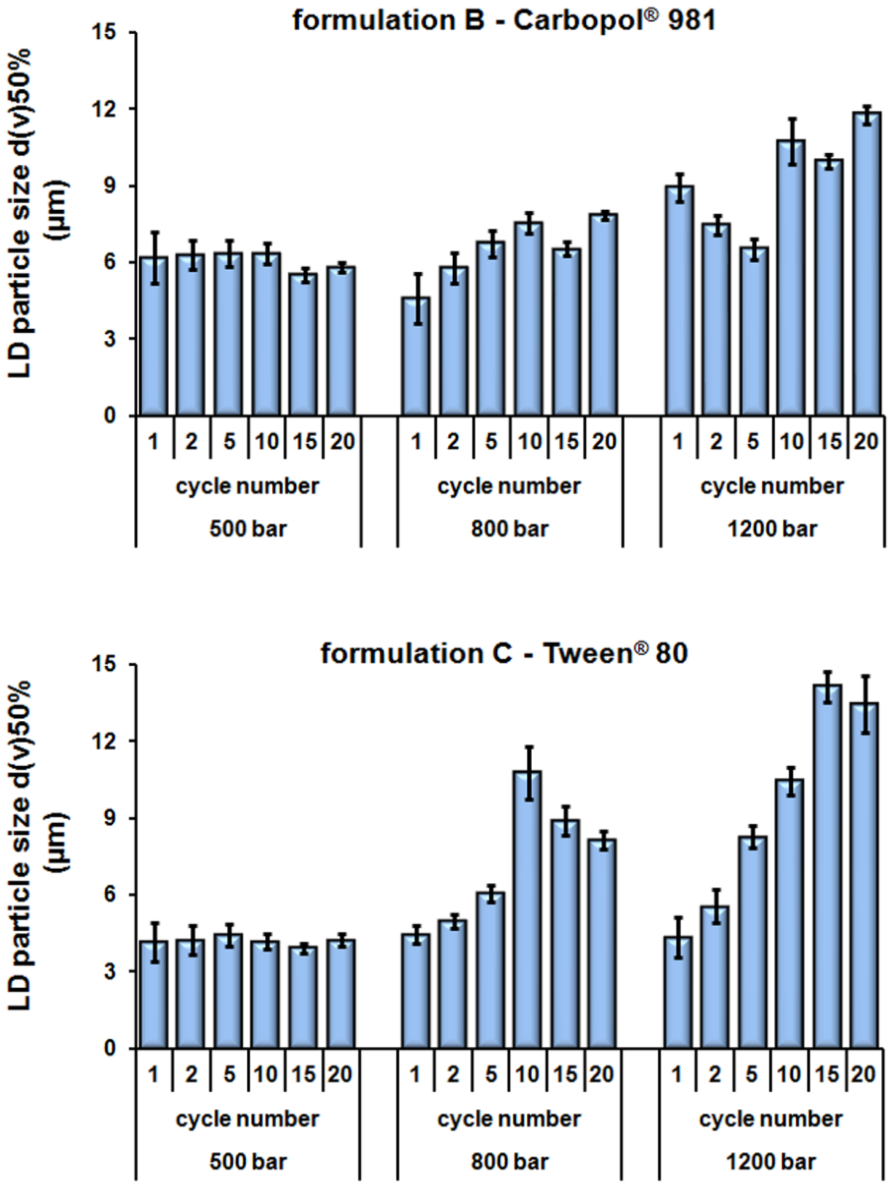

Figure 6-3: Particle size of caffeine crystals as a function of homogenization cycles produced by HPH at three pressures (LD data, *d(v)* 50%). Three formulations (A to C) stabilized with PVP 40, Carbopol® 981 and Tween® 80, respectively, were investigated.

As shown in Figure 6-3, for formulation A stabilized with PVP 40, slightly increase in particle size was observed when applied varied pressures. Similar phenomenon was obtained for formulation B stabilized with Carbopol® 981. When applied a homogenization pressure of 1,200 bar, smallest particle size was obtained after 5 cycles. Further homogenization cycles led to an increase in particle size from 7 ± 0.5

µm to 12 ± 0.4 µm. As with Tween® 80 stabilized formulation, particle size has been maintained the same during the 20 cycles of homogenization at 500 bar. However, a continuous increase in particle size was observed when applied a higher pressure. The biggest particle size reached to approximately 15 µm after 20 cycles of homogenization at 1,200 bar, which was even bigger than the starting caffeine powder with *d(v)* 50% of 13 µm.

When producing caffeine nanocrystals in such a high energy process of HPH, supersaturation effects led to pronounced crystals growth (Ostwald ripening effects) (Figure 6-4, left). During homogenization cycles, input of energy breaks the crystal and diminutes the size by overcoming the binding forces between crystal lattice. However, extra energy could enhance the kinetic energy of the crystals, cause agglomeration and accelerate crystal growth (Kakran et al., 2012b). After production, the macrocrystals started to grow to extremely long fibres, leading to a cotton swab appearance (Figure 6-4, middle and right).

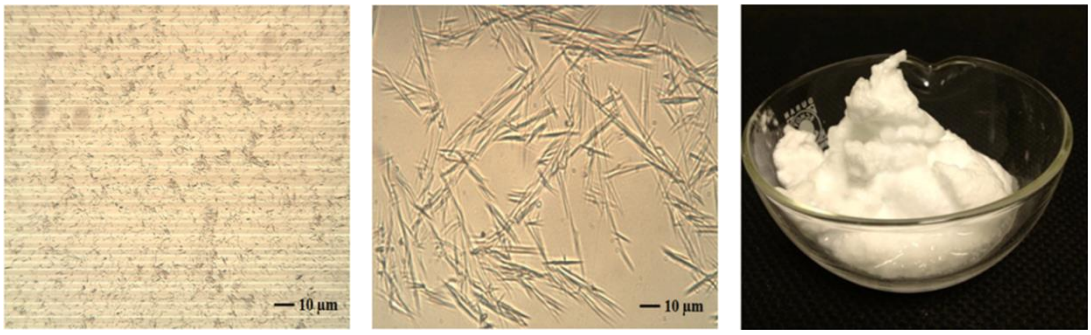

Figure 6-4: Caffeine crystals produced by HPH (formulation A): fibres formed immediately after applying 20 cycles homogenization at 1,200 bar (left, microscope). The fibres continue to grow leading to extremely long fibres (middle, 630 fold magnification), and a cotton swab appearance of the caffeine suspension (right).

6.3.2.2 PM – influence of dispersion medium on caffeine nanocrystals

A special process was developed based on low energy pearl milling in combination with low dielectric constant solvents (water-ethanol mixtures) to reduce the recrystallization of caffeine nanocrystals. Caffeine pre-suspension was charged into the milling chamber of the pearl mill along with the beads and the crystal size

reduction was achieved utilizing the grinding forces generated by the movement of the beads.

The formulations D to F employed 1% (w/w) Tween® 80 as stabilizer for the production of 20% (w/w) caffeine nanocrystals. Preliminary study was performed to evaluate the solubility of caffeine in varied water-ethanol mixtures (Fratus, 2011). To reduce the recrystallization, water-ethanol mixtures in ratios of 1:9, 3:7 and 5:5 with lower caffeine solubility were selected as dispersion medium (Table 6-1). Figure 6-5 shows the z-average and PI of the caffeine nanocrystals as a function of milling time. A steady decrease in z-average was observed for formulation D. After milling for 180 minutes, a z-average of 375 nm and a PI of 0.205 were obtained. No more decrease in particle size and PI was observed when applying further milling (data not shown). Formulation E showed an efficient size reduction in the first 90 min. A z-average reduction from approx. 1,600 nm to 500 nm and a PI diminishment from approx. 0.4 to 0.2 were observed. However, pearl milling for the next 90 min only led to slightly decrease in PI and steady state of the particle size with a z-average of 420 nm and a PI of 0.176. A similar phenomenon was observed in formulation F within the first 90 min pearl milling. However, pearl milling for the last 90 min led to an increase in particle size to 586 nm. Besides this, the broadening in size distribution (increase in PI) indicated the agglomeration due to van der Waals force or crystal growth caused by Ostwald ripening.

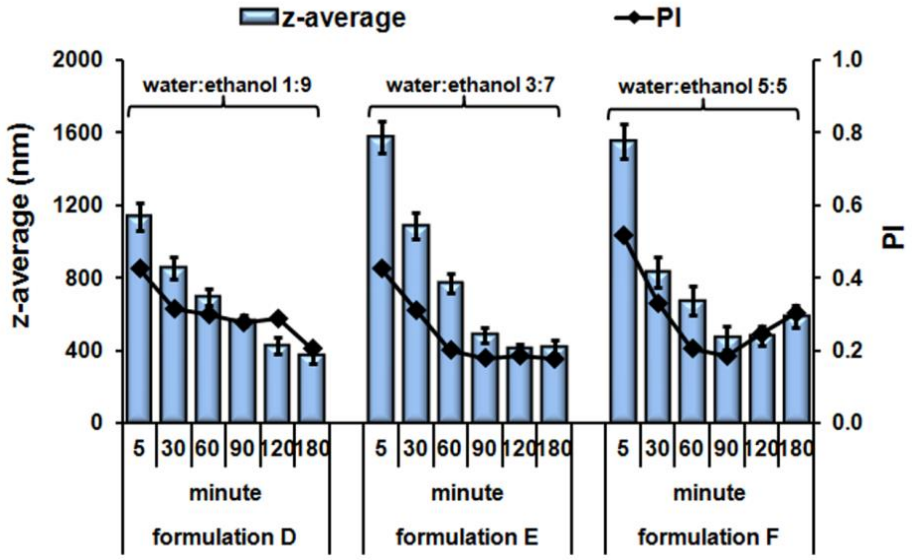

Figure 6-5: Caffeine nanocrystals produced by PM: influence of dispersion medium on particle size as function of milling time. Water and ethanol mixtures in ratios of 1:9, 3:7 and 5:5 were used as dispersion medium, respectively. Z-average and PI were obtained by PCS immediately after production (stabilizer: 1% Tween® 80).

In a nanosuspension system, Ostwald ripening refers to the phenomena that smaller crystals dissolve and the dissolved molecules deposit on the surface of larger crystals so as to reach a more thermodynamically stable state (Zhang et al., 2010). According to the Kelvin equation, the saturation solubility of smaller crystals is higher than that of larger crystals, which results in the diffusion of drug molecules from the surrounding region of the smaller crystals to the less concentrated solution around the larger crystals. In the end, the Ostwald ripening process leads to the growth of the larger crystals and size reduction or even disappearance of the smaller crystals (Kakran et al., 2012a). Therefore, from the physical stability aspect it is essential to produce homogeneous nanosuspensions with a uniform particle size. To have a more intuitive understanding of Ostwald ripening, micrographs of caffeine nanocrystals were taken by light microscopy after being freshly produced and after 24 hours storage at 4°C.

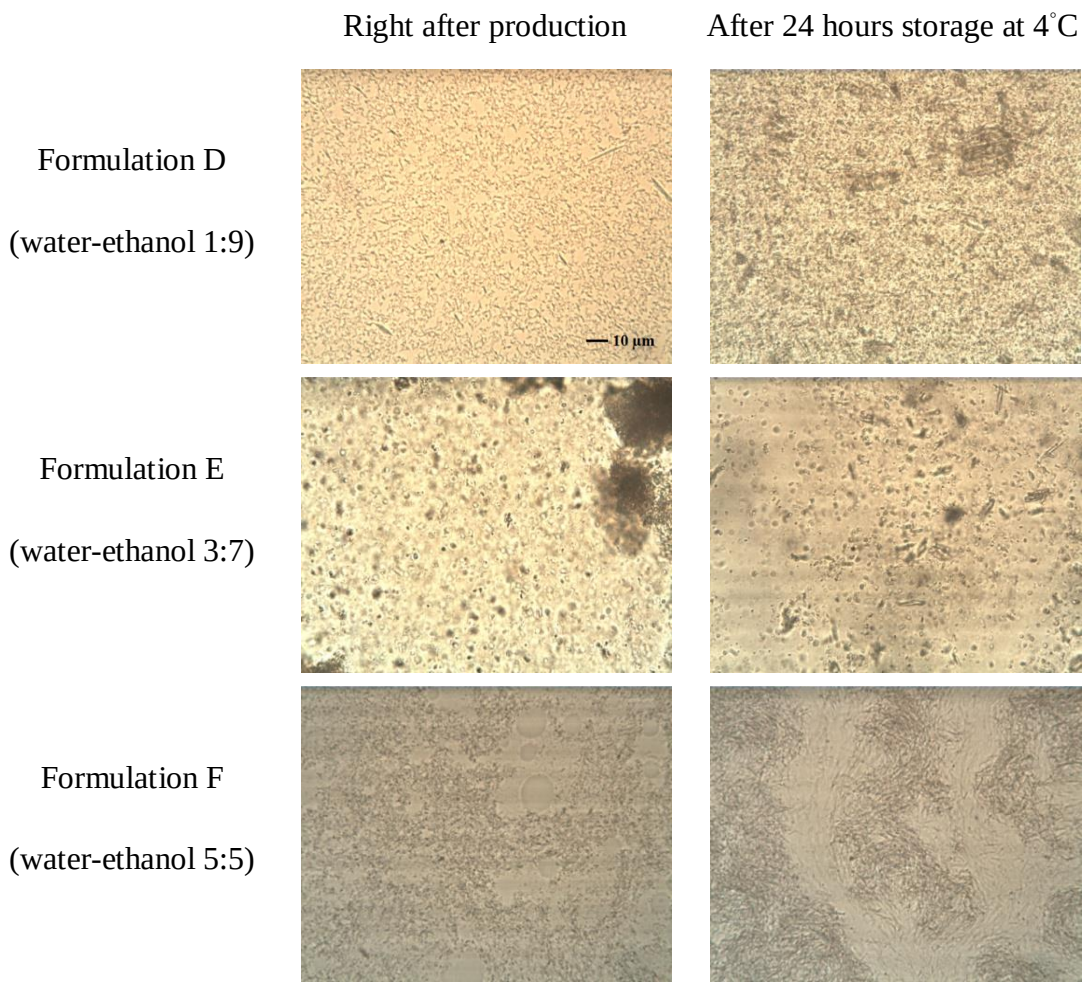

Figure 6-6: Light microscopy pictures of caffeine nanocrystals produced by PM: freshly prepared (left) and after 24 hours storage at 4°C (right) (magnification 630×; scale =10 µm). Increased water content from D to E of the dispersion medium facilitated the recrystallization and crystal growth (stabilizer: 1% Tween® 80).

As shown in Figure 6-6, individual needle-like microcrystals could be observed in formulation D after production, while clear agglomeration appeared after 24 hours. In formulation E, freshly produced nanosuspension already showed individual agglomeration and after storage only micro-sized crystals could be observed. As illustrated by the Lifshitz-Slyozov-Wagner theory, Ostwald ripening is directly correlated to the solubility of the particle material (Zeeb et al., 2012). Increased solubility of caffeine in the higher water content dispersion medium strongly facilitated the Ostwald ripening process in formulation F. After storage for only 24 hours, nanocrystals grew up to fibre-like microcrystals and agglomeration could also be observed. Based on the results above, water-ethanol mixture in a ratio of 1:9 was

selected to perform further investigations to screen for more efficient stabilizer, i.e. to replace Tween® 80.

6.3.2.3 PM – influence of stabilizer on caffeine nanocrystals

In the drug nanocrystallization process, the disintegration of coarse powder implies the creation of new additional surfaces and is associated with an increased surface free energy. Freshly manufactured drug nanocrystals are thermodynamically unstable and tend to agglomerate to minimize the total energy. Thus, the right choice of stabilizers is critical for the stabilization of nanocrystals. Both ionic and nonionic surfactants as well as polymers have been commonly applied as stabilizers. Possible stabilization mechanism of ionic surfactants is the electrostatic repulsion due to the formation of charged surfaces. As to nonionic surfactants and polymers, the repulsive barrier against agglomeration is mainly based on the steric effect (Choia et al., 2005; Eerdenbrugh et al., 2008). In addition, adsorbed polymers on crystal surface can act as crystallization inhibitor, e.g. exploited in sugar coating of tablets.

However, for dermal application the number of accepted ionic surfactants is relatively low due to the high irritation potential. Therefore in the present study the focus was put on nonionic substances to be tested. Three formulations of caffeine nanosuspension stabilized with 2% (w/w) PVP 40, Carbopol® 981 and Tween® 80, respectively, were developed. The influence of different stabilizers on resulting caffeine nanocrystals size is illustrated by PCS data (Figure 6-7). A continuous reduction in particle size was observed as a function of milling time for all applied stabilizers when analyzed by using both PCS and light microscopy (Figure 6-7). This constant reduction was observed until 120 min followed by only minor change in z-average between 120 and 180 min. Caffeine nanosuspension stabilized with Carbopol® 981 showed the highest steady decrease followed by the suspensions stabilized with Tween® 80 and at least with PVP 40. After milling for 180 min, the z-average was 250 nm and 350 nm for Carbopol® 981 and Tween® 80 stabilized nanosuspensions, whereas it was around 600 nm for PVP 40 stabilized nanosuspension.

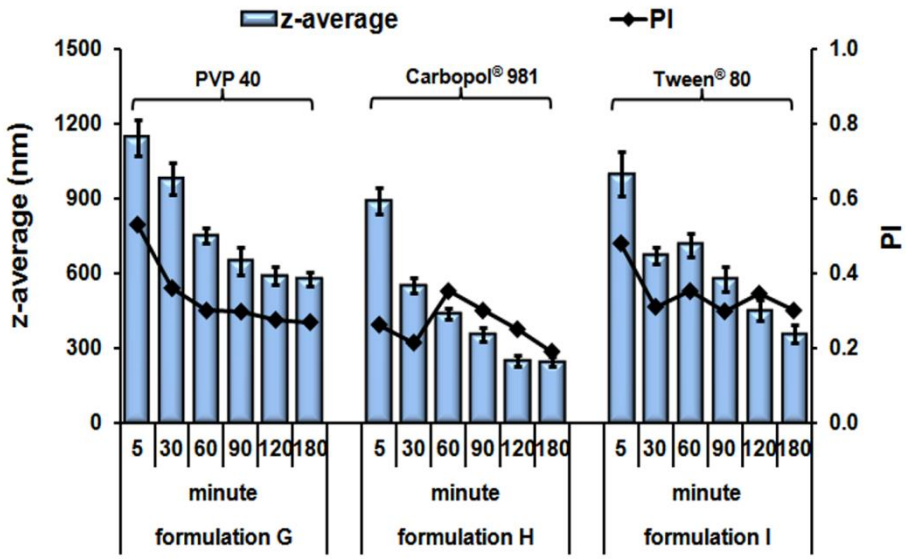

Figure 6-7: Caffeine nanocrystals produced by PM: influence of stabilizers (PVP 40, Carbopol® 981 and Tween® 80) on particle size as function of milling time. Z-average and PI were obtained by PCS immediately after production (dispersion medium: water-ethanol 1:9).

Previous studies have demonstrated that the final particle size of nanocrystals produced by pearl milling is mainly determined by the rotating speed and the diameter of applied milling beads (Peltonem and Hirvonen, 2010). Furthermore, the stabilizers play an important role to prevent agglomeration during the production as well as during the following storage of nanosuspensions. For this, the molecular weight, affinity to the newly generated crystal surfaces and diffusion velocity of the stabilizers are of extraordinary importance (Kakran et al., 2012a). That means, in all three formulations the generated particle size is identical and differences measured in size are due to absence or different extent of agglomeration. Under the same production conditions, the inefficient size reduction indicates the formation of agglomerations and a poor affinity of PVP 40 to caffeine nanocrystals. PVP 40 has amide functional groups, while the other two polymers process ether carboxyl or hydroxyl functional groups.

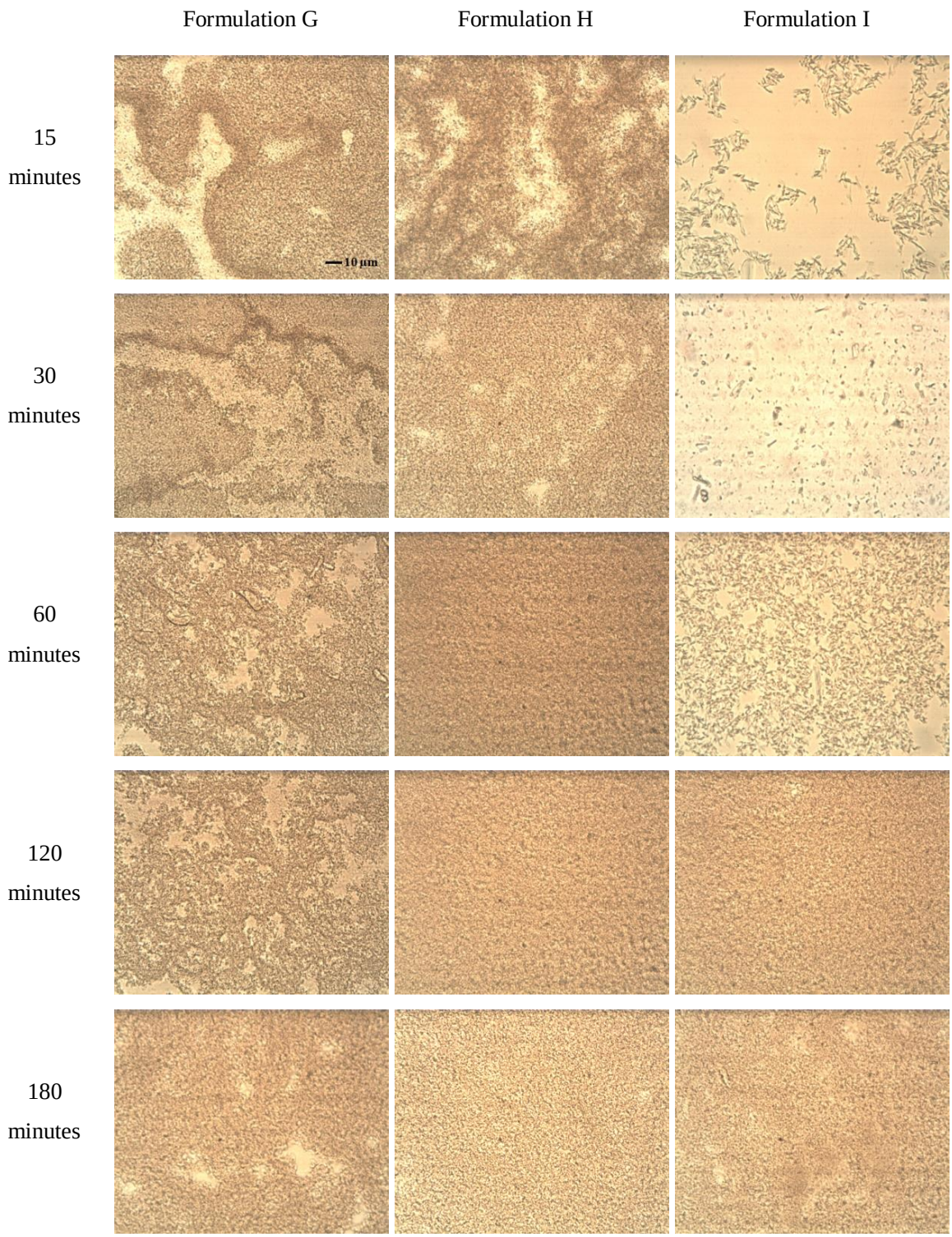

Figure 6-8: Light microscopy images of caffeine nanosuspensions during the process of milling (magnification 630×; scale =10 µm). Three formulations (G, H and I) stabilized with PVP 40, Carbopol® 981 and Tween® 80, respectively, were investigated (dispersion medium: water-ethanol 1:9).

Light microscopy is commonly used to detect the agglomerations and potentially large crystals exist in the formulation (> 1 μm). It helps to confirm the results from PCS or LD under lower magnification and to estimate the surfactant efficiency by observing the movement and spatial arrangement of particles under the microscope under higher magnification (i.e. 1000×). Figure 6-8 shows the microscopy images of the three formulations in the process of pearl milling. The size difference which is indicated in the pictures of 630 fold magnification is not as obvious as the PCS results. Formulation G and I stabilized with PVP 40 and Tween® 80 showed obvious agglomerations after milling for 180 minutes, most pronounced for formulation G. In contrast, formulation H stabilized with Carbopol® 981 indeed presented the smallest nanocrystals and a uniform distribution, being well in agreement with the PCS data. Both for the efficiency of nanonization and for avoiding agglomeration, the advantage of Carbopol® 981 has been proven by direct observation.

6.3.2.4 PM – development of formulation with decreased ethanol content

Ethanol is widely used in all kinds of products with direct exposure to the human skin e.g. pharmaceutical preparations, medicinal products and especially cosmetics due to a pleasant cooling effect. In previous experiments, caffeine nanosuspension was successfully produced with low dielectric constant dispersion medium (water-ethanol mixture 1:9) and was expected to increase skin penetration via increased saturation solubility (Figure 6-9, upper) and hair follicle accumulation (Figure 6-10, middle).

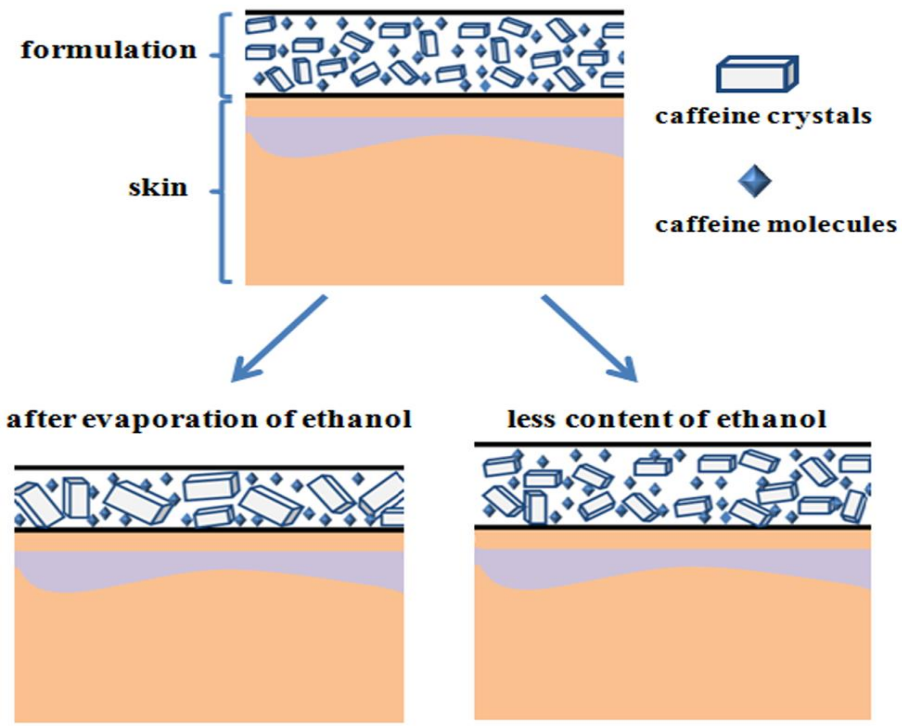

Figure 6-9: The concept to decrease ethanol content in caffeine nanosuspension: evaporation of ethanol leads to a supersaturated solution and micro-sized crystals caused by recrystallization (lower left); decreased ethanol content helps to maintain a constant crystal size (lower right).

However, ethanol possesses lower boiling point than water as ethanol molecules do not form a strong network of hydrogen bonding between carbon and hydrogen components. When a mixture of water and ethanol is evaporating, the ethanol will evaporate faster. After application of caffeine nanosuspension onto the skin (with a temperature of approximately 32°C) fast evaporation of ethanol leads to a highly supersaturated solution as ethanol accounts for 90% of the medium. Supersaturation effects can lead to pronounced crystal growth on the skin, even to micro size (Figure 6-9, lower left). Thus the caffeine concentration gradient between the formulation and the skin decreases due to the relatively lower saturation solubility of micro-sized crystals. The skin penetration of caffeine decreases as well. On contrary, decreased ethanol content in the formulation slows down the evaporation of the medium, which helps to maintain a constant particle size (or only slight increase in particle size) of caffeine nanocrystals and correspondingly constant skin penetration (Figure 6-9,

lower right). This is especially the case, when the second compound in the solvent mixture is not water but an even slower evaporating glycol.

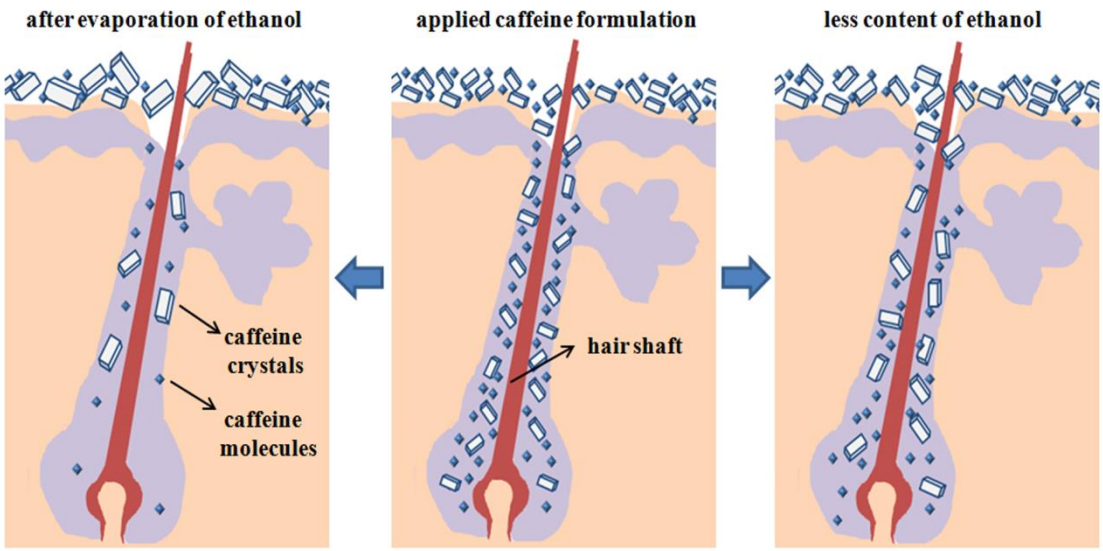

Figure 6-10: The concept to decrease ethanol content in caffeine nanosuspension: caffeine nanocrystals can accumulate in hair follicles, increasing the penetration into surrounding cells (middle); evaporation of ethanol leads to the formation of bigger nanocrystals or even micro-sized crystals which can not sufficiently accumulate in hair follicles (left); decreased ethanol content helps to maintain a constant crystal size and sufficient accumulation in hair follicles (right).

Caffeine nanocrystals with optimal particle size around 700 nm can accumulate in hair follicles, increasing the penetration into surrounding cells (Figure 6-10, middle). After application of high ethanol-content caffeine nanosuspension onto the skin, ethanol evaporates very fast. Supersaturation effects lead to pronounced crystal growth even to micro size. Particles larger than 900 nm show little flow into the hair follicles or can only accumulate in the upper infundibulum part (Figure 6-10, left). Skin penetration of caffeine decreases if the hair follicle penetration is reduced or even suspended. Decreased ethanol content helps to maintain constant crystal size, sufficient accumulation in hair follicles and increased skin penetration (Figure 6-10, right). In previous experiments, formulations possessing a lower ethanol content were also developed, i.e. water-ethanol mixtures in ratios of 3:7 and 5:5 were used as dispersion medium. However, even with 70% ethanol, the resulting caffeine nanocrystals were not stable for 24 hours. Agglomerations and micro-sized crystals

emerged immediately after production as higher water content increased the solubility of caffeine and facilitated the Ostwald ripening process (in section 6.3.2.2). Thus it is essential to develop formulations applying dispersion medium with lower solubility and reduced Ostwald ripening effect, identically also with lower evaporation velocity.

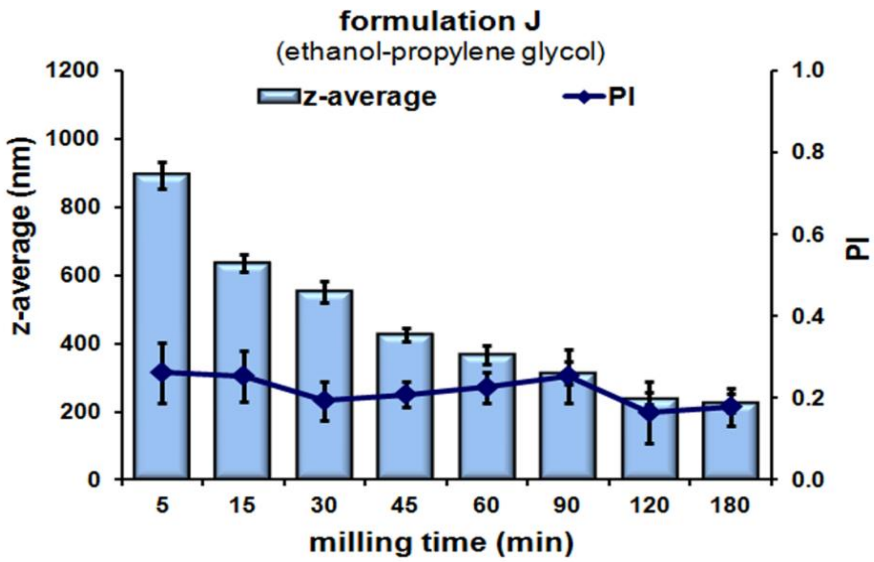

Figure 6-11: Caffeine nanocrystals produced by PM: particle size reduction as function of milling time. Ethanol-propylene glycol mixture in a ratio of 3:7 was used as dispersion medium (stabilizer: 2% Carbopol® 981). Z-average and PI were obtained by PCS immediately after production.

Propylene glycol is one of the most widely used ingredients in cosmetics. It is also used in foods and pharmaceuticals. Propylene Glycol is a skin conditioning agent that has the ability to attract water and acts as a moisturizer in cosmetic products (Fiume et al., 2012). Propylene glycol possesses a boiling point of approximately 188°C and evaporates much slower than ethanol and water under the same condition. On the other hand, the skin penetration of caffeine solution (2.5% w/w, in ethanol-propylene glycol mixture 3:7) has already been estimated in human (Sindy Trauer et al., 2009). The role of hair follicles in the percutaneous absorption of caffeine was also investigated (Otberg et al., 2008). It will be helpful to verify whether caffeine nanosuspension is really superior to the caffeine solution by using the same medium. Thus ethanol-propylene glycol mixture in a ratio of 3:7 was applied as dispersion medium for the production of caffeine nanosuspension. PCS data shows constant

reduction in the particle size starting from the first 5 minutes of milling (Figure 6-11). After 15 minutes caffeine nanocrystals with a particle size of 635 nm and a PI of 0.217 were obtained. At the end of the milling process, the smallest particle size of 220 nm was observed. No agglomerations were detected by investigating the withdrawn samples under light microscope. Compared with the results obtained from water-ethanol dispersed formulations, ethanol-propylene glycol dispersed formulation represented generally smaller particle size and narrower size distribution.

6.3.3 Saturation solubility

From a chemical or a thermodynamic point of view, each compound has only one constant solubility value at a fixed pressure and temperature. The thermodynamic solubility is the concentration of the substance in solution at equilibrium state in the presence of undissolved powder. The kinetic or apparent solubility is higher than the thermodynamic solubility, e.g. achieved by the amorphous state of powders or by size reduction (Saal and Petereit, 2012). The kinetic solubility is physically instable, and after an infinite equilibrium time it will decrease to the level of the constant thermodynamic solubility by precipitation of crystals.

The kinetic saturation solubility of caffeine nanocrystals was investigated over 7 days. As predicted before, the solubility of caffeine was increased by nanonization of coarse powder (Figure 6-12). The kinetic solubility of two bathes water-ethanol dispersed caffeine nanocrystals (660 nm and 250 nm) were 23.9 ± 0.7 mg/ml and 29.2 ± 0.9 mg/ml, respectively. These were distinctly higher than that of caffeine coarse powder (17.5 ± 0.7 mg/ml). The equilibrium of the solubility was achieved after 6 hours for all tests. The fluctuations in solubility within the first several hours could be due to the supersaturation effect and later on the precipitation.

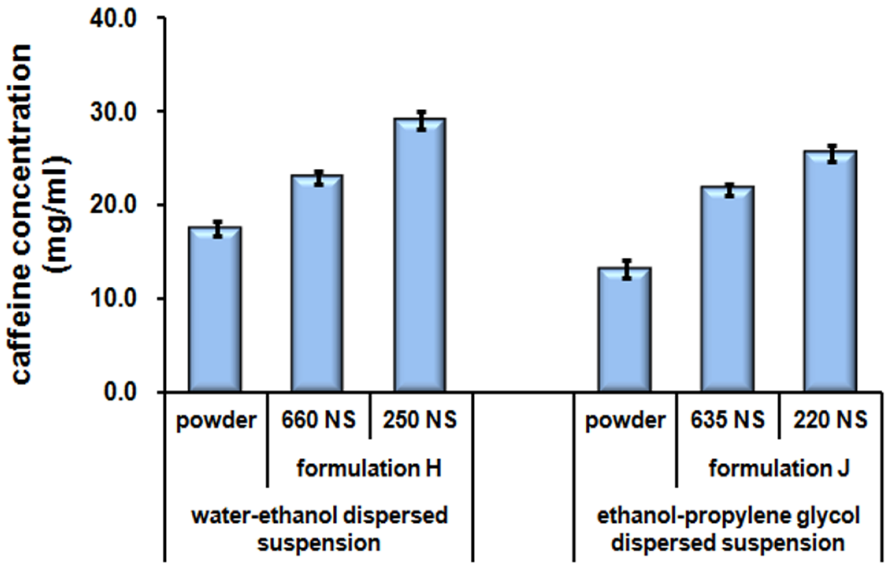

Figure 6-12: Saturation solubility of water-ethanol (1:9) dispersed nanocrystals and ethanol-propylene glycol (3:7) dispersed nanocrystals in original dispersion medium. Two batches of each formulation with different particle size generated by different milling times (30 minutes and 180 minutes, respectively), were investigated. The solubility of caffeine coarse powder was also investigated and compared. (Powder: caffeine coarse powder; NS: caffeine nanocrystals; the number refers to the particle size with a unit of nm).

Similar phenomena were observed with ethanol-propylene glycol dispersed caffeine nanocrystals. The solubility results were generally slightly lower than that of water-ethanol dispersed ones, e.g. 20.3 $\pm$0.6 mg/ml for 635 nm nanocrystals and 24.2 $\pm$0.9 mg/ml for 220 nm nanocrystals (Figure 6-12). It is generally acknowledged that the reduction of the particle size to the nanometer range can improve the kinetic saturation solubility of the substance. As with caffeine, the increase in solubility is only around 35% by 660 nm nanocrystals and 70% by generating 250 nm nanocrystals, dispersed in water-ethanol mixture. The increase is not as high as reported for other compounds, e.g. increase by a factor of 500 for coenzyme Q_{10} nanocrystals (Mauludin et al., 2008). However, the limited improvement in solubility will still benefit the application of caffeine nanocrystals in a dermal formulation as dissolving depot. Certain amount of nanocrystal state caffeine should be maintained in the formulation to be dissolved to maintain a constant concentration gradient (Figure 6-1).

6.3.4 Short term stability

Figure 6-13 shows the PCS mean diameters of the three differently stabilized nanosuspensions at the three storage temperatures. As PVP 40 was not efficient enough to stabilize the caffeine nanosuspension during pearl milling, the stability data of PVP 40 present predicted results. At all three storage temperatures, particle size increased considerably along with the PI. Similar results were observed for Tween® 80 stabilized formulation, although it has proven to be optimal during the production of caffeine nanosuspension. Carbopol® 981 stabilized nanosuspensions showed practically unchanged PCS diameters when stored at both 4°C and 25°C during the first month. Only negligible increase in particle size was observed after two months. Continuous increase in particle size and PI was observed when stored at stress condition of 40°C. The solubility of caffeine is reported to be substantially temperature dependent. Storage at 40°C increases its solubility, thus the crystal size could be reduced due to the dissolution of the nanocrystals. For example, the thermodynamic solubility of caffeine in water is 2.0 g/100 ml at room temperature and 4.4 g/100 ml at 40°C (Shalmashi and Golmohammad, 2010). The differences are even more pronounced in the nano size range.

However, according to the Ostwald ripening theory, the smaller crystals will dissolve or even disappear, while the larger ones remain or even grow up to micro size, leading to an increase in mean particle size. Smaller crystals possess relatively higher solubility therefore the growth rate of the particle size was even higher for 250 nm nanocrystals compared with the 660 nm ones, which is perfectly in line with the theory.

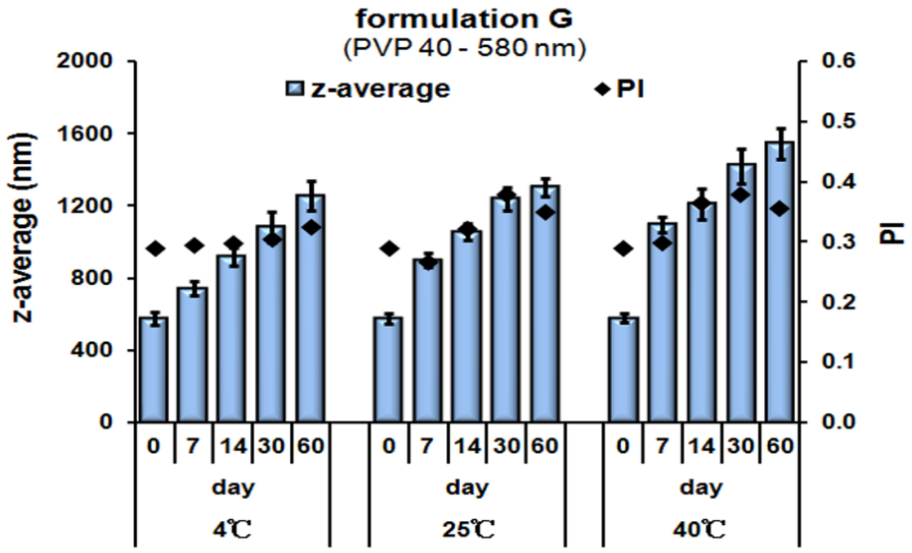
formulation G
(PVP 40 - 580 nm)
z-average
PI
z-average (nm)
PI
2000
1600
1200
800
400
0
0.6
0.5
0.4
0.3
0.2
0.1
0.0
0 7 14 30 60
day
4℃
25℃
40℃

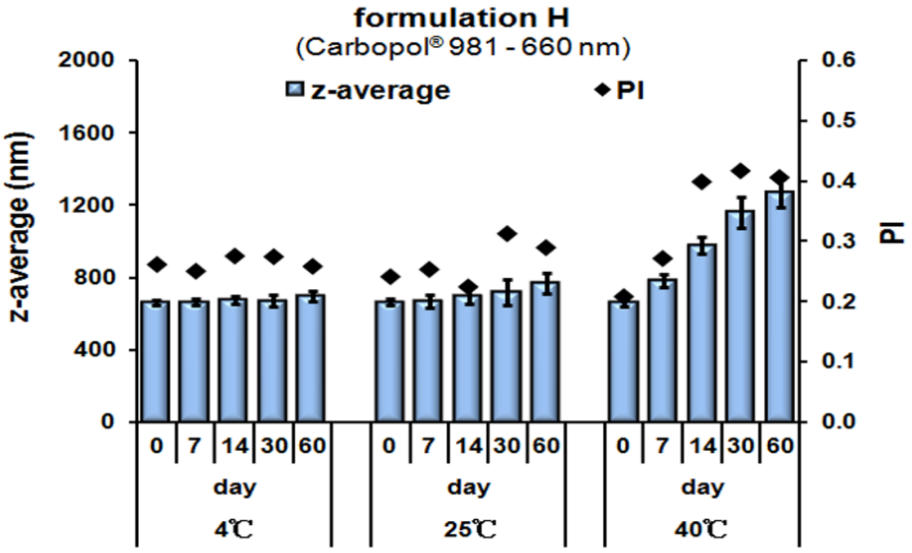
formulation H
(Carbopol® 981 - 660 nm)
z-average
PI
z-average (nm)
PI
2000
1600
1200
800
400
0
0.6
0.5
0.4
0.3
0.2
0.1
0.0
0 7 14 30 60
day
4℃
25℃
40℃

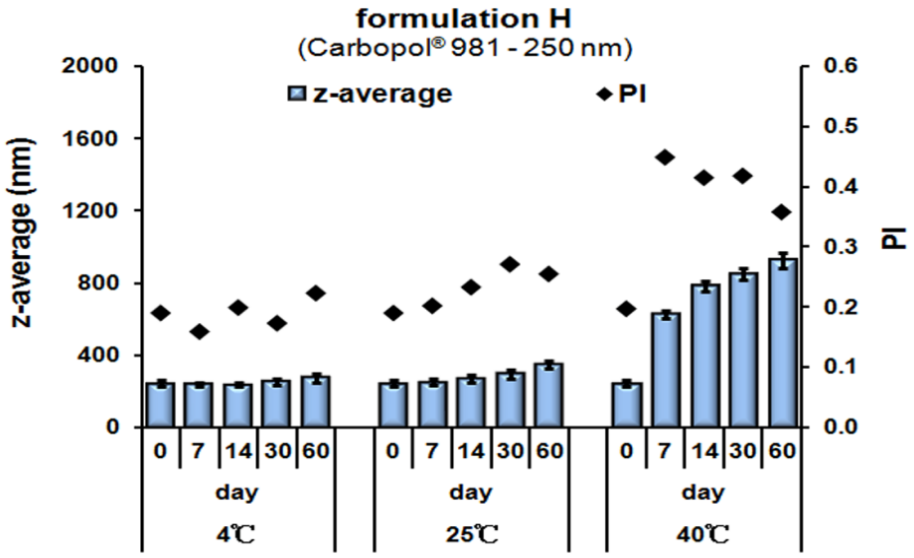

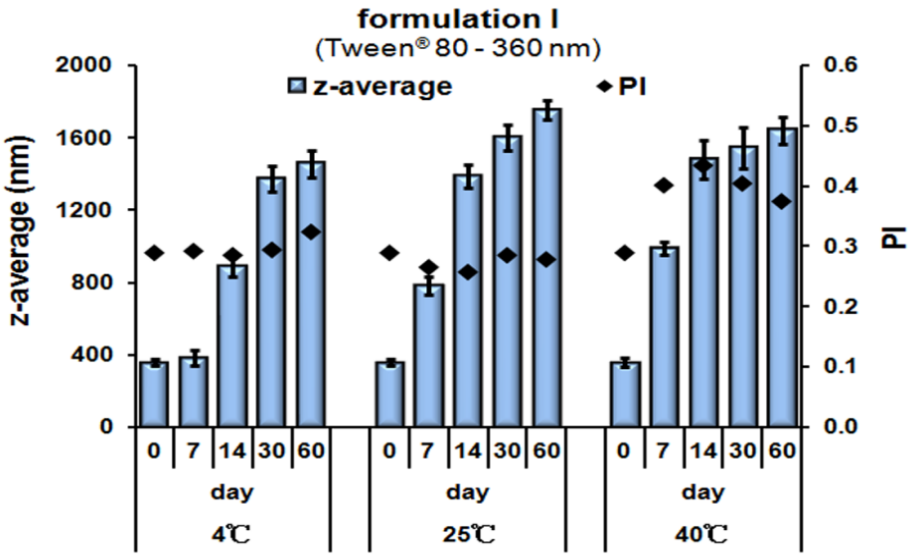

Figure 6-13: Short term stability test of caffeine nanocrystals produced by PM over a time period of two months at three different temperatures. Three formulations (G to I) stabilized with PVP 40, Carbopol® 981 and Tween® 80, respectively, were investigated (dispersion medium: water-ethanol 1:9). For Carbopol® 981 stabilized nanocrystals, two batches with sizes of 660 nm and 250 nm, generated by different milling times (30 minutes and 180 minutes, respectively), were investigated. Particle size analysis was performed by PCS.

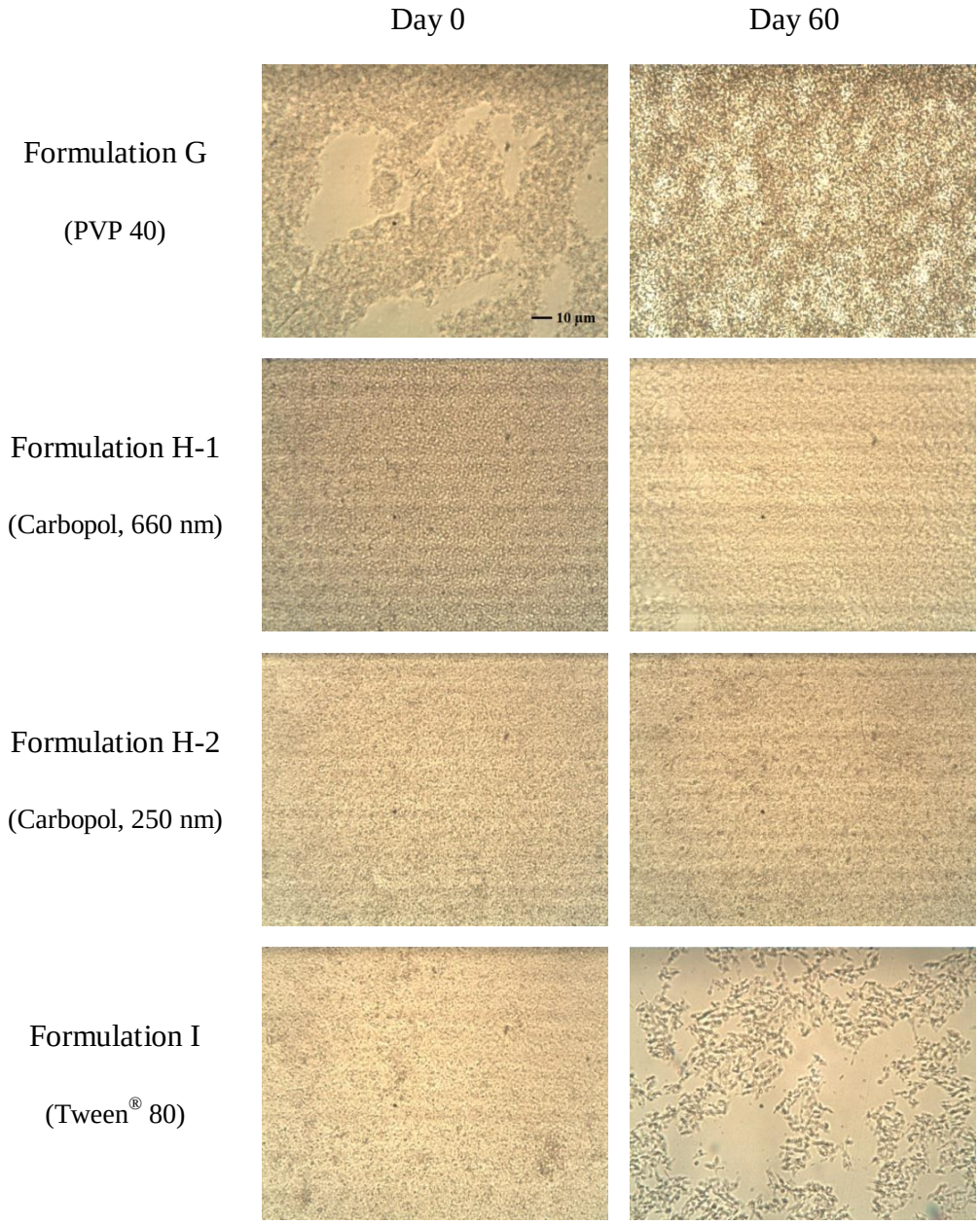

Figure 6-14: Light microscopy pictures of caffeine nanocrystals produced by PM, on the day of production (day 0) and after two months storage (day 60) at 25°C (magnification 630 ×; bar = 10 µm). Formulation H stabilized with Carbopol® 981 possessed the best physical stability, as no agglomeration or big crystals was observed in both two batches of caffeine nanocrystals (660 nm and 250 nm).

Via microscopic investigation directly after production and after two months of storage at 25°C, it can be clearly seen that there were no microcrystals or apparent agglomerations in the presence of Carbopol® 981 (Figure 6-14). However, in PVP 40 stabilized nanosuspension agglomerations could be found directly after production

and the Tween® 80 stabilized nanosuspension showed agglomerations after two months storage at 25°C. This confirms the results obtained by PCS measurements, that Carbopol® 981 is a very efficient stabilizer for the production and stabilization of caffeine nanocrystals.

Carbopol® 981 consists of cross-linked acrylic acid and has been commonly used in controlled release formulations as gelling agent or viscosity enhancer. Once dispersed in water, the acrylic acids can be deprotonated and the tightly coiled acidic molecules begin to hydrate and partially uncoil due to electrostatic repulsion. When an appropriate neutralizer is added, maximum thickening effect could be observed (Grażyna, 2009). In the present study, even without neutralization, the partially uncoiled structure of Carbopol® 981 provides sufficient steric effect for the stabilization of caffeine nanosuspension. In the case of multifunctional caffeine, there are several sites which could be protonated including the oxygen of carbonyl groups and the nitrogen of imine group (Bahrami et al., 2013). The ability to protonate and positively charge newly created crystal surfaces, consequently enhance their interactions with deprotonated carboxyl groups of Carbopol® 981 could be the reason why only this polymer presented satisfactory performance in the stabilization of caffeine nanosuspension.

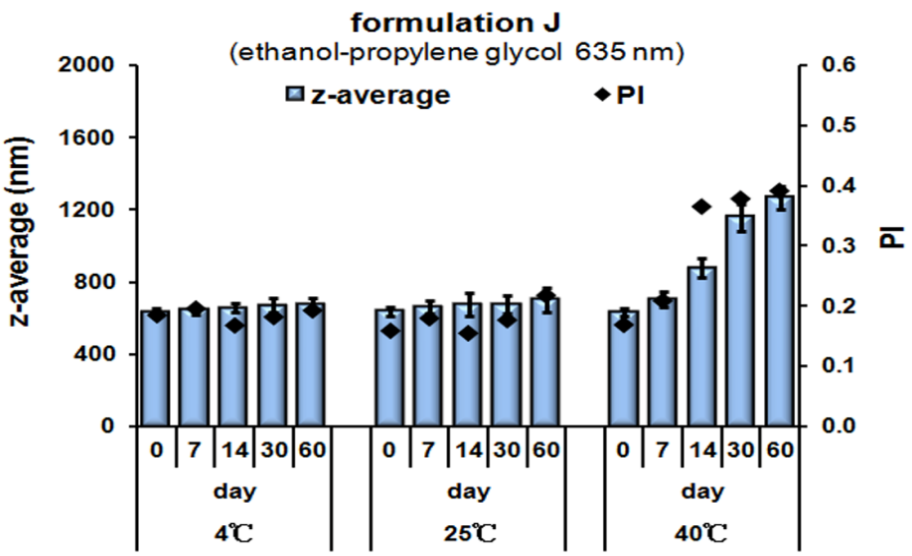

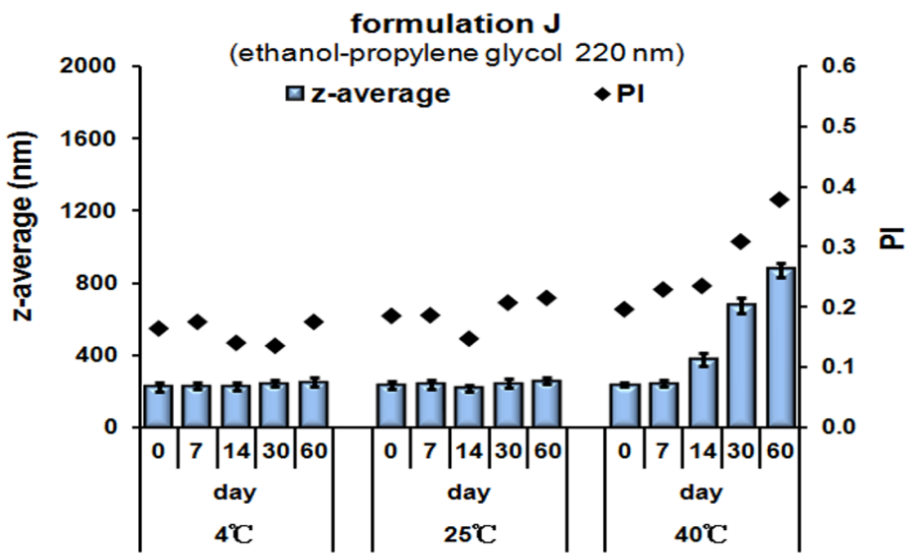

Figure 6-15: Short term stability test of ethanol-propylene glycol dispersed caffeine nanocrystals (stabilizer: 2% Carbopol® 981). Two batches with sizes of 635 nm and 220 nm, generated by different milling times (15 and 180 minutes, respectively), were investigated. Particle size analysis was performed by PCS.

Stability of two batches of ethanol-propylene glycol dispersed caffeine nanocrystals was also investigated. As depicted in Figure 6-15, particle size and PI of two batches caffeine nanocrystals remained stable after two months when stored at both 4 and 25°C. Increase in particle size was only observed when stored at 40°C after two weeks. The results of the light microscopy evaluation confirmed the data obtained by PCS measurements. No microcrystals or apparent agglomerations were observed for both two bathes nanocrystals when stored at 25°C for two months (Figure 6-16).

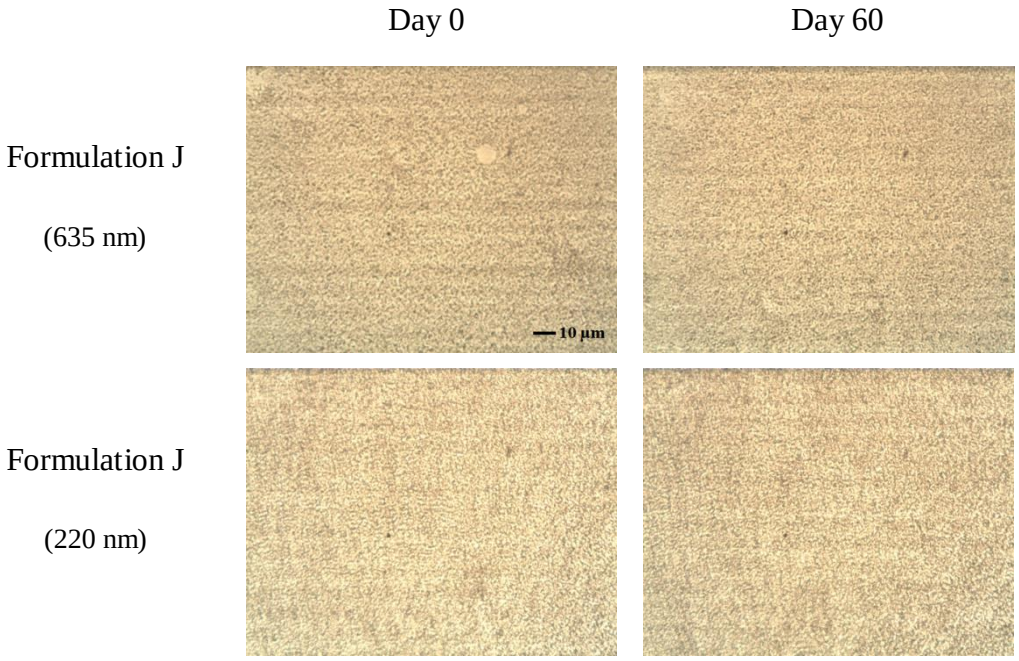

Figure 6-16: Light microscopy pictures of ethanol-propylene glycol dispersed caffeine nanocrystals (stabilizer: 2% Carbopol® 981), on the day of production (day 0) and after two months storage (day 60) at 25°C (magnification 630 ×; bar = 10 µm). Two batches with sizes of 635 nm and 220 nm, generated by different milling times (15 and 180 minutes, respectively), were investigated.

Compared with water-ethanol dispersed caffeine nanocrystals the ethanol-propylene glycol dispersed ones possessed even better stability. This was due to the fact that the solubility of caffeine in ethanol-propylene glycol mixture (3:7) was 13.2 ± 0.6 mg/ml which was relatively lower than in water-ethanol mixture (1:9). In addition, ethanol-propylene glycol dispersed caffeine nanosuspensions possess narrower size distributions as the PI values are lower than 0.2 after production. All these points help to slow down the Ostwald ripening process as illustrated in section 6.3.2.2.

6.4 Conclusions

As demonstrated by caffeine, not only nanocrystals of poorly soluble but also medium soluble actives can be produced. Crystal growth caused by supersaturation effects can be eliminated by appropriate production conditions (e.g. low energy process, low dielectric constant of dispersion medium and optimal stabilizers). Nanocrystals with varied sizes can now be produced in a controlled process, e.g. 660 nm (optimal for

hair follicle accumulation) to 250 nm (optimal for fast dissolution). Essential next step is to verify whether the performance of the nanocrystal suspension on human skin is really superior to a caffeine solution. If yes – this principle & production method could be applied to other medium soluble actives and introduced as a novel dermal delivery concept.

7 Summary

1. Production and characterization of ultrafine GNPs

Several parameters of the classical two-step desolvation technique including the starting gelatin concentration, the precipitation time, the pH value, the desolvation temperature and the desolvating agent were optimized. Ultrafine GNPs were successfully produced by the modified two-step desolvation technique. The preparation temperature can be lowered to 40°C, which facilitates the application of GNPs as carriers for proteins and peptides. The *in vitro* characterization results showed that GNPs possess spherical conformation with a mean particle size of 56 ± 4 nm. A good compatibility of GNPs with different gels was observed, as the particle size and PI remained stable after incorporation into a variety of gels over one month. The results of the long term stability test indicated Euxyl® PE 9010 to be an optimal preservative for GNPs based dermal formulations.

2. Ultrafine GNPs versus traditional GNPs: characterization and comparison using lysozyme as model enzyme

Ultrafine GNPs were produced by the modified two-step desolvation technique developed in the preceding chapter while traditional GNPs were produced via the classical desolvation method. Lysozyme loading was performed at different production steps of GNPs. Limited increase in particle size was observed when drug loading was performed at the second desolvation step or after formation of particles. Whereas for both ultrafine and traditional GNPs, the first desolvation step was demonstrated to be an inappropriate choice for drug loading as noticeable increase in particle size was observed. The results of the *in vitro* characterization demonstrated ultrafine GNPs to be a more promising delivery system for dermal application of enzymes. Compared to traditional GNPs, ultrafine GNPs possess smaller particle size, higher drug loading capacity, faster drug release and preserved biological activity of lysozyme. A fast drug release was observed when drug loading was performed after the formation of GNPs, as lysozyme molecules were mainly adsorbed onto the particle surface. A biphasic pattern of drug release was observed when drug loading was performed prior to the formation of particles. The initial burst is due to desorption of surface associated lysozyme and the prolonged release is due to the release of lysozyme from particle matrix. The lower drug loading capacity and much slower

drug release of traditional GNPs are due to the large particle size and smaller specific surface area compared to ultrafine GNPs.

3. Production and characterization of caffeine nanocrystals

A novel concept was introduced for the first time to transfer medium soluble actives into nanocrystals for dermal application, utilizing the depot function of nanocrystals. Caffeine nanocrystals were produced by both high pressure homogenization and low energy pearl milling. Pronounced crystals growth was observed due to supersaturation effects when applying high energy homogenization technique. Caffeine nanocrystals with particle size of 660 nm (optimal for hair follicle accumulation) or 250 nm (with high C_s and dissolution velocity) were obtained by pearl milling generated by different milling times. Several stabilizers were evaluated and Carbopol® 981 showed the best stabilization effect. This is due to the steric effect caused by the uncoiled acrylic acid molecules. Furthermore, Carbopol® 981 can protonate and positively charge crystal surfaces. Thus electrical repulsion also contributes to the stabilization of caffeine nanosuspension. A variety of water-ethanol mixtures and ethanol-propylene glycol mixture were applied as dispersion medium. The dispersed caffeine nanosuspension possessed better physical stability with ethanol-propylene glycol in a ratio of 7:3 compared to the water-ethanol dispersed ones due to the lower solubility of caffeine in the medium and consequently reduced Ostwald ripening process.

8 Zusammenfassung

1. Herstellung und Charakterisierung ultrafeiner GNPs

Mehrere Parameter der klassischen Zwei-Stufen-Desolvatisierungstechnik, wie die Ausgangskonzentration der Gelatine, die Fällungszeit, der pH-Wert, die Temperatur der Desolvatisierung und die Auswahl des Desolvatisierungsmittels wurden variiert und optimiert um ultrafeine GNPs erfolgreich herzustellen. Die Ergebnisse der in vitro Untersuchungen zeigten eine kugelförmige Form GNPs mit einer mittleren Teilchengröße von 56 ± 4 nm. Nach Einarbeiten der GNPs in verschiedene Gelgrundlagen blieben sowohl die Teilchengröße als auch der PdI über einen Monat stabil, wodurch eine gute Kompatibilität der GNPs mit verschiedenen Gelgrundlagen nachgewiesen werden konnte. Die Ergebnisse der Studie zur Ermittlung der Langzeitstabilität zeigten, dass Euxyl® PE 9010 das optimale Konservierungsmittel für GNP basierte dermale Formulierungen ist.

2. Charakterisierung und Vergleich von ultrafeinen GNPs und herkömmlichen GNPs beladen mit Lysozym als Modellenzym

Ultrafeine GNPs wurden durch die modifizierte Zwei-Stufen-Desolvatisierungstechnik, welche im vorhergehenden Kapitel entwickelt wurde, produziert. Die traditionellen GNPs hingegen wurden unverändert über den klassischen Weg hergestellt. Die Beladung mit dem Modellenzym Lysozym erfolgte bei verschiedenen Produktionsschritten der GNPs. Eine geringe Zunahme der Partikelgröße konnte dann beobachtet werden, wenn die Wirkstoffbeladung bei dem zweiten Schritt der Desolvatisierung oder nach der Ausbildung der Partikel erfolgte. Die Zugabe des Lysozyms im ersten Stritt der Desolvatisierung dagegen zeigte sowohl bei der Zwei-Stufen-Desolvatisierungstechnik als auch beim klassischen Produktionsverfahren der GNPs eine deutliche Zunahme der Partikelgrößen und wurde folglich als ungeeigneter Zeitpunkt zur Wirkstoffbeladung ermittelt. Die Ergebnisse der in vitro Charakterisierung haben gezeigt, dass ultrafeine GNPs ein vielversprechendes Abgabesystem für die dermale Anwendung von Enzymen ist. Im Vergleich zu herkömmlichen GNPs, besitzen sie kleinere Partikelgrößen, eine höhere Beladbarkeit mit Wirkstoffen, eine schnellere Wirkstofffreisetzung und die Möglichkeit der Konservierung von biologisch aktivem Lysozym.

3. Herstellung und Charakterisierung von Koffeinnanokristallen

Erstmals wurde ein Verfahren zur Produktion von Nanokristallen mittellöslicher Wirkstoffe entwickelt und angewandt um von der bekannten Depotwirkung der Nanokristalle zu profitieren. Koffeinnanokristalle wurden sowohl durch die Hochdruckhomogenisation als auch durch die Perlenmühle hergestellt. Bei der Produktion mittels Hochdruckhomogenisation konnte aufgrund der hohen Energiezufuhr ein Übersättigungseffekt beobachtet werden, einhergehend mit starkem Wachstum der Kristalle. Mithilfe der Perlenmühle, ein Verfahren mit geringer Energiezufuhr, konnten erfolgreich durch Variation der Mahlzeit Koffeinnanokristalle mit Partikelgrößen von 660 nm (optimal für die Akkumulation in Haarfollikeln) oder 250 nm (mit höherer Sättigungskonzentration und Auflösungsgeschwindigkeit) hergestellt werden. Mehrere Stabilisatoren wurden untersucht, wobei Carbopol® 981 den besten Stabilisierungseffekt zeigte. Die ungewundenen Acrylsäuremoleküle sorgen für eine sterische Stabilisierung. Darüber hinaus besitzt Carbopol® 981 die Fähigkeit zur Protonierung und bewirkt dadurch eine positive Aufladung der Kristalloberflächen. Eine elektrische Abstoßung trägt somit ebenfalls zur Stabilisierung der Suspension bei. Wasser-Ethanol Mischungen in variierenden Volumenverhältnissen und ein Ethanol-propylenglykol Gemisch wurden auf ihre Tauglichkeit als Dispersionsmedium untersucht. In einem Gemisch aus Ethanol und Propylenglykol, in einem Volumenverhältnis von 3 zu 7, suspendierte Koffeinnanokristalle besaßen eine bessere physikalische Stabilität als in einem Gemisch aus Wasser und Ethanol aufgrund der geringeren Löslichkeit von Koffein im erstgenannten Medium und dadurch reduzierten Ostwald Reifung.

9 References

Arroyo-Maya, I.J., Rodiles-Lopez, J.O., Cornejo-Mazon, M., Gutierrez-Lopez, G.F., Hernandez-Arana, A., Toledo-Nunez, C., Barbosa-Canovas, G.V., Flores-Flores, J.O., Hernandez-Sanchez, H., 2012. Effect of different treatments on the ability of alpha-lactalbumin to form nanoparticles. J Dairy Sci 95, 6204-6214.

Azarmi, S., Huang, Y., Chen, H., McQuarrie, S., Abrams, D., Roa, W., Finlay, W.H., Miller, G.G., Lobenberg, R., 2006. Optimization of a two-step desolvation method for preparing gelatin nanoparticles and cell uptake studies in 143B osteosarcoma cancer cells. J Pharm Pharm Sci 9, 124-132.

Bahrami, H., Tabrizchi, M., Farrokhpour, H., 2013. Protonation of caffeine: A theoretical and experimental study. Chem Phys 415, 222-227.

Bajpai, A.K., Choubey, J., 2006. In vitro release dynamics of an anticancer drug from swellable gelatin nanoparticles. J Appl Polym Sci 101, 2320-2332.

Barratt, G., 2003. Colloidal drug carriers: achievements and perspectives. Cell Mol Life Sci 60, 21-37.

Bolzinger, M.A., Briançon, S., Pelletier, J., Chevalier, Y., 2012. Penetration of drugs through skin, a complex rate-controlling membrane. Curr Opin Colloid In 17, 156-165.

Bourquin, C., Wurzenberger, C., Heidegger, S., Fuchs, S., Anz, D., Weigel, S., Sandholzer, N., Winter, G., Coester, C., Endres, S., 2010. Delivery of immunostimulatory RNA oligonucleotides by gelatin nanoparticles triggers an efficient antitumoral response. J Immunother 33, 935-944.

Bouwstra, J., Pilgram, G., Gooris, G., Koerten, H., Ponec, M., 2001. New aspects of the skin barrier organization. Skin Pharmacol Appl Skin Physiol 14 Suppl 1, 52-62.

Cal, C.F., Bakowsky, U., Rytting, E., Schaper, A.K., Kissel, T., 2008. Charged nanoparticles as protein delivery systems: A feasibility study using lysozyme as model protein. Eur J Pharm Biopharm 69, 31-42.

Cascone, M.G., Lazzeri, L., Carmignani, C., Zhu, Z., 2002. Gelatin nanoparticles produced by a simple W/O emulsion as delivery system for methotrexate. J Mater Sci Mater Med. 13, 523-526.

Cascone, M.G., Lazzeri, L., Carmignani, C., Zhu, Z., 2002. Gelatin nanoparticles produced by a simple W/O emulsion as delivery system for methotrexate. J Mater Sci Mater Med. 13, 523-526.

Cevc, G., 2004. Lipid vesicles and other colloids as drug carriers on the skin. Adv Drug Deliv Rev 56, 657-711.

Charalambopoulou, G.C., Karamertzanis, P., Kikkinides, E.S., Stubos, A.K., Kanellopoulos, N.K., Papaioannou, A.T., 2000. A study on structural and diffusion properties of porcine stratum corneum based on very small angle neutron scattering data. Pharm Res 17, 1085-1091.

Che, E., Zheng, X., Sun, C., Chang, D., Jiang, T., Wang, S., 2012. Drug nanocrystals: a state of the art formulation strategy for preparing the poorly water-soluble drugs. Asian J Pharm 7, 85-95.

Choia, J.Y., Yooa, J.Y., Kwakb, H.S., Namc, B.U., Lee, J., 2005. Role of polymeric stabilizers for drug nanocrystal dispersions. Curr Appl Phys 5, 472-474.

Coester, C.J., Langer, K., Von Briesen, H., Kreuter, J., 2000. Gelatin nanoparticles by two step desolvation - a new preparation method, surface modifications and cell uptake. J Microencapsul 17, 187-193.

Eerdenbrugh, B.V., Mooter, G.V.d., Augustijns, P., 2008. Top-down production of drug nanocrystals: nanosuspension stabilization, miniaturization and transformation into solid products. Int J Pharm 364, 64-75.

Elzoghby, A.O., 2013. Gelatin-based nanoparticles as drug and gene delivery systems: Reviewing three decades of research. J Control Release 172, 1075-1091.

Elzoghby, A.O., Samy, W.M., Elgindy, N.A., 2012. Protein-based nanocarriers as promising drug and gene delivery systems. J Control Release. 161, 38-49.

Ethirajan, A., Schoeller, K., Musyanovych, A., Ziener, U., Landfester, K., 2008. Synthesis and optimization of gelatin nanoparticles using the miniemulsion process. Biomacromolecules 9, 2383-2389.

Farris, S., Song, J., Huang, Q., 2010. Alternative reaction mechanism for the cross-linking of gelatin with glutaraldehyde. J Agric Food Chem 58, 998-1003.

Farrugia, C.A., Groves, M.J., 1999. Gelatin behaviour in dilute aqueous solution: designing a nanoparticulate formulation. J Pharm Pharmacol 51, 643-649.

Fiume, M.M., Bergfeld, W.F., Belsito, D.V., Hill, R.A., Klaassen, C.D., Liebler, D., Marks, J.J., Shank, R.C., Slaga, T.J., Snyder, P.W., Andersen, F.A., 2012. Safety assessment of propylene glycol, tripropylene glycol, and PPGs as used in cosmetics. Int J Toxicol 31, 245-260.

Flory, P.J., Weaver, E.S., 1960. Helix coil transitions in dilute aqueous collagen solutions. J Am Chem Soc 82, 4518-4525.

Fratus, M., 2011. Development and characterization of caffeine nanocrystals for dermal delivery. Diploma dissertation, Freie Universität Berlin.

Gady, B., Schleef, D., Reifenberger, R., Rimai, D., Demejo, L.P., 1996. Identification of electrostatic and van der Waals interaction forces between a micrometer-size sphere and a flat substrate. Phys Rev B 15, 8065-8070.

Gaihre, B., Aryal, S., Khil, M.S., Kim, H.Y., 2008. Encapsulation of Fe_3O_4 in gelatin nanoparticles: effect of different parameters on size and stability of the colloidal dispersion. J Microencapsul 25, 21-30.

Goswami, S., Bajpai, J., Bajpai, A.K., 2010. Designing gelatin nanocarriers as a swellable system for controlled release of insulin: an in-vitro kinetic study. J Macromol Sci 47, 119-130.

Grażyna, S., 2009. The effect of various types of Carbopol and different neutralizing bases on pharmaceutical availability of morphine hydrochloride from hydrogel preparations. Polim Med 39, 25-37.

Hadgraft, J., 2001. Modulation of the barrier function of the skin. Skin Pharmacol Appl Skin Physiol 14 Suppl 1, 72-81.

Hoffmann, F., Sass, G., Zillies, J., Zahler, S., Tiegs, G., Hartkorn, A., Fuchs, S., Wagner, J., Winter, G., Coester, C., Gerbes, A.L., Vollmar, A.M., 2009. A novel technique for selective NF-kappaB inhibition in Kupffer cells: contrary effects in fulminant hepatitis and ischaemia-reperfusion. Gut 58, 1670-1678.

Jahanshahi, M., Sanati, M.H., Hajizadeh, S., Babaei, Z., 2008. Gelatin nanoparticle fabrication and optimization of the particle size. Phys Status Solidi A 205, 2898-2902.

Jain, A., Gulbake, A., Shilpi, S., Hurkat, P., Jain, S.K., 2012. Development of surface-functionalised nanoparticles for FGF2 receptor-based solid tumour targeting. J Microencapsul 29, 95-102.

Junghanns, J.U., Müller, R.H., 2008. Nanocrystal technology, drug delivery and clinical applications. Int J Nanomedicine 3, 295-309.

Kakran, M., Shegokar, R., Sahoo, N.G., Gohla, S., Li, L., Muller, R.H., 2012. Long-term stability of quercetin nanocrystals prepared by different methods. J Pharm Pharmacol 64, 1394-1402.

Kakran, M., Shegokar, R., Sahoo, N.G., Shaal, L.A., Li, L., Muller, R.H., 2012. Fabrication of quercetin nanocrystals: comparison of different methods. Eur J Pharm Biopharm 80, 113-121.

Karthikeyana, S., Prasada, N.R., A. Ganamanib, Balamurugana, E., 2013. Anticancer activity of resveratrol-loaded gelatin nanoparticles on NCI-H460 non-small cell lung cancer cells. Biomedicine & Preventive Nutrition 3, 64-73.

Kaul, G., Amiji, M., 2002. Long-circulating polyethylene glycol)-modified gelatin nanoparticles for intracellular delivery. Pharm Res-Dord 19, 1061-1067.

Kawai, K., Suzuki, S., Tabata, Y., Ikada, Y., Nishimura, Y., 2000. Accelerated tissue regeneration through incorporation of basic fibroblast growth factor-impregnated gelatin microspheres into artificial dermis. Biomaterials 21, 489-499.

Keck, C.M., 2006. Cyclosporine Nanosuspensions: optimised size characterisation & oral formulations. Doctoral dissertation, Freie Universität Berlin.

Keck, C.M., Müller, R.H., 2006. Drug nanocrystals of poorly soluble drugs produced by high pressure homogenisation. Eur J Pharm Biopharm 62, 3-16.

Khan, S., Pace, G.W., 2002. Composition and method of preparing microparticles of water-insoluble substances, US patent, 6337092.

Knorr, F., Lademann, J., Patzelt, A., Sterry, W., Blume-Peytavi, U., Vogt, A., 2009. Follicular transport route - research progress and future perspectives. Eur J Pharm Biopharm 71, 173-180.

Kobierski, S., Ofori-Kwakye, K., Muller, R.H., Keck, C.M., 2011. Resveratrol nanosuspensions: interaction of preservatives with nanocrystal production. Pharmazie 66, 942-947.

Kommareddy, S., Shenoy, D.B., Amiji, M.M., 2005. Gelatin nanoparticles and their biofunctionalization. Nanotechnologies for the Life Sciences, Vol. 1 Biofunctionalization of Nanomaterials, 330-352.

Kuo, W.T., Huang, H.Y., Chou, M.J., Wu, M.C., Huang, Y.Y., 2011. Surface modification of gelatin nanoparticles with polyethylenimine as gene vector. J Nanomater, 1-5.

Lademann, J., Patzelt, A., Schanzer, S., Richter, H., Thiede, G., Havlickova, B., Günther, C., Friedrich, M., Sterry, W., Fluhr, J.W., Seifert, S., 2012. Non-invasive analysis of penetration and storage of Isoconazole nitrate in the stratum corneum and the hair follicles. Eur J Pharm Biopharm 80, 615-620.

Lademann, J., Otberg, N., Richter, H., Weigmann, H.J., Lindemann, U., Schaefer, H., Sterry, W., 2001. Investigation of follicular penetration of topically applied substances. Skin Pharmacol Appl 14, 17-22.

Lademann, J., Richter, H., Teichmann, A., Otberg, N., Blume-Peytavi, U., Luengo, J., Weiss, B., Schaefer, U.F., Lehr, C.M., Wepf, R., Sterry, W., 2007. Nanoparticles - An efficient carrier for drug delivery into the hair follicles. Eur J Pharm Biopharm 66, 159-164.

Langer, K., Balthasar, S., Vogel, V., Dinauer, N., von Briesen, H., Schubert, D., 2003. Optimization of the preparation process for human serum albumin (HSA) nanoparticles. Int J Pharm 257, 169-180.

Lee, E.J., Khan, S.A., Park, J.K., Lim, K.H., 2012. Studies on the characteristics of drug-loaded gelatin nanoparticles prepared by nanoprecipitation. Bioproc Biosystems Eng 35, 297-307.

Lee, S., 2011. Solute-solvent interactions in folded and unfolded proteins. Doctoral dissertation, University of Toronto.

Leo, E., Cameroni, R., Forni, F., 1999. Dynamic dialysis for the drug release evaluation from doxorubicin-gelatin nanoparticle conjugates. Int J Pharm 180, 23-30.

Li, J.K., Wang, N., Wu, X.S., 1998. Gelatin nanoencapsulation of protein/peptide drugs using an emulsifier-free emulsion method. J Microencapsul 15, 163-172.

Li, W.M., Liu, D.M., Chen, S.Y., 2011. Amphiphilically-modified gelatin nanoparticles: Self-assembly behavior, controlled biodegradability, and rapid cellular uptake for intracellular drug delivery. J Mater Chem 21, 12381-12388.

Liang, M.T., Davies, N.M., Blanchfield, J.T., Toth, I., 2006. Particulate systems as adjuvants and carriers for peptide and protein antigens. Curr Drug Deliv 3, 379-388.

Liao, Y.H., Brown, M.B., Martin, G.P., 2001. Turbidimetric and HPLC assays for the determination of formulated lysozyme activity. J Pharm Pharmacol 53, 549-554.

Liversidge, G.G., Cundy, K.C., 1995. Particle size reduction for improvement of oral bioavailability of hydrophobic drugs: I. Absolute oral bioavailability of nanocrystalline danazol in beagle dogs. Int J Pharmaceut 125, 91-97.

Liversidge, G.G., Cundy, K.C., Bishop, J.F., Czekai, D.A., 1992. Surface modified drug nanoparticles. US patent, 5145684.

Lu, Z., Yeh, T.K., Tsai, M., Au, J.L., Wientjes, M.G., 2004. Paclitaxel-loaded gelatin nanoparticles for intravesical bladder cancer therapy. Clin Cancer Res 10, 7677-7684.

M. Rajan, V.R., 2013. Formation and characterization of chitosan-polylacticacid-polyethylene glycol-gelatin nanoparticles: a novel biosystem for controlled drug delivery. Carbohydr Polym 98, 951-958.

Magadala, P., Amiji, M., 2008. Epidermal growth factor receptor-targeted gelatin-based engineered nanocarriers for DNA delivery and transfection in human pancreatic cancer cells. AAPS J 10, 565-576.

Marty, J.J., Oppenheim, R.C., Speiser, P., 1978. Nanoparticles - a new colloidal drug delivery system. Pharm Acta Helv 53, 17-23.

Mauludin, R., Hommoss, A., Knauer, J., Müller, R.H., 2008. Physicochemical characteristics of lyophilised coenzyme Q10 nanocrystals, Int Symp Control Rel Bioact Mater, New York City.

Menendez-Arias, L., Gavilanes, J.G., Rodriguez, R., 1985. Amino acid sequence around the cysteine residues of pigeon egg-white lysozyme: comparative study with other type c lysozymes. Comp Biochem Physiol B 82, 639-642.

Migneault, I., Dartiguenave, C., Bertrand, M.J., Waldron, K.C., 2004. Glutaraldehyde: behavior in aqueous solution, reaction with proteins, and application to enzyme crosslinking. Biotechniques 37, 790-796 798-802.

Mohanty, B., Aswal, V.K., Kohlbrecher, J., Bohidar, H.B., 2005. Synthesis of gelatin nanoparticles via simple coacervation. J Surface Sci Technol 21, 149-160.

Morsky, P., 1983. Turbidimetric determination of lysozyme with Micrococcus lysodeikticus cells: reexamination of reaction conditions. Anal Biochem 128, 77-85.

Müller, R.H., 1996. Zetapotential und Partikelladung in der Laborpraxis-Einführung in die Theorie, praktische Meßdurchführung, Dateninterpretation. Wissenschaftliche Verlagsgesellschaft Stuttgart, 254 S.

Müller, R.H., Becker, R., Kruss, B., Peters, K., 1999. Pharmaceutical nanosuspensions for medicament administration as systems with increased saturation solubility and rate of solution. US patent, 5858410.

Müller, R.H., Gohla, S., Keck, C.M., 2011. State of the art of nanocrystals - special features, production, nanotoxicology aspects and intracellular delivery. Eur J Pharm Biopharm 78, 1-9.

Müller, R.H., Mäder, K., Krause, K., 2000. Verfahren zur schonenden Herstellung von hochfeinen Micro-/Nanopartikeln. PCT/EP00/06535.

Nahar, M., Mishra, D., Dubey, V., Jain, N.K., 2008. Development, characterization, and toxicity evaluation of amphotericin B-loaded gelatin nanoparticles. Nanomedicine 4, 252-261.

Narayanan, D., Geena, M.G., Koyakutty, M., Nair, S., Menon, D., 2013. Poly-(ethylene glycol) modified gelatin nanoparticles for sustained delivery of the anti-inflammatory drug Ibuprofen-Sodium: an in vitro and in vivo analysis. Nanomedicine 9, 818-828.

Nezhadi, S.H., Choong, P.F., Lotfipour, F., Dass, C.R., 2009. Gelatin-based delivery systems for cancer gene therapy. J Drug Target 17, 731-738.

Noyes, A.A., Whitney, W.R., 1897. The rate of solution of solid substances in their own solutions. J Am Chem Soc 19, 930-934.

Ofokansi, K., Winte, R.G., Fricker, G., Coester, C., 2010. Matrix-loaded biodegradable gelatin nanoparticles as new approach to improve drug loading and delivery. Eur J Pharm Biopharm 76, 1-9.

Ossadnik, M., Czaika, V., Teichmann, A., Sterry, W., Tietz, H., Lademann, J., Koch, S., 2007. Differential stripping: introduction of a method to show the penetration of topically applied antifungal substances into the hair follicles. Mycoses 50, 457-462.

Otberg, N., Patzelt, A., Rasulev, U., Hagemeister, T., Linscheid, M., Sinkgraven, R., Sterry, W., Lademann, J., 2008. The role of hair follicles in the percutaneous absorption of caffeine. Br J Clin Pharmacol 65, 488-492.

Otberg, N., Richter, H., Schaefer, H., Blume-Peytavi, U., Sterry, W., Lademann, J., 2004. Variations of hair follicle size and distribution in different body sites. J Invest Dermatol 122, 14-19.

Patzelt, A., Lademann, J., 2013. Drug delivery to hair follicles. Expert Opin Drug Deliv 10, 787-797.

Patzelt, A., Richter, H., Knorr, F., Schafer, U., Lehr, C.M., Dahne, L., Sterry, W., Lademann, J., 2011. Selective follicular targeting by modification of the particle sizes. J Control Release 150, 45-48.

Peltonem, L., Hirvonen, J., 2010. Pharmaceutical nanocrystals by nanomilling: critical process parameters, particle fracturing and stabilization methods. J Pharm Pharmacol 62, 1569-1579.

Peng, Z.G., Hidajat, K., Uddin, M.S., 2004. Adsorption and desorption of lysozyme on nano-sized magnetic particles and its conformational changes. Colloid Surface B 35, 169-174.

Petersen, R., 2006. Nanocrystals for use in topical cosmetic formulations and method of production thereof. US patent, 60/8866233.

Piao, H., Kamiya, N., Hirata, A., Fujii, T., Goto, M., 2008. A novel solid-in-oil nanosuspension for transdermal delivery of diclofenac sodium. Pharm Res 25, 896-901.

Pinkus, H., 1951. Examination of the epidermis by the strip method of removing horny layers. I. Observations on thickness of the horny layer, and on mitotic activity after stripping. J Invest Dermatol 16, 383-386.

Proksch, E., Brandner, J.M., Jensen, J.M., 2008. The skin: an indispensable barrier. Exp Dermatol 17, 1063-1072.

Prow, T.W., Grice, J.E., Lin, L.L., Faye, R., Butler, M., Becker, W., Wurm, E.M., Yoong, C., Robertson, T.A., Soyer, H.P., Roberts, M.S., 2011. Nanoparticles and microparticles for skin drug delivery. Adv Drug Deliv Rev 63, 470-491.

Qazvini, N.T., Zinatloo, S., 2011. Synthesis and characterization of gelatin nanoparticles using CDI/NHS as a non-toxic cross-linking system. J Mater Sci Mater Med 22, 63-69.

Quintanar-Guerrero, D., Allemann, E., Fessi, H., Doelker, E., 1998. Preparation techniques and mechanisms of formation of biodegradable nanoparticles from preformed polymers. Drug Dev Ind Pharm 24, 1113-1128.

Rachmawati, H., Al Shaal, L., Müller, R.H., Keck, C.M., 2013. Development of curcumin nanocrystal: physical aspects. J Pharm Sci 102, 204-214.

Rizzieri, R., Mahadevan, L., Vaziri, A., Donald, A., 2006. Superficial wrinkles in stretched, drying gelatin films. Langmuir 22, 3622-3626.

Roth, C.M., Lenhoff, A.M., 1995. Electrostatic and van der Waals contributions to protein adsorption: Comparison of theory and experiment. Langmuir 11, 3500-3509.

Saal, C., Petereit, A.C., 2012. Optimizing solubility: Kinetic versus thermodynamic solubility temptations and risks. Eur J Pharm Sci 47, 589-595.

Saxena, A., Sachin, K., Bohidar, H.B., Verma, A.K., 2005. Effect of molecular weight heterogeneity on drug encapsulation efficiency of gelatin nano-particles. Colloids Surf B Biointerfaces 45, 42-48.

Schreiber, R., Gareis, H., 2007. Gelatine Handbook: Theory and Industrial Practice.

Schwick, H.G., Heide, K., 1969. Immunochemistry and immunology of collagen and gelatin. Bibl Haematol 33, 111-125.

Shaal, L.A., 2011. smartCrystals® - investigations on preparation, preservation and long-term stability. Doctoral Dissertation, Freie Universität Berlin.

Shalmashi, A., Golmohammad, F., 2010. Solubility of caffeine in water, ethyl acetate, ethanol, carbon tetrachloride, methanol, chloroform, dichloromethane, and acetone between 298 and 323 K. Lat Am appl res 40, 283-285.

Shegokar, R., Müller, R.H., 2010. Nanocrystals: industrially feasible multifunctional formulation technology for poorly soluble actives. Int J Pharm 399, 129-139.

Simonelli, A.P., Mehta, S.C., Higuchi, W.I., 1970. Inhibition of sulfathiazole crystal growth by polyvinylpyrrolidone. J Pharm Sci 59, 633-638.

Sinha, B., Müller, R.H., Moeschwitzer, J., 2013. Bottom-up approaches for preparing drug nanocrystals: Formulations and factors affecting particle size. Int J Pharm 453, 126-141.

Soppimath, K.S., Aminabhavi, T.M., Kulkarni, A.R., Rudzinski, W.E., 2001. Biodegradable polymeric nanoparticles as drug delivery devices. J Control Release 70, 1-20.

Storp, B., Engel, A., Boeker, A., Ploeger, M., Langer, K., 2012. Albumin nanoparticles with predictable size by desolvation procedure. J Microencapsul 29, 138-146.

Sussman, E.M., Clarke, M.B., Jr., Shastri, V.P., 2007. Single-step process to produce surface-functionalized polymeric nanoparticles. Langmuir 23, 12275-12279.

Teichmann, A., Jacobi, U., Ossadnik, M., Richter, H., Koch, S., Sterry, W., Lademann, J., 2005. Differential stripping: Determination of the amount of topically applied substances penetrated into the hair follicles. J Invest Dermatol 125, 264-269.

Teichmann, A., Otberg, N., Jacobi, U., Sterry, W., Lademann, J., 2006. Follicular penetration: development of a method to block the follicles selectively against the penetration of topically applied substances. Skin Pharmacol Physiol 19, 216-223.

Toll, R., Jacobi, U., Richter, H., Lademann, J., Schaefer, H., Blume-Peytavi, U., 2004. Penetration profile of microspheres in follicular targeting of terminal hair follicles. J Invest Dermatol 123, 168-176.

Trauer, S., Patzelt, A., Otberg, N., Knorr, F., Rozycki, C., Balizs, G., Büttemeyer, R., Linscheid, M., Liebsch, M., Lademann, J., 2009. Permeation of topically applied caffeine through human skin - a comparison of in vivo and in vitro data. Br J Clin Pharmacol 68, 181-186.

Vandervoort, J., Ludwig, A., 2004. Preparation and evaluation of drug-loaded gelatin nanoparticles for topical ophthalmic use. Eur J Pharm Biopharm 57, 251-261.

Venkataramani, S., Truntzer, J., Coleman, D.R., 2013. Thermal stability of high concentration lysozyme across varying pH: A Fourier Transform Infrared study. J Pharm Bioallied Sci 5, 148-153.

Vogt, A., Combadiere, B., Hadam, S., Stieler, K.M., Lademann, J., Schaefer, H., ., Autran, B., Sterry, W., Blume-Peytavi, U., 2006. 40 nm, but not 750 or 1,500 nm, nanoparticles enter epidermal CD1a+ cells after transcutaneous application on human skin. J Invest Dermatol 126, 1316-1322.

Wang, H., Zou, Q., Boerman, O.C., Nijhuis, A.W., Jansen, J.A., Li, Y., Leeuwenburgh, S.C., 2013. Combined delivery of BMP-2 and bFGF from nanostructured colloidal gelatin gels and its effect on bone regeneration in vivo. J Control Release 166, 172-181.

Wang, H.A., Boerman, O.C., Sariibrahimoglu, K., Li, Y.B., Jansen, J.A., Leeuwenburgh, S.C.G., 2012. Comparison of micro- vs. nanostructured colloidal gelatin gels for sustained delivery of osteogenic proteins: Bone morphogenetic protein-2 and alkaline phosphatase. Biomaterials 33, 8695-8703.

Weber, C., Coester, C., Kreuter, J., Langer, K., 2000. Desolvation process and surface characterization of protein nanoparticles. Int J Pharm 194, 91-102.

Wissing, S.A., Müller, R.H., 2002. Solid lipid nanoparticles as carrier for sunscreens: in vitro release and in vivo skin penetration. J Control Release 81, 225-233.

Yamamoto, M., Ikada, Y., Tabata, Y., 2001. Controlled release of growth factors based on biodegradation of gelatin hydrogel. J Biomater Sci Polym Ed 12, 77-88.

Young, S., Wong, M., Tabata, Y., Mikos, A.G., 2005. Gelatin as a delivery vehicle for the controlled release of bioactive molecules. J Control Release 109, 256-274.

Zeeb, B., Gibis, M., Fischer, L., Weiss, J., 2012. Influence of interfacial properties on Ostwald ripening in crosslinked multilayered oil-in-water emulsions. J Colloid Interface Sci 387, 65-73.

Zhai, X.Z., Müller, R.H., Coester, C., 2011. Production of ultrafine gelatin nanoparticles for dermal application, AAPS annual meeting, Washington DC USA.

Zhang, J., Huang, F., Lin, Z., 2010. Progress of nanocrystalline growth kinetics based on oriented attachment. Nanoscale 2, 18-34.

Zhao, B., Xie, J., Zhao, J., 2004. A novel water-soluble nanoparticles of hypocrellin B and their interaction with a model protein: C-phycocyanin. Bba-Biomembranes 1670, 113-120.

Zhao, Y.Z., Li, X., Lu, C.T., Xu, Y.Y., Lv, H.F., Dai, D.D., Zhang, L., Sun, C.Z., Yang, W., Li, X.K., Zhao, Y.P., Fu, H.X., Cai, L., Lin, M., Chen, L.J., Zhang, M., 2012. Experiment on the feasibility of using modified gelatin nanoparticles as insulin pulmonary administration system for diabetes therapy. Acta Diabetologica 49, 315-325.

Zhong, J., Shen, Z., Yang, Y., Chen, J., 2005. Preparation and characterization of uniform nanosized cephradine by combination of reactive precipitation and liquid anti-solvent precipitation under high gravity environment. Int J Pharm 301, 286-293.

Zillies, J.C., Zwiorek, K., Hoffmann, F., Vollmar, A., Anchordoquy, T.J., Winter, G., Coester, C., 2008. Formulation development of freeze-dried oligonucleotide-loaded gelatin nanoparticles. Eur J Pharm Biopharm 70, 514-521.

Zwiorek, K., 2006. Gelatin nanoparticles as delivery system for nucleotide-based drugs. Doctoral dissertation, Ludwig-Maximilians-University München.

Zwiorek, K., Kloeckner, J., Wagner, E., Coester, C., 2005. Gelatin nanoparticles as a new and simple gene delivery system. J Pharm Pharm Sci 7, 22-28.

Abbreviations

BA	bioavailability
BCS	Biopharmaceutics classification system
CMC-Na	sodium carboxymethyl cellulose
C_s	saturation solubility
DLE	drug loading efficiency
DLS	dynamic light scattering
FDA	US Food & Drug Administration
GNPs	gelatin nanoparticles
HMW	high molecular weight
HPLC	high performance liquid chromatography
HPH	high pressure homogenization
IEP	isoelectric point
LD	laser diffractometry
LMW	low molecular weight
LTG	lysozyme loaded traditional GNPs
LUG	lysozyme loaded ultrafine GNPs
PCS	photon correlation spectroscopy
PI	polydispersity index
PM	pearl milling
PVP	polyvinylpyrrolidone

RT	room temperature
TEM	transmission electron microscope
UTG	unloaded traditional GNPs
UUG	unloaded ultrafine GNPs
UV	ultraviolet

Publication list

Abstracts

1. Zhai, X., Keck, C. M., Staufenbiel, S., Müller, R. H., Caffeine nanocrystals – a novel concept to increase skin delivery by transferring medium solubles into nanocrystals, T2074, AAPS Annual Meeting, San Antonio, 10-14 November 2013.

2. Zhai, X., Keck, C. M., Müller, R. H., Lysozyme loaded ultra small gelatin nanoparticles for dermal delivery: Physicochemical characterization and in vitro release, p67, 7th Polish-German Symposium on Pharmaceutical Sciences: Interdisciplinary research for Pharmacy, Gdansk, 24-25 May 2013.

3. Zhai, X., Keck, C. M., Müller, R. H., Nanocrystals of medium soluble drugs/actives – a novel concept for improved skin delivery, p28, 7th Polish-German Symposium on Pharmaceutical Sciences: Interdisciplinary research for Pharmacy, Gdansk, 24-25 May 2013.

4. Zhai, X., Keck, C. M., Müller, R. H., Preparation method for ultra small gelantin nanoparticles for dermal delivery of peptides & enzymes, P10, Jahrestagung der Gesellschaft für Dermopharmazie (GD), Mainz, 21-23 March 2013.

5. Zhai, X., Keck, C. M., Müller, R. H., Caffeine nanocrystals – novel concept for improved dermal delivery & production method, P8, Jahrestagung der Gesellschaft für Dermopharmazie (GD), Mainz, 21-23 March 2013.

6. Zhai, X., Shegokar, R., Müller, R. H., Lysozyme loaded ultra small gelatin nanoparticles for dermal application: loading capacity, release profile and activity, R6047, AAPS Annual Meeting, Chicago, 14-18 October 2012.

7. Zhai, X., Shegokar, R., Müller, R. H., Preparation of ultra small gelatin nanoparticles for dermal delivery: optimization of production parameters, „Tag der Pharmazie“, DPhG Landesgruppe Berlin-Brandenburg, Berlin, 6 July 2012.

8. Zhai, X., Müller, R., Coester, C., Production of ultrafine gelatin nanoparticles for dermal delivery, T2137, AAPS Annual Meeting, Washington D.C., 23-27 October 2011.

9. Zhai, X., Shegokar, R., Müller, R. H., Coester, C., Preparation of below 100 nm gelatin nanoparticles – influence of production parameters, PO-129, Annual Joint Meeting, DPhG, Innsbruck, 20-23 September 2011.

Proceeding

1. Zhai, X., Staufenbiel, S., Keck, C. M., Müller, R. H., Caffeine nanocrystals – a novel concept for improved skin delivery, The 40th Annual Meeting & Exposition of the Controlled Release Society, Honolulu, Hawaii, 21-24 July 2013.

Curriculum Vitae

For reasons of data protection,

the curriculum vitae is not included in the online version

For reasons of data protection,

the curriculum vitae is not included in the online version

Acknowledgements

First of all, I would like to express my deepest gratitude to Prof. Dr. Rainer H. Müller, for his guidance, support, patience as well as encouragement during the three years of my research and the compilation of this thesis. I appreciate very much this opportunity to perform my doctoral study in his famous international research group. What I have learned from him is invaluable for my work and life in the future.

Secondly, greatest appreciation goes to Prof. Dr. Cornelia M. Keck, for her productive ideas to enrich my research. I highly appreciated the expert suggestions of her concerning the production of caffeine nanocrystals. It saves me a lot of time and energy to get meaningful results.

Special thanks go to Dr. Ranjita shegokar, for her scientific guidance and valuable suggestions, especially during the first two years. Much thanks to her for the daily support while sharing with me the joy in good times and suffering the depression in bad times!

I would like to thank China Scholarship Council for the financial support during the past three years, which enables my doctoral study at Freie Universität Berlin.

I would like to thank PharmaSol GmbH (Berlin, Germany) for sponsoring my participation in international conferences. These conferences help me to broad my scientific horizon.

Special thanks to Ms. Gabriela Karsubke, Ms. Corinna Schmidt, Ms. Inge Volz, Dr. Lothar Schwabe and Mr. Alfred Protz for their help and support in administrative and practical issues.

I would also like to owe many thanks to Sung Min Pyo, for her careful proofreading of this thesis, even though she was also busy with her own thesis during the past several months.

This thesis would not have been possible without the support and accompanying from my lovely colleagues. Happiness and sorrows, we spend every minute together. We will always remember and appreciate this precious experience in the future.

Last but not least, I would like to dedicate my endless appreciation and gratitude to my parents and my family members for the support, love and faith.